

Department of Materials Science and Engineering

Properties of Pulsed Electric Current Sintered Copper and Copper Composites

Riina Ritasalo

Properties of Pulsed Electric Current Sintered Copper and Copper Composites

Riina Ritasalo

A doctoral dissertation completed for the degree of Doctor of Science (Technology) to be defended, with the permission of the Aalto University School of Chemical Technology, at a public examination held at the lecture hall V1 of the school on 23 May 2014 at 12.

Aalto University
School of Chemical Technology
Department of Materials Science and Engineering
Advanced and Functional Materials Group

Supervising professor

Professor Simo-Pekka Hannula

Thesis advisor

Professor Simo-Pekka Hannula

Preliminary examiners

Research Professor, Joanna R. Groza
University of California, Davis, California, USA

Professor, Veli-Tapani Kuokkala
Department of Materials Science,
Tampere University of Technology, Finland

Doctor Ludger Weber, Group Leader at the
Laboratory of Mechanical Metallurgy,
EPF Lausanne, Switzerland

Opponents

Doctor Janis Grabis, Director, Head of Plasma
Process Laboratory Institute of Inorganic Chemistry,
Riga Technical University, Latvia

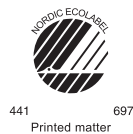
Aalto University publication series
DOCTORAL DISSERTATIONS 53/2014

© Riina Ritasalo

ISBN 978-952-60-5654-8
ISBN 978-952-60-5655-5 (pdf)
ISSN-L 1799-4934
ISSN 1799-4934 (printed)
ISSN 1799-4942 (pdf)
<http://urn.fi/URN:ISBN:978-952-60-5655-5>

Unigrafia Oy
Helsinki 2014

Finland



Author

Riina Ritasalo

Name of the doctoral dissertation

Properties of Pulsed Electric Current Sintered Copper and Copper Composites

Publisher School of Chemical Technology

Unit Department of Materials Science and Engineering

Series Aalto University publication series DOCTORAL DISSERTATIONS 53/2014

Field of research Physical Metallurgy and Materials Science

Manuscript submitted 10 February 2014

Date of the defence 23 May 2014

Permission to publish granted (date) 8 April 2014

Language English

Monograph

Article dissertation (summary + original articles)

Abstract

This work focuses on the processing and properties of Cu-based materials by the non-conventional and innovative method of pulsed electric current sintering (PECS), also known as spark plasma sintering (SPS). In particular, the aim is to produce materials with fine microstructures and determine the relationships between the manufacturing and the resulting properties of the bulk compacts. This includes process optimization to provide dense samples with controlled microstructures, in terms of grain size and reinforcement distribution, as well as an investigation on the properties of the final materials. The mechanical, nanomechanical, thermal, electrical, and tribological properties are of main interest.

The experimental studies employed commercial and experimental powders and their mixtures as the starting materials for consolidation. The PECS process optimization yielded highly dense Cu and Cu-composite samples, mostly ranging between 97.0 and 99.7% of theoretical density (T.D.). Overall, the studied additives, their size, amount, and distribution in Cu matrixes resulted in a variety of influences on their properties. It was found that all the dispersoids decreased the tendency of grain growth during PECS process. Furthermore, a linear relationship between Cu and Cu₂O grain growth was observed. Cu₂O prevented grain growth of Cu, the effectiveness increasing up to about 20 vol% Cu₂O remaining at the same level beyond that. The hindrance of Cu grain growth by Cu₂O could be described by the cluster model of Flores. All of the reinforcements in the present study, such as Cu₂O, Al₂O₃, TiB₂ and nano/submicron-sized diamond (ND/SMD), were found to noticeably improve the microhardness compared to plain sm-Cu (submicron-sized copper). Large amount of small size reinforcements is the most effective. At best, these composites also resulted in improved thermal properties, moderate electrical conductivity, lower CoFs (coefficient of friction) and a reduced wear rate as compared to plain Cu. However, the properties greatly depended on the composite type and do not as such present general rules. The comparison between the PECS and HIP processes and the accompanied properties verified that the shorter time needed for proper densification by PECS resulted in finer grain structure and improved mechanical properties as compared to HIP.

Overall, this study shows that PECS can be used to produce high quality Cu-composites with superior properties when compared to those of sm-Cu. On the whole, this research is supportive of the development of new alternative Cu-based materials for various applications, where enhanced thermal properties together with excellent mechanical properties are desired.

Keywords pulsed electric current sintering, copper, metallic matrix composites, microstructure, dispersion strengthening, mechanical properties, thermal properties, tribological properties, electrical properties

ISBN (printed) 978-952-60-5654-8

ISBN (pdf) 978-952-60-5655-5

ISSN-L 1799-4934

ISSN (printed) 1799-4934

ISSN (pdf) 1799-4942

Location of publisher Helsinki

Location of printing Helsinki

Year 2014

Pages 183

urn <http://urn.fi/URN:ISBN:978-952-60-5655-5>

Tekijä

Riina Ritasalo

Väitöskirjan nimi

PECS menetelmällä kiinteitettyjen kuparin ja kuparikomposiittien ominaisuudet

Julkaisija Kemian tekniikan korkeakoulu**Yksikkö** Materiaalitekniikan laitos**Sarja** Aalto University publication series DOCTORAL DISSERTATIONS 53/2014**Tutkimusala** Metall- ja materiaalioppi**Käsitteilypvm** 10.02.2014**Väitöspäivä** 23.05.2014**Julkaisuluvan myöntämispäivä** 08.04.2014**Kieli** Englanti **Monografia** **Yhdistelmäväitöskirja (yhteenvedo-osa + erillisartikkelit)****Tiivistelmä**

Työn tavoitteena on määrittää kuparipohjaisten materiaalien ominaisuudet kiinteytettäessä niitä pulssitettua tasavirtaa hyödyntävällä sintraustekniikalla (PECS), tunnettu myös kipinäplasma sintraustekniikkana (SPS). Pyrkimyksenä on tuottaa materiaaliin hienojakoinen mikrorakenne ja ymmärtää ominaisuuksiin vaikuttavien prosessimuuttujien sekä niihin yhteydessä olevien materiaali koostumusten vaikutuksia. Tutkimuksessa optimoidaan prosessiparametreja tiiviiden ja mikrorakenteeltaan tasalaatuisten bulkinäytteiden aikaansaamiseksi sekä määritetään niiden ominaisuuksia. Erityisesti tarkastellaan mekaanisia, nanomekaanisia, termisiä, sähköisiä ja tribologisia ominaisuuksia.

Kiinteityksessä lähtöaineina käytettiin sekä kaupallisia että kokeellisesti valmistettuja jauheita ja niiden kombinaatioita. Prosessioptimoinnin tuloksena saavutettiin teoreettiseen tiheyteen verrattuna 97.0 - 99.7% tiiviitä kappaleita, joissa materiaaliominaisuuksiin vaikuttivat sekä lujitetyt ja -määrä että lujitepartikkeleiden koko ja jakauma. Kaikki lujitetyt hidastivat kuparin rakeen kasvua PECS -prosessoinnissa. Lisäksi raekoon kasvu kuparin ja kupriitin (Cu_2O) välillä noudatti lineaarista riippuvuutta. Cu_2O :n raekoon kasvua kontrolloiva vaikutus kasvoi 20 til.% asti, säilyen samalla tasolla tämän jälkeen. Kuparin rakeen kasvu Cu_2O :n vaikutuksesta voitiin mallintaa Florensin 'klustereihin' perustuvan mallin avulla. Kaikki lujitteet, ts. Cu_2O , Al_2O_3 , TiB_2 sekä nano/submikronin kokoiset timanttipartikkelit, paransivat kovuutta verrattuna raekooltaan submikronin luokkaa olevaan puhtaaseen kupariin (sm-Cu). Kuten odotettua, pienempi koko ja suurempi lujitemäärä tehostivat vaikutusta. Parhaimmillaan lujitteet kohensivat sekä termisiä että tribologisia ominaisuuksia. Lisäksi sähköiset ominaisuudet säilyivät kohtuullisina. Ominaisuudet riippuivat kuitenkin merkittävästi lujitetyypistä.

PECS -menetelmän avulla saavutettuja materiaaliominaisuuksia verrattiin HIP:n vastaaviin. Tulokset osoittivat, että tiiviiden kappaleiden aikaansaamiseksi HIP -menetelmällä vaadittiin pidempi aika, mikä johti merkittävämpään raekokoon kasvuun ja sen myötä heikompiin mekaanisiin ominaisuuksiin.

Tutkimus osoittaa, että PECS -menetelmällä voidaan tuottaa laadukkaita Cu-komposiitteja, jotka ovat ominaisuuksiltaan selkeästi parempia kuin puhdas PECS kiinteitetty sm-Cu. Tutkittuja materiaaleja voidaan pitää huomioon otettavina vaihtoehtoina käyttökohteissa, joissa vaaditaan hyviä lämpöteknisiä ja kuparia parempia mekaanisia ominaisuuksia.

Avainsanat sintraus tasavirtapulssien avulla (PECS, SPS), kupari, metalli matriisi komposiitit, mikrorakenne, mekaaniset ominaisuudet, lämpötekniset ominaisuudet, tribologiset ominaisuudet, sähköjohtavuus

ISBN (painettu) 978-952-60-5654-8**ISBN (pdf)** 978-952-60-5655-5**ISSN-L** 1799-4934**ISSN (painettu)** 1799-4934**ISSN (pdf)** 1799-4942**Julkaisupaikka** Helsinki**Painopaikka** Helsinki**Vuosi** 2014**Sivumäärä** 183**urn** <http://urn.fi/URN:ISBN:978-952-60-5655-5>

Preface

The research work presented in this thesis was conducted at Aalto University, formerly known as Helsinki University of Technology. The majority of the research was carried out in the Department of Materials Science and Engineering at the School of Chemical technology. Part of the experiments were carried out in the Catholic University of Leuven, Belgium, in FCT Systeme GmbH, Germany, in Tallinn University of Technology, Estonia, at Outotec Research Center and Luvata Inc., in Pori and at VTT Technical Research Centre in Tampere and Espoo, which are gratefully acknowledged. For the financial support, I wish to express my sincere gratitude to The Finnish Academy via the Graduate School of Advanced Materials and Processes at Aalto University, between the years of 2011 - 2013.

The most precious appreciation I would like to address, is to my Supervisor, Professor Simo-Pekka Hannula. With his approval, I became a member of the group of Advanced and Functional Materials, initially as a post-graduate student with an assistant position. With his support, guidance and knowledge, I have had a great chance to work towards my 'long-lived' goal.

I would like to thank the pre-examiners of my thesis for their reviews and comments.

I wish to thank all the co-authors of my Publications. A special thanks goes to Outi Söderberg for all the advice she gave me. Her exceptionally positive attitude amazes me over and over again. For MsC Ulla Kanerva, Dr Yanling Ge and Dr Xuwen Liu, I wish to show my gratitude for their efforts in participating and helping my work. Erkin, 'my SPS-guru', you have taught me so much and have always had time for me. I have enjoyed all the travels, discussions and chats with you. Thanks for being my friend for all these years!! Pirjo, I want to thank you for all time you spent in helping me in the lab.

For my friends, colleagues and ex-colleagues: thanks to you all, for just being there and lightening my days!! IP, you are the 'spirit' of the whole group! And Juha, you are the nicest person ever, such a great company and always there when I needed

help, advice or someone special to talk to. Mostly, I want to thank you for being my friend!

Finally, many thanks to my beloved parents and to my two brothers and their families! As well, I would like to thank my parents-in-law and their other son. Having you around helps me to keep my sense!

Foremost; to my husband Teemu and our son Oskari, you mean the world to me!!!!

Riina Ritasalo

Espoo, 2014

List of Publications

The thesis consists of an overview of the properties of spark plasma sintered Cu and Cu-composites. The results of the work have been presented in the following Publications which are referred to in the text by their Roman numerals.

- I** R. Ritasalo, M. E. Cura, X.W. Liu, O. Söderberg, T. Ritvonen, S-P. Hannula, Spark plasma sintering of submicron-sized Cu-powder - influence of processing parameters and powder oxidization on microstructure and mechanical properties, *Materials Science & Engineering A*, 527 (2010) 2733-2737.
- II** R. Ritasalo, X.W. Liu, O. Söderberg, A. Keski-Honkola, V. Pitkänen, S-P. Hannula, The microstructural effects on the mechanical and thermal properties of pulsed electric current sintered Cu-Al₂O₃ composites, *Procedia Engineering*, 10 (2011) 124-129.
- III** R. Ritasalo, M.E. Cura, X.W. Liu, Y. Ge, T. Kosonen, U. Kanerva, O. Söderberg, S-P. Hannula, Microstructural and mechanical characteristics of Cu-Cu₂O composites compacted with pulsed electric current sintering and hot isostatic pressing, *Composites Part A: Applied Science and Manufacturing*, 45 (2013) 61-69.
- IV** R. Ritasalo, U. Kanerva, Y. Ge, S-P. Hannula, Mechanical and thermal properties of pulsed electric current sintered (PECS) Cu-diamond -compacts, *Metallurgical and Materials Transaction B*, 45 (2) (2014) 489-496.
- V** R. Ritasalo, U. Kanerva and S-P. Hannula, Thermal stability of PECS - compacted Cu-composites, *Key Engineering Materials*, 527 (2013) 113-118.
- VI** R. Ritasalo, M. Antonov, R. Veinthal, S-P. Hannula, Comparison of the wear and frictional properties of Cu matrix composites prepared by pulsed electric current sintering, *Proceedings of the Estonian Academy of Sciences*, 63 (1) (2014) 62-74.

Brief Description of the Publications

Publication I: “Spark plasma sintering of submicron-sized Cu-powder - influence of processing parameters and powder oxidization on microstructure and mechanical properties.”

The microstructures and nanomechanical properties of copper, consolidated from oxidized submicron-sized Cu powder by Spark Plasma Sintering (SPS) were studied. It was shown that a good compact density of between 97.6 and 99.7% of T.D. (theoretical density), a small grain size close to the starting powder size and high microhardness were achieved by 6 min SPS of the Cu powder with about 20 vol.% Cu₂O at 100 MPa and 873 K. Higher sintering temperatures led to an increase in grain size and a decrease in hardness. For the sample made by hot isostatic pressing (HIP), the grain growth was more pronounced, most probably due to the longer process time, thus yielding lower hardness. The nanoindentation measurements indicated no notable difference between the hardness values of Cu and the Cu₂O phases, whereas, it revealed a lower elastic modulus for Cu₂O.

The results in this Publication show that the SPS process is superior to HIP consolidation in terms of the microhardness and microstructure of the final material. Furthermore, the presence of Cu₂O had no marked effect on the SPS densification process confirmed by the high density values achieved.

Publication II: “The microstructural effects on the mechanical and thermal properties of pulsed electric current sintered Cu-Al₂O₃ composites.”

In this Publication, the influences of microstructure on the mechanical and thermal properties of pulsed electric current sintered (PECS) Cu-Al₂O₃ composites were investigated. The PECS resulted in dense samples (98 - 99.6% of T.D.) after process optimization for all four grades of composite powders. The samples compacted from commercial internally oxidized (IO) powders demonstrated a higher hardness and better thermal stability than those made from the chemically synthesized experimental (Exp.) powders. The results suggest that the differences can be attributed to the distribution and size of Al₂O₃ particles in the two types of

composites. The coefficient of thermal expansion (CTE) values of all the compacts lay in the same range, despite the different amount and distribution of alumina. This study confirms that PECS can be used to produce dense, high quality Cu-Al₂O₃ composites with comparable properties to those prepared by conventional methods.

Publication III: “Microstructural and mechanical characteristics of Cu-Cu₂O composites compacted with pulsed electric current sintering and hot isostatic pressing.”

Two methods, pulsed electric current sintering (PECS) and hot isostatic pressing (HIP), were applied for the consolidation of Cu-Cu₂O composite powders. The objective was to study the resulting properties of these compacts.

In PECS, a fine-grained structure was obtained, while in HIP the grain growth was more noticeable, mostly due to the longer process time. The results showed that the Cu₂O (cuprite) phase distributed in a Cu matrix increased microhardness, giving comparable values for submicron-sized Cu-Cu₂O composites and those reported for pure nanosized Cu, with a near-Hall-Petch -type of relationship for hardness depending on grain size. The high microhardness values were consistent with the high hardness values measured with nanoindentation. In addition, these nanoindentation measurements revealed the different elastic behaviour for the Cu and Cu₂O phases; demonstrating a lower modulus and larger elastic recovery upon unloading, for cuprite than for copper. This Publication also suggests that the Cu₂O phase distributed in a Cu matrix prevented the grain growth of Cu during high-temperature processing. The effectiveness of Cu₂O in grain growth control increased until about 20 vol.% of Cu₂O, remaining at the same level beyond that.

Publication IV: “Mechanical and thermal properties of pulsed electric current sintered (PECS) Cu-diamond -compacts.”

The Publication focuses on the dispersion strengthening (DS) of Cu by nano- and submicron-sized diamonds (ND and SMD). Mechanical alloying (MA) in an argon atmosphere by high-energy vibratory ball mill resulted in composite powders with diamond particles strongly adhering onto the surfaces of Cu particles. The prepared PECS compacts had a high density (> 97% of T.D.), with quite evenly distributed diamonds, and a higher hardness than that of pure submicron-sized copper (sm-Cu). It was shown that the experimental microhardness values mostly correlated to

the theoretical ones calculated by the Hall-Petch and Orowan strengthening models.

The results of this Publication revealed that the content of diamond dispersoids influenced the thermal stability. It was also revealed that increased amount of diamond dispersoids led to more stable structures and lower CTEs. By nanoindentation, a well-bonded interface between the diamonds and Cu was demonstrated. At best, both types of Cu-diamond composites clearly possess better mechanical and thermal properties compared to sm-Cu.

Publication V: “Thermal stability of PECS -compacted Cu-composites.”

Metal matrix composites (MMCs) with higher strength and better temperature stability than reference submicron-sized copper (sm-Cu) was of interest in this Publication. The pulsed electric current sintered (PECS) samples of plain sm-Cu and Cu with dispersoids of cuprite (Cu_2O), alumina (Al_2O_3), titaniumdiboride (TiB_2), and nano- or submicron-sized diamonds (ND or SMD) were chosen for the study. The results revealed that the incorporation of dispersoids notably improved the room temperature mechanical properties as well as the high-temperature stability of Cu. The effects were more noticeable with smaller sizes of dispersoids and also with a higher amount of reinforcement. A similar trend was also noted in the case of CTE. It was shown that Cu-ND, Cu-SMD and Cu- Cu_2O composites are suitable for use at moderate temperatures, whereas, the more stable composites of Cu- Al_2O_3 and Cu- TiB_2 are suitable for much higher temperatures. The Hall-Petch strengthening, Orowan strengthening, and in the case of Cu- TiB_2 the contribution of hard and coarse TiB_2 attributed to the overall strength of the compacts.

This Publication suggests that PECS can be used to produce high-quality Cu-composites, which can be considered to be promising candidates for applications where enhanced thermal properties together with high mechanical properties are desired.

Publication VI: “Comparison of the wear and frictional properties of Cu matrix composites prepared by pulsed electric current sintering.”

The Publication presents the tribological properties of copper and Cu with dispersoids of cuprite (Cu_2O), alumina (Al_2O_3), titaniumdiboride (TiB_2), and diamond in non-lubricated sliding tests. The ball-on-flat tests demonstrated a great dependence of the coefficient of friction (CoF), wear rate and mechanism on the counter material. The tests against ceramic alumina counterparts led to low CoFs

and wear rates, whereas the tests against metallic Cr-steel counterparts led to much higher wear values in all the tests, mostly due to the difference in wear mechanisms. Of the composites, Cu with diamond dispersoids showed the lowest wear rate and Cu-Cu₂O and Cu with diamond (5 nm) dispersoids showed the lowest CoF against alumina. The main wear mechanism was oxidative wear. In some cases the reciprocating sliding caused material pile-up onto the sides of the tracks. In contrast, the tests against metallic Cr-steel showed adhesive/abrasive wear and reactivity against the metallic test samples; Cu-Cu₂O yielded the lowest CoF and wear rate. In this Publication it was confirmed that both the type of dispersed particles and the counter material have a notable effect on the tribological features in Cu-composites. It is believed that the present work gives new insights for materials selection e.g., in electronic connector parts.

Author's Contribution

The author is the responsible author for all the Publications and has contributed the major part of the planning and design of the research, as well as the writing of all the Publications from I to VI presented in this Thesis. Of the experimental work, she has been responsible for the PECS experiments stated in the Publications of II and IV-VI. She has also conducted the majority of materials characterization, including optical microscopy, scanning electron microscopy (SEM), and a part of transmission electron microscopy (TEM) evaluations. Additionally, she has carried out the Archimedes density measurements, Vickers' hardness measurements, X-ray diffraction (XRD) measurements, annealing experiments, and the majority of the nanoindentation measurements. The author also analyzed most of the results, including the thermal expansion measurements. Finally, all the non-lubricated sliding tests were conducted by the author.

The co-authors have contributed to the following parts of the experimental work and preparation of the manuscripts:

- Prof. S-P. Hannula: provided important scientific guidance for the research work, participated in the preparation, analysis and reviewing's of all the manuscripts prior to their submission for Publication.
- Prof. R. Veinthal: provided the possibility for the author to carry out the non-lubricated sliding tests and reviewed the manuscript for Publication VI.
- Dr. Y. Ge: carried out most of the TEM work and analysis for Publications III and IV together with the author.
- Dr. X.W. Liu: conducted the nanoindentation experiments of Publication I together with the author and gave his guidance for nanoindentation analysis for Publications II and III.
- Dr. O. Söderberg: provided important scientific guidance for the research and analysis and also reviewed the manuscripts for Publications I-III.

- MSc. M.E. Cura: participated in the organizing and planning of the SPS - experiments for Publication I and gave valuable comments for Publication III.
- MSc. A. Keski-Honkola: conducted the thermal expansion measurements for Publications II, IV and V.
- MSc. U. Kanerva: provided the Cu-composite powders (Cu-TiB₂ and Cu-diamond) for Publications IV - VI. She also participated in the organizing and planning of the HIP (hot isostatic pressing) experiments and gave valuable comments for Publication III.
- MSc. M. Antonov: participated in the planning of the non-lubricated sliding tests, gave valuable comments, and reviewed the manuscript for Publication VI.
- MSc. T. Ritvonen: participated in organizing HIP experiment for Publication I.
- T. Kosonen: conducted the HIP experiments for Publication III.
- V. Pitkänen: participated in the thermal stability experiments for Publication II.

Professor, Simo-Pekka Hannula

Espoo, 2014

Contents

Preface	i
List of Publications	iii
Brief Description of the Publications	v
Author's Contribution	ix
Contents	xi
Nomenclature	xiii
List of Abbreviations	xvii
List of Figures and Tables	xix
1. Introduction	1
1.1 Characteristics of two-phase composites.....	1
1.1.1 Strengthening of metals	2
1.1.2 Thermal properties of MMCs	8
1.1.3 Influence of dispersed particles on tribological properties	10
1.2 Copper: properties and applications.....	11
1.2.1 Properties of copper	12
1.2.2 Dispersion strengthened copper	12
1.2.3 Applications of Cu-based materials	13
1.3 Preparation of Cu-composite powders	16
1.3.1 Mixing	16
1.3.2 Mechanical alloying	17
1.3.3 Internal oxidation	18
1.3.4 Self-propagating high-temperature synthesis.....	18
1.4 Preparation of bulk UFG and nanosized Cu-composites	19
1.4.1 Hot isostatic pressing.....	19
1.4.2 Pulsed electric current sintering.....	21
1.5 PECS processed Cu-based materials and their properties	24
1.6 Aim of the work.....	26
2. Experimental	29
2.1 Preparation and characteristics of Cu matrix composite powders	29
2.2 Consolidation of the powders.....	31
2.2.1 Pulsed electric current sintering	31
2.2.2 Hot Isostatic Pressing	33
2.3 Sample preparation for materials characterization.....	33
2.4 Characterization of the bulk samples	34
2.4.1 Density.....	34
2.4.2 Microstructure.....	34
2.4.3 Mechanical and nanomechanical properties	35
2.4.4 Oxygen content	35

2.4.5	Electrical properties	36
2.4.6	Thermal properties	36
2.4.7	Tribological properties	37
3.	Summary of the Results	39
3.1	The microstructural characteristics of Cu and Cu-composites	39
3.1.1	Pure copper	39
3.1.2	Cu-Cu ₂ O composites	39
3.1.3	Cu-Al ₂ O ₃ composites	41
3.1.4	Cu-TiB ₂ composites	43
3.1.5	Cu-diamond composites	45
3.2	The mechanical properties of Cu-composites	47
3.2.1	Microhardness	47
3.2.2	Nanomechanical properties of Cu-composites	51
3.3	Thermal stability and thermal expansion of Cu-composites	53
3.4	Electrical properties	55
3.5	Friction and wear properties of Cu-composites	55
4.	Discussion	59
4.1	Densification of Cu-composite powders	59
4.2	Influence of the dispersoids on the hardness and grain growth	60
4.2.1	Microhardness	60
4.2.2	Grain growth	62
4.2.3	Strengthening	63
4.2.4	Nanomechanical properties	64
4.3	Thermal properties of Cu MMCs	67
4.3.1	Thermal stability	67
4.3.2	Coefficient of thermal expansion	68
4.4	Electrical properties of Cu-composites	70
4.5	Tribological characteristics of Cu-composites	71
4.5.1	Coefficient of friction	71
4.5.2	Wear track profiles	72
4.5.3	Wear rate and mechanisms	73
5.	Conclusions	75
	Bibliography	79
	Errata	93

Nomenclature

A	volume
b	Burgers vector
c	solute concentration
c-Cu	coarse Cu
CNF	carbon nanofiber
CNT	carbon nanotubes
Cu	copper
Cu ₂ O	copper oxide, cuprite
d	grain size
D	diamond
DWCNT	double-walled carbon nanotube
E	elastic modulus
Exp.	experimental
f	obstacle strength
f _v	volume fraction
F _w	weight fraction
F _p	applied load
G	shear modulus
H	hardness
H ₀	initial hardness
HE	hot extrusion

HV	Vickers' hardness
h-BN	hexagonal boron nitride
K_H	material dependent constants/Hall-Petch constant
K	bulk modulus
k	coarsening kinetic coefficient
L	distance
M	Taylor factor
MWCNT	multi-walled carbon nanotubes
N	Newton
n	grain growth exponent
n_c	grain/cell size exponent
nc	nanocrystalline
n-Cu	nanosized Cu
ND	nanodiamonds
nanoD	single-digit nanodiamonds
q	variable (depends on the average obstacle spacing)
R	particle radius/size
R_c	critical grain size
r_e	effective particle radius
sm	submicron-sized
SMD	submicron-sized diamonds
T	line tension
t	time
T_m	melting temperature
ν	Poisson ratio

V	volume loss
vol. %	volume percent
wt. %	weight percent
$\gamma\text{-Al}_2\text{O}_3$	gamma-alumina
α_i	CTE of element i
β	proportionality constant
μ	shear modulus
σ_{TiB_2}	fracture strength of TiB ₂
σ_Y	yield strength/stress
σ_0	friction/intrinsic stress
σ_s	yield stress by solutes
λ	distance between the dispersoids
ρ	density
Cr-steel	chromium-steel
ΔT	temperature change
$\Delta L/L_0$	relative linear expansion

List of Abbreviations

BF	bright field
CMC	ceramic matrix composites
CoF	coefficient of friction
CTE	coefficient of thermal expansion
DC	direct current
DS	dispersion strengthening
ECAP	equal channel angular pressing
EDS	energy dispersive spectroscopy
EDX	energy dispersive X-ray
EFTEM	energy-filtered transmission electron microscopy
FAST	field assisted sintering technology
FEG	field emission gun
FGM	functionally graded material
GBS	grain boundary sliding
GIF	gatan imaging filter
H-P	Hall-Petch
HIP	hot isostatic pressing
HP	hot pressing
IO	internal oxidation
MA	mechanical alloying
MMC	metallic matrix composites

OR	Orowan equation
PECS	pulsed electric current sintering
PM	powder metallurgical
PMC	polymer matrix composites
SAD	selected area diffraction
SADP	selected area diffraction pattern
SEM	scanning electron microscopy
SHS	self-propagating high-temperature synthesis
SPM	scanning probe microscopy
SPS	spark plasma sintering
STEM	scanning transmission electron microscope
TC	thermocouple
T.D.	theoretical density
TEM	transmission electron microscopy
UFG	ultra-fine grained
XRD	X-ray diffraction
%IACS	International annealed copper standard

List of Figures and Tables

Fig. 1.1.	Hardening in particle strengthened materials: illustration of a transition between the cutting and bowing at a critical particle size R (Arzt, 1998, with permission from Elsevier).	6
Fig. 1.2.	A sketch of the effect of the particle clustering (or agglomeration) on the diminution of the pinning force due to a reduction on the available superficial area of the particle: fewer particles are now acting as obstacles to the grain boundary motion (Flores et al., 2004, reprinted with permission from Springer).	7
Fig. 1.3.	Approximate effect of impurity elements on the electrical conductivity of copper (© Copper Development Association, 2013).	14
Fig. 1.4.	Transport mechanisms occurring during sintering of powders (Kaysser et al., 1988, with permission from Maney Publishing).	20
Fig. 1.5.	A schematic representation of a PECS unit.	23
Fig. 2.1.	(a) A FCT HP D 25 -type PECS equipment, (b) a vacuum chamber, and (c) a mold placed in the chamber between the electrodes.	31
Fig. 3.1.	Microstructures of the samples after etching: (a) PECS 1 (873 K/6 min), (b) PECS 2 (973 K/3 min), (c) PECS 4 (1073 K/1 min), (d) HIP 1 (948 K/30 min), (e) HIP 2 (1073K/30min), and (f) HIP 3 (1073 K/120 min) with a small insert in the top-left corner indicating the distribution of Cu_2O particles appearing with light borders. In (a) to (c) Cu_2O particles appear lighter than the Cu matrix.	40
Fig. 3.2.	The grain size of Cu and Cu_2O present in compacted Cu- Cu_2O samples as a function of process temperature in comparison with the values reported by Zhang et al. (2008) for (1 μm) Cu powder by PECS.	41
Fig. 3.3.	The microstructures of the composite samples: (a) $2.5\text{Al}_2\text{O}_3$ (IO) and (b) $2.5\text{Al}_2\text{O}_3$ (Exp.). Inserts in the top-left corners show Al_2O_3 particle distributions.	42

Fig. 3.4.	(a) - (b) STEM micrographs of the sample $2.5\text{Al}_2\text{O}_3$ (IO) with SAD and (c) - (d) STEM micrographs of the sample $2.5\text{Al}_2\text{O}_3$ (Exp.), the former with SAD.	43
Fig. 3.5.	Optical microscopy images of Cu-TiB ₂ -composites: (a) 12TiB ₂ , (b) 36TiB ₂ , and (c) 79TiB ₂ . TiB ₂ appears darker in the micrographs.	44
Fig. 3.6.	XRD results of the Cu-TiB ₂ composite samples.	44
Fig. 3.7.	SEM micrographs of the Cu-composite samples: (a) 6SMD (Cu - 6 vol.% submicron-sized diamonds), (b) 6ND (Cu - 6 vol.% 50 nm diamonds), and (c) 6nanoD (Cu - 6 vol.% 5 nm diamonds). Diamonds appear light in all micrographs.	45
Fig. 3.8.	(a) EFTEM micrograph of the Cu sample with 6 vol.% nanodiamonds (6ND), (b) the corresponding carbon map, and (c) STEM micrograph showing lighter spots, which indicate the sizes and placement of nanodiamonds in sample 6ND.	46
Fig. 3.9.	The hardness increment ($H - H_0$) as a function of grain size (d) obtained through the study of Cu-Cu ₂ O in comparison with the earlier reported values for Cu. Sources for the points marked with A - Das et al. (2006), B - Youngdahl et al. (1997), C - Khan et al. (2008), D - Chokshi et al. (1989), and E - present study. The samples of the present study with more than 30 vol.% Cu ₂ O are emphasized with filled marks and arrows. The trendlines are fitted for each data series.	48
Fig. 3.10.	(a) Fraction of clusters present in samples as a function of Cu ₂ O content and (b) dependence on the R_c/R ratio of the volume fraction of the second-phase as a comparison to the model presented by Flores et al. (2004).	49
Fig. 3.11.	Comparison of the experimental (exp.) and theoretical strengths (stacked bars). The numbers indicate the vol.% of dispersoids.	51
Fig. 3.12.	(a) The SPM image after indentation on HIP 3 and (b) the nanoindentation load-displacement curves corresponding to the points in (a).	52

Fig. 3.13.	(a) An SPM image of sample 6SMD (Cu with 6 vol.% submicron-sized diamonds) showing elevated lighter formations (diamonds) above the polished surface and marks from the (3 x 4) indent pattern and (b) the load vs. displacement curves for the indicated indents shown in (a).	53
Fig. 3.14.	Influence of one-hour (1h) heat treatment on the hardness of the compacts.	54
Fig. 3.15	The measured CTE values between the marked temperature ranges and the theoretical predictions based on Eq. (1.8).	55
Fig. 3.16.	The steady state coefficient of friction (CoF) as a function of vol.% dispersoids against Cr-steel and alumina counter balls. Note that the scales are different. The red marks are reference values for Cu (c-Cu for Cu-Al ₂ O ₃ composites and sm-Cu for others).	56
Fig. 3.17.	Optical images for (a) c-Cu, (b) 37Cu ₂ O, and (c) 6ND showing wear tracks after sliding against alumina (upper images) and Cr-steel (middle images), as well as ball surfaces after sliding against Cr-steel (lower images).	57
Fig. 3.18.	Typical wear profiles of the tracks made by (a) the Cr-steel and (b) the alumina counter ball.	58
Fig. 3.19.	Logarithmic presentation of the wear rates as a function of vol.% dispersoids against Cr-steel and alumina. The reference Cu values are marked as red (values of c-Cu for Cu-Al ₂ O ₃ composites due to the coarse matrix and sm-Cu for others).	58
Fig. 4.1.	Contribution of the reinforcements to the strength of Cu. Reference values for Cu have been taken from Khan et al. (2008).	64
Fig. 4.2.	Comparison of micro- and nanohardness values for selected samples.	66
Table 2.1.	Process parameters used in the experiments for Cu-composite powders showing the sintering temperature, holding time, pressure, and heating rate.	33
Table 3.1.	Properties of the PECS samples.	47

1. Introduction

1.1 Characteristics of two-phase composites

Composite materials include several types of combinations of two different materials separated by a distinct interface (Clyne & Withers, 1993). The most significant reason to apply second-phase particles (reinforcements) into the matrix is to enhance the properties compared to its constituents, e.g., in strength, strength to weight ratio, toughness, fatigue, ductility, tribological properties, corrosion resistance, or thermal properties (Clyne & Withers, 1993; Kainer, 2006). The reinforcing phases are usually in the form of particles, fibres or sheets (Clyne & Withers, 1993; Kainer, 2006), whereas the matrix materials can be polymers, ceramics or metals. On this basis, the composites can be classified in various ways. For example, based on reinforcement, the composites can be classified as (i) particle reinforced composites (spheres, rods, wires, whiskers), (ii) fiber reinforced composites, and (iii) structural composites (e.g. multilayer systems) (Clyne & Withers, 1993; Kainer, 2006). On the basis of matrix material, the major categories are (i) polymer matrix composites (PMC), (ii) ceramic matrix composites (CMC), (iii) metal matrix composites (MMC), and (iv) hybrid composites (Clyne & Withers, 1993). Furthermore, the composites with a metal matrix can be divided into subcategories of dispersion or particle strengthened composites, layer composites, fiber composites, and infiltration composites (Kainer, 2006).

The composites can be prepared from their constituents by solid-phase, liquid-phase, vapour state methods or their combinations (Clyne & Withers, 1993). In this work, the focus is on solid phase methods in preparing dispersion hardened MMCs. For reinforcements, the main requirements are thermodynamic and chemical stability, mechanical and chemical compatibility, high compression and tensile strength, low diffusivity, and low solubility (Groza, 1992; Groza & Gibeling, 1993; Kainer, 2006). It is widely recognized that the composite properties are controlled by the size, amount and type of reinforcement, as well as the nature of the interface between the constituents (Groza, 1992; Tjong & Ma, 2000). It is possible to approximate the characteristics of the composite by models; however these often represent the ideal conditions (Kainer, 2006).

1.1.1 Strengthening of metals

Metals can be strengthened with various alloying strategies including strain hardening, solid solution strengthening, and with precipitation or age hardening (Groza, 1992; Nadkarni & Synk, 1984). It is also possible to introduce particles into the metallic matrix by applying dispersion strengthening (DS) methods. In all these cases, the strengthening effect is due to obstacles, which block or retard the motion of lattice dislocations (Arzt, 1998). Additionally, the grain size decrement is considerably associated with enhanced strength (Chokshi et al., 1989; Conrad, 2003 & 2004). The additive elements can change the characteristics of the base material, or lose their affect at higher temperatures, or when subjected to static or dynamic loads. Thus, when choosing the suitable strengthening method the further treatment and application of the final product should be kept in mind.

Grain refinement

It is widely known that a fine grain size has a great impact on the strength. The strengthening of polycrystals by grain boundaries has been established ever since Hall proposed the relation between the grain size and the yield stress (Hall, 1951; Petch, 1953). The Hall-Petch relation suggests that the yield strength of a material should increase with decreasing grain size. The mathematically described Hall-Petch relation, Eq. (1.1), between yield stress and grain size, has shown validity to different systems (Chokshi et al., 1989; Conrad, 2003 & 2004; Conrad & Jung, 2005; Hannula et al., 2004; Khan et al., 2008; Kim et al., 2000; Youngdahl et al., 1997).

$$\sigma_Y = \sigma_o + k_H d^{-1/n_c} \quad (1.1)$$

where σ_Y is the yield stress, σ_o is the intrinsic stress/friction stress of the material (presenting other strengthening contributions) and k_H is material dependent constant, d is the average grain size and n_c is the grain/cell size exponent (with $n_c = 2$, the Eq. (1.1) represents a Hall-Petch relation).

Grain growth is a process in which the grain size of a single-phase polycrystalline material increases with time, thus leading to a decrement in strength (El-Khozondar et al., 2006; Finsy, 2004; German, 1996). The driving force for grain growth is the reduction of the total grain boundary energy when the total grain boundary area of a system is reduced (El-Khozondar et al., 2006; German, 1996; Zheng et al., 2006). During the grain growth, a grain boundary tends to migrate towards its curvature centre (Ashby, 1974). The large grains grow and the small grains shrink and finally disappear, thus resulting in an increase in grain size. (El-Khozondar et al., 2006; Finsy, 2004; German, 1996; Zheng et al., 2006).

In a single-phase system (e.g. pure metals and ceramics), the grain/cell size exponent n_c is close to 2, which represents a Hall-Petch relation (El-Khozondar et al., 2006; Zheng et al., 2006). However, some variation in grain size exponent has been reported, e.g., for deformed metals, where boundary strengthening is not a constant and the Hall-Petch relation must be modified. These variations can result from dislocation strengthening, deformation-induced high angle boundaries embedded in the structure or other structure factors (lamellae, etc.) (Hansen, 2004). Several different, fundamental approaches have been considered to describe the Hall-Petch behaviour (Chandrasekaran, 2003; Kim et al., 2000). Additionally, it is noticed that the Hall-Petch relation cannot be extrapolated to very fine grain sizes of around a few tens of nanometers (Chokshi et al., 1989; Conrad, 2003 & 2004; Conrad & Jung, 2005; Kim et al., 2000; Meyers et al., 2006). Instead, the inverse Hall-Petch relation or softening has been reported. This has been attributed to grain boundary diffusion creep and grain boundary sliding/shear (Arzt, 1998; Chokshi et al., 1989; Conrad, 2003). For instance, Conrad (2003 & 2004; Conrad & Jung, 2005) presented different rate-controlling mechanisms responsible for the Hall-Petch relation for different grain size regimes, i.e. intersection of dislocations (Regime I, when $d = 10^{-6} - 10^{-3}$ m), grain boundary shear promoted by the pile-up of dislocations (Regime II, when $d = 10^{-8} - 10^{-6}$ m), and grain boundary shear without pile-up (Regime III, when $d = < 10^{-8}$ m). While grain size hardening dominates in Regimes I and II, grain size softening occurs in Regime III.

Grain size in the presence of particles

For two-phase systems, the grain growth of matrix is greatly suppressed due to the presence of the other phase (Akbarpour et al., 2013; Fan et al., 1997a,b & 1998; Tian et al., 2006; Zheng et al., 2006). Zener pinning is a phenomenon in which the second-phase particles impede the grain growth of the matrix phase, by pinning the motion of grain boundaries (Fan et al., 1998; Smith, 1948). The correlation between the grain size of matrix phase and size of non-coarsening second-phase particles can be expressed as:

$$d = \frac{c}{f_v^m} R \quad (1.2)$$

where d is the grain size of the matrix, R is the size of second-phase particles, f_v is the volume fraction and c and m are constants. The value $m = 1$ correlates to the early Zener model (Smith, 1948), whereas $m = 1/2$ is suggested for two-dimensional non-random systems and $m = 1/3$ for three-dimensional, high-volume fraction systems (Fan et al., 1998). However, in many systems the m value differs from the above-mentioned because of nano-grains, microstructural defects, dispersoid distribution, and the shape or structural factors (El-Khozondar et al., 2006; Fan et al., 1998; Solomatov et al., 2002; Zheng et al., 2006).

The Zener pinning model assumes that the dispersed particles are spherical, mono-sized, randomly distributed, stable, incoherent, and non-coarsening (Smith, 1948). Even if the grain size of the matrix does coarsen, the second-phase particles retain their sizes. However, in some two phase systems the grain growth in the matrix and Ostwald ripening of second-phase particles can occur concurrently (El-Khozondar et al., 2006; Fan et al., 1998; Solomatov et al., 2002). The second-phase particles may show a tendency to coarsen by diffusing through the matrix and grow at the expense of smaller ones (El-Khozondar et al., 2006; Fan et al., 1997b & 1998). The growth kinetics can be predicted, e.g., by the power law as in Eq. (1.3) (Brodhag & Herwegh, 2010; El-Khozondar et al., 2006; Fan et al., 1997a,b & 1998):

$$R_t^n - R_0^n = kt \quad (1.3)$$

where n is the grain growth exponent, k is the coarsening kinetic coefficient, t is time and R is the average size of particles. The grain growth exponent describes the method of grain growth in Ostwald ripening; it is 3 for volume diffusion, 4 for grain boundary diffusion, and 5 for diffusion on dislocations (Ardell, 1972; Lifshitz & Slyozov, 1961; Wagner, 1961). The growth by the power law is suggested to be independent of the initial microstructure or volume fraction (Fan et al., 1997a,b & 1998). Nevertheless, the coarsening kinetic coefficient depends on the volume fraction of second-phase particles and the diffusivity and mobility between the phases. It is also affected by the boundary energies and the interphase boundary energy (Brodhag & Herwegh, 2010; Fan et al., 1997a,b; Zheng et al., 2006). Within the clusters of the same phase grains the grain growth occurs faster, which results in larger kinetic coefficients (Brodhag & Herwegh, 2010; Fan et al., 1997a,b).

Altogether, the matrix grain growth in the two-phase system depends on the grain boundary width that is pinned by the second-phase particles and the dispersoid volume fraction (Zener pinning effect) (El-Khozondar et al., 2006; Fan et al., 1997b; Solomatov et al., 2002). This applies if the second-phase particles are stable and non-coarsening. On the other hand, in some systems the second-phase particles can undergo Ostwald ripening by long-range diffusion, where the diffusion distance correlates to the distance between dispersed grains (El-Khozondar et al., 2006; Fan et al., 1997a,b & 1998; Solomatov et al., 2002).

Solid solution hardening

Solid solution hardening is the simplest alloy-hardening mechanism. Solid solution strengthening is accomplished by adding other elements to the base metal. A solid solution forms when the atoms of the additive elements enter into the crystal lattice of the metal, and thus cause widespread lattice distortions and strains. The additive

atoms inhibit the slip of dislocations thus resisting plastic deformation. Generally, the solutes are considered weak obstacles (Arzt, 1998), and strengthening depends on the extent that atoms are interfering dislocation motion in lattice. The most significantly influencing factors are the size and shear modulus differences, while, the amount (concentration) of solutes and the temperature have also affect (Caron, 2001a; Chandrasekaran, 2003; Zheng et al., 2006). The strengthening effect due to solutes at 0 K is expressed as in Eq. (1.4) (Chandrasekaran, 2003):

$$\sigma_s = \mu f^q c^m \quad (1.4)$$

where σ_s is the yield stress, μ is the shear modulus, f the obstacle strength, c the solute concentration, q varies depending on the nature of obstacles and m on the average spacing of obstacles. However, the expression ignores the temperature dependency of the yield stress. Overall, the drawback for solid solution strengthening is that these type of materials lose much of their strength at relatively low temperatures. Moreover, the additive elements alter the properties of the base metal. (Caron, 2001a; Chandrasekaran, 2003; Liang & Fan, 1999).

Age hardening / precipitation hardening

Age hardening/precipitation hardening involves three distinct steps: (i) solution treatment to minimize segregation in the alloy, (ii) quenching to create a supersaturated solid solution, and (iii) aging or precipitation heat treatment to facilitate the formation of hard second-phase particles in the base matrix. The method relies on changes in solid solubility with temperature to produce separate particulate phases. In practice, the aging reaction is induced by heat treatments between room temperature and the solvus with carefully chosen parameters. The final properties depend on the type and amount of alloying element, as well as the process conditions (Caron, 2001a; Chandrasekaran, 2003). As another phase with new interfaces is formed, the precipitates are incoherent ('strong' obstacles). The treatment can result also in coherent ('weak' obstacles) or semi-coherent fine precipitates, e.g., pre-precipitates with non-equilibrium composition and crystal structure that nearly fit the parent matrix. The precipitation kinetics initially follows the path of minimum activation energy, i.e., a homogeneous nucleation with a coherent interface, followed by the transformation to one or more intermediate semi-coherent phases before a final transformation to the equilibrium precipitate. The degree of strengthening is affected by the elastic strains between the matrix and precipitate phases. The strains, on the other hand, are influenced by the shape and size of precipitates, as well as by the anti-phase boundaries (sheared precipitates) and interfaces between the matrix and precipitate phases (Arzt, 1998; Chandrasekaran, 2003). When the size increases, precipitates are more likely to be present incoherently. Overall, a dislocation can bypass obstacles by several ways,

such as shearing through them, by bowing out between them (Orowan mechanism) or by cross-slip or climb at higher temperatures. The bypassing stress or ‘Orowan stress’ shear for ‘strong’, fine obstacles is given by (Arzt, 1998; Kocks, 1977):

$$\sigma_{OR} \approx 2T/b\lambda \approx Gb/R \quad (1.5)$$

where T is the line tension, b the Burgers vector of the dislocation, λ is the distance between obstacles, G is the shear modulus of the matrix material, and R the obstacle size. The equation describes the maximum increase in flow stress that an obstacle can impart in a dislocation-dominated material. This follows the $1/R$ dependence of the bypassing stress (Arzt, 1998). On the other hand, when the obstacles are not impenetrable to dislocation, (known as ‘weak’ obstacles e.g. coherent precipitates), they give a shear stress increment substantially below the Orowan stress (Arzt, 1998) resulting in \sqrt{R} dependence of the cutting stress. There is a transition between the cutting and bowing at a critical particle size R , see Fig. 1.1, where a maximum yield stress can be achieved (Arzt, 1998; Caron, 2001a; Chandrasekaran, 2003; Jacobs, 1999). To avoid the loss of strength, the precipitated metal should not be heated above the initial precipitation heat treatment temperature.

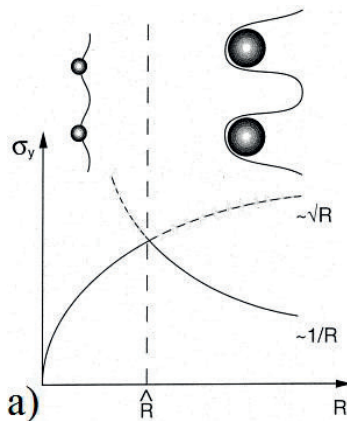


Fig. 1.1. Hardening in particle strengthened materials: illustration of a transition between the cutting and bowing at a critical particle size R (Arzt, 1998, with permission from Elsevier).

Dispersion strengthening

Dispersoids can strengthen metals by various ways. The stable particles dispersed throughout the matrix can limit the grain growth during processing and decrease dislocation mobility, thus inducing internal stresses which increases the hardness value (Caron, 2001a; Chen et al., 2006; Groza & Gibeling, 1993; Nadkarni &

Synk, 1984). The interface planes of the matrix and dispersoids have a very different atomic configuration from each other. Thus, even with a well-bonded interface, there is no possibility of a good match across the interface and the boundary becomes incoherent (Caron, 2001a; Groza & Gibeling, 1993).

Resistance to coarsening leads to a requirement for low diffusivity and solubility of the particle constituents into the matrix (Groza & Gibeling, 1993). In addition, the dispersed particles must retain their size and distribution without phase transformations or matrix recrystallization (Davis, 2001; Groza, 1992; Groza & Gibeling, 1993; Nadkarni & Synk, 1984). The effect of fine and evenly distributed particles to the yield strength increment can be predicted by the Orowan strengthening equation, as in Eq. (1.5). On the other hand, with the same content of clustered particles their influence on strengthening is less as compared to isolated particles, see Fig. 1.2.

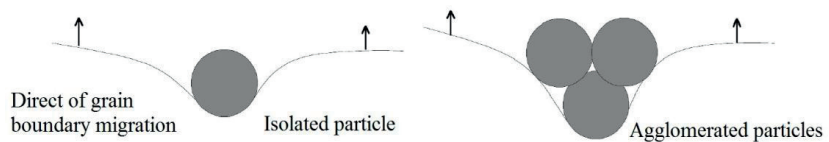


Fig. 1.2. A sketch of the effect of the particle clustering (or agglomeration) on the diminution of the pinning force due to a reduction on the available superficial area of the particle: fewer particles are now acting as obstacles to the grain boundary motion (Flores et al., 2004, reprinted with permission from Springer).

The dispersoids can be introduced into the metal matrix in several different ways (section 1.3). The choice of the technique depends upon the nature of the matrix metal and the kinetics of the critical reactions involved (e.g. in internal oxidation).

Strain/work hardening

In strain hardening, the metal is subjected to cold work or plastic deformation, e.g. rolling, drawing, swaging, forging, or compression below its recrystallization temperature (Caron, 2001a). The recrystallization temperature is between one-third and one-half of the melting points of pure metals. In general, as a metal is cold worked during processing, ductility decreases as strength increases, requiring annealing of the worked alloy before further cold work (Caron, 2001a,c). The annealing provides the thermal energy required to allow the dislocation defects to rearrange themselves by diffusion. However, if the metal is heated to the recrystallization temperature, the effect of strengthening will be lost.

The crucial point in deformation/work hardening is the evolution of dislocation density with strain (Chandrasekaran, 2003; Kim et al., 2000). The obstacles are described as forest dislocations, and their spacing or density correlates to the hardening behaviour (Arzt, 1998). Taylor first explained the work hardening behaviour and it can be expressed as in Eq. (1.6) (Chandrasekaran, 2003).

$$\sigma_f = \sigma_0 + M\beta\mu b\rho^{1/2} \quad (1.6)$$

where σ_f is the flow stress, σ_0 is the friction stress (presenting other strengthening contributions), M is the average Taylor factor, μ is the shear modulus, b is the Burgers vector, β the proportionality constant, and ρ the dislocation density. A number of theories have been introduced to describe deformation hardening since then (Meyers et al., 2006). For example, ultrafine-grained (UFG) materials cannot sustain uniform tensile elongation as well as materials with coarser structures (Diouf, 2013; Meyers et al., 2006; Nachum et al., 2010). The lower strain hardening rate is suggested to relate to the annihilation of dislocations into the grain boundaries, thus resulting in early localized deformation (Meyers et al., 2006).

1.1.2 Thermal properties of MMCs

When the dispersed particles are stable, resistant to coarsening and have sufficient size and spacing, even prolonged heating does not lead to matrix recrystallization. This phenomenon is associated with softening and coarsening resistance (section 1.1.1), or in other words, thermal stability (Davis, 2001; Groza & Gibeling, 1993). However, the differences in the properties of constituents may lead to several types of changes when exposed to high temperatures. The influencing factors consist of, for example, the matrix properties (elastic, elastic-plastic or elastic-viscoplastic), second-phase particles (their properties and volume fraction), thermal history of the composite, and the cooling rate from the fabrication temperature (Choo et al., 2001).

The coefficient of thermal expansion (CTE) is one of the most important properties of composites when operating at elevated temperatures (Choo et al., 2001; Weiss, 2000). It is generally stated that CTE values reflect the level of misfit strains introduced in the matrix from the reinforcement, impurities, defects, or microstructural changes (Qian et al., 2002; Weiss, 2000). The CTE can be calculated from the expansion data with the following equation:

$$CTE = \frac{\Delta L}{L_0} \frac{1}{\Delta T} \quad (1.7)$$

where $\Delta L/L_0$ is the relative linear expansion and ΔT is the temperature change (Fathy & El-Kady, 2013; Shao et al., 2009). Theoretically, the CTEs can be

predicted by the simplest model of rule of mixture (Shao et al., 2009). However, the more precise models take into account the Young's modulus, the bulk modulus, or the shear modulus of the constituents (Kerner, 1956; Shao et al., 2009; Turner, 1946). In theoretical relations derived by Turner Eq. (1.8) (Turner, 1946) and by Kerner Eq. (1.9) (Kerner, 1956), the CTEs of composites are expressed as follows:

$$CTE = \frac{\alpha_1 K_1 \frac{F_{w1}}{\rho_1} + \alpha_2 K_2 \frac{F_{w2}}{\rho_2}}{K_1 \frac{F_{w1}}{\rho_1} + K_2 \frac{F_{w2}}{\rho_2}} \quad (1.8)$$

$$CTE = \alpha_1 + f_{v2}(\alpha_2 - \alpha_1) \times \frac{K_1(3K_2 + 4G_1)^2 + (K_2 - K_1)(16G_1^2 + 12G_1K_2)}{(4G_1 + 3K_2)[4G_1f_{v2}(K_2 - K_1) + 3K_1K_2 + 4G_1K_1]} \quad (1.9)$$

where α_1 and α_2 are CTEs for constituents of the composite, K is the bulk modulus, G is the shear modulus, F_w is the weight fraction, f_v is the volume fraction, and ρ is the density of the constituent. One inherent issue in most composites is the presence of thermal residual stress due to CTE differences between the matrix metal and the reinforcement. On cooling from the fabrication temperature, the thermal mismatch between the reinforcement and the matrix can lead to residual stresses, i.e., stress and strain distributions within the phases (Choo et al., 2001). The residual stresses are often caused by the differences in the elastic moduli of the constituents (Addleman & Webster, 1973). The material constituents may undergo stages of compression and tensile stresses during the fabrication or thermal cycling, with some stresses remaining in the elements (Addleman & Webster, 1973; Choo et al., 2001; Weiss, 2000).

Consideration of creep is necessary if the composite is exposed to elevated temperatures under stress. Generally, the creep of materials is associated with time-dependent plasticity under a fixed stress at an elevated temperature, often above $0.5 T_m$ (Kassner & Hayes, 2003). The temperature increment can result in inelastic stress relaxation by creep plasticity, diffusional flow deformation, or decohesion (Choo et al., 2001; Kassner & Hayes, 2003). The stress is highest at the interfaces and the cavities and voids frequently nucleate on grain and phase boundaries or against hard particles due to strain concentrations and dislocations interactions (Addleman & Webster, 1973; Choo et al., 2001; Kassner & Hayes, 2003; Weiss, 2000). At high temperatures, the lattice dislocations can circumvent obstacles by climb or cross-slip, and the associated strain field can be partially relaxed by diffusion in the interface (Arzt, 1998).

In practice, the type of defect (point defects such as vacancies, line defects i.e. dislocations, and planar defects i.e. grain boundaries) plays a role in determining the creep behaviour (Langdon, 2006). Among the established diffusional creep mechanisms in materials are the Nabarro-Herring creep, which involves vacancy flow through the lattice and Coble creep, which involves vacancy flow along the

grain boundaries (Cai et al., 1999; Coble, 1963; Herring, 1950; Kim et al., 2000; Meyers et al., 2006). In these, the creep mechanisms do not require a lattice dislocation movement. On the other hand, creep with a lattice dislocation processes is often referred to as Harper-Dorn creep (Harper & Dorn, 1957). Two separate types of grain boundary sliding (GBS) mechanisms can also participate in creep deformation, i.e., Rachinger GBS in conventional creep and Lifshitz in diffusion creep (Langdon, 2006). In GBS there exists a displacement, which occurs when, in response to an external stress, two grains slide in relation to each other at their mutual interface. In Rachinger GBS the displacement results from the movement of intergranular dislocations, where the grains retain their shape but show visible displacement with respect to each other. The Lifshitz-sliding GBS occurs in Nabarro-Herring creep and Coble diffusion creep and refers to boundary offset as a consequence of stress-directed diffusion of vacancies. For nanocrystalline materials, the volume fraction of grain boundaries is high. It is considered that creep is dominantly controlled by grain boundary sliding/shear (Arzt, 1998; Chokshi et al., 1989; Conrad, 2003) or grain/phase boundary diffusion, i.e. 'interface controlled diffusional creep', consisting of the diffusion, emission, and absorption of atoms/vacancies at the grain boundary (Cai et al., 1999; Conrad & Jung, 2005). The avoidance of internal stresses is critical, especially in devices exposed to cyclic temperature variations. Things to consider are material combinations (constituents with CTEs close to each other), process parameters (proper cooling and heating rates) and post-annealing at low-temperature (Choo et al., 2001).

1.1.3 Influence of dispersed particles on tribological properties

Any wear characteristics must be related to the complete system, i.e. the material components, the counter material as well as their relevant properties and interactions. Additionally, the operating variables and environment are highly influential. This declares that the wear characteristics of materials should not be treated in analogy to the classical strength characteristics of materials, but a different approach is needed (Peterson & Winer, 1980).

One of the main functions of a lubricant is to reduce wear. Any material that reduces friction or wear, for instance, by preventing or reducing adhesive junctions/asperities or damage on opposing surfaces, can by definition be regarded as a lubricant (Peterson & Winer, 1980). Certain additives reduce wear by forming a surface film which prevents metal-metal contact or can induce a self-lubricative film (MoS₂, Teflon, graphite, CNT, h-BN etc.) (Chen et al., 2008; Guiderdoni et al., 2011; Hashimoto et al., 2008; Rajkumar & Aravindan, 2013). E.g., the CoF for MoS₂ is about 0.04 and for h-BN it is 0.06 against Cr-steel (Hashimoto et al., 2008). For CNT the calculated CoF is 0.15 (Trinh et al., 2010), and for fine

graphite powder composites against steel it is 0.15 - 0.16 (Kováčik et al., 2008). On the contrary, some additives (e.g. carbides, borides, nitrides) have much higher hardness and wear resistance than the base metal, thus decreasing the damage in a matrix metal by acting as a load-bearing element (Dhokey & Paretkar, 2008; Tjong & Lau, 2000). Some lubricants work by oxidation or decomposition during operation. Powder metallurgy (PM) technologies enable also porous metals where the pores can be impregnated with liquid lubricants and work as lubricant reservoirs (Davis, 2001; Peterson & Winer, 1980).

The friction coefficient for a composite material can be estimated with a rule of mixture. Based on this approach, Trinh et al. (2010) developed a new equation for CoF of composites. In the calculations, the strain of additives is assumed equal to that of the matrix, ending up with the expression:

$$CoF = \frac{CoF_1(A-A_2)E_1 + CoF_2A_2E_2}{A_2E_2 + (A-A_2)E_1} \quad (1.10)$$

where CoF is the coefficient of friction of the composite, CoF_1 and CoF_2 are the coefficient of friction of the matrix and additive respectively, A the total volume of the composite, A_2 the volume covered by the additive, and E_1 and E_2 are the respective modulus of the matrix and additives. Trinh et al. (2010) found the expression appropriate for the prediction of the CoF for Cu/CNT composites. However, the environmental constraints of physical (temperature, moisture), chemical (atmosphere, lubricant composition, bonding etc.), and mechanical (load, stress, counter material) nature are issues to be dealt with as well (Peterson & Winer, 1980).

1.2 Copper: properties and applications

With atomic number 29, copper is a member of subgroup IB in the periodic table of elements. The other elements in the same group, silver (Ag) and gold (Au), share the properties of chemical stability and high ductility. The known characteristics of high electrical and thermal conductivity along with its red colour are a result of copper's atomic structure ($1s^2 2s^2 p^6 3s^2 p^6 d^{10} 4s^1$); its filled 3d state, loosely bound 4s electrons and the optical transitions between them (Kundig & Cowie, 2006).

Copper is produced from three major raw materials; sulphide copper minerals, oxidized copper minerals and scrap. Nowadays copper is the most commonly used non-ferrous metal in metallurgy after aluminium. In powder metallurgy (PM) parts fabrication, the use of copper and Cu-based powders are next to iron and steel in volume (Davis, 2001). Currently, almost two-thirds of pure copper PM parts produced are used for electrical and electronic applications, although a wide list of

optional functions exists. The final products can be in the form of wires, cables, tubes, rods, bars, strips, sheets, plates, castings, and powder (Caron, 2001a; Kundig & Cowie, 2006).

1.2.1 Properties of copper

The important properties of copper, which make it desirable in a variety of applications are high electrical and thermal conductivities, favorable combinations of strength and ductility, ease of machinability and joining properties, as well as resistance to corrosion, and aesthetic appeal (Caron, 2001a; Kundig & Cowie, 2006; Nadkarni & Synk, 1984; Suryanarayana & Al-Aqeeli, 2013). However, copper has quite low tensile and yield strength. Low thermal stability and considerably a high CTE also limits the use of Cu at higher temperatures. To circumvent these disadvantages the characteristics of Cu can be enhanced to meet various requirements by combining it with suitable additives or by heat treating (Caron, 2001a; Groza, 1992; Kundig & Cowie, 2006; Nadkarni & Synk, 1984; Tian et al., 2006). Generally, the major reason for alloying Cu is to increase strength and softening resistance without losing too much of inherent properties (Caron, 2001a,b).

1.2.2 Dispersion strengthened copper

By introducing stable and insoluble particles into the Cu matrix it is possible to produce metal matrix composites (MMCs) with improved properties. Depending on the application the dispersoids can be oxides (e.g. Al_2O_3 , ZrO_2 , SiO_2 , ThO_2), borides (e.g. TiB_2 , ZrB_2), nitrides (e.g. TiN , ZrN , h-BN), carbides (e.g. SiC , ZrC , VC , WC , B_4C , NbC , TaC , TiC), or other elements (e.g., graphite, CNT, diamond) (Chen et al., 2008; Davis, 2001; Groza, 1992; Groza & Gibeling, 1993; Hanada et al., 2004 & 2007; Ichikawa & Achikita, 1991; Kaczmar et al., 2000; Rajkumar & Aravindan, 2013; Trinh et al., 2010; Upadhyaya, 2000). In most cases, oxides make the best dispersoids due to their hardness, stability, and insolubility in the matrix metals (Nadkarni & Synk, 1984). Some metal oxides such as copper oxide or nickel oxides are not as stable at higher temperatures, and thus are not as potential. Overall, dispersion strengthened (DS) copper materials are significant from the point of view of their strength and creep resistance at elevated temperatures (Upadhyaya, 2000). They also retain many of the inherent properties of copper (Nadkarni & Synk, 1984).

Conventional melting and casting techniques are not useful routes to produce DS metals due to the high interfacial energy between molten metal and additives and/or density disparities between them. These would lead to flocculation or segregation in the melt. Generally the manufacturing methods involve PM techniques for the preliminary preparations (Davis, 2001; Upadhyaya, 2000).

While dense PM Cu-based parts can be produced for electrical components, the low-density parts are typically used as self-lubricating bearings or filters where the pores act as oil reservoirs (Davis, 2001). Both the physical and mechanical properties of Cu-based materials depend greatly both on the density and the amount/type of additive elements.

1.2.3 Applications of Cu-based materials

The main consumption areas for Cu and Cu-based materials are electrical and electronic applications, heat transfer, and structural and frictional applications (Caron, 2001a; Davis, 2001; Kundig & Cowie, 2006; © Copper Development Association, 2013). Cu-based materials have also been used in manufacturing processes and applications relying on good corrosion resistance or its fine appearance, e.g., automotive, marine, aircraft, and building industries as well as coinage, medallion, and jewellery applications (Brock, 2001; Caron, 2001a,b, Kaczmar et al., 2000; Suryanarayana & Al-Aqeeli, 2013, © Copper Development Association, 2013).

Cu-composites for electrical applications

Electrical contacts/connectors are metal devices that make and break electrical circuits and are designed for occasional or frequent insertions and removals (Davis, 2001; Murty, 2001). These consist of contact points for resistance welding electrodes, electrodes generally, electrical switches, and wires for electrical motors (Davis, 2001; Kaczmar et al., 2000; Nadkarni & Klar, 1973). Electrical connectors can also be used in permanent applications in fixed wire terminations, e.g., solder joints (Murty, 2001). In majority of applications (computer, telecommunication, aerospace, or automotive industry), a stable performance with a good contact interface is required (Murty, 2001).

Several Cu-composites containing carbides or borides have the potential to operate in electric devices and applications. The need has always existed for high electrical conductivity (> 80%IACS) Cu-based conductors with a good creep resistance and tensile strength at temperatures above 773 K (500 °C). The good creep and rupture resistance, as well as thermal stability, of DS Cu-Al₂O₃ composites prevent the electrode tip from deforming and sticking against galvanized steel (Nadkarni & Synk, 1984). For resistance welding electrodes, electrical contact materials, and electrodes for automatic welding, Cu-W and Cu-TiC have been applied (Kaczmar et al., 2000) while, Cu-Co has been used in components of electronic systems (Kaczmar et al., 2000). Due to the electrical conductivity and electric erosion resistance of TiB₂, it has been introduced into Cu for electrical use (Jin et al., 2005; Korchagin & Dudina, 2007; López et al., 2005). Similarly, Cu-Cu₂O (Martínez-Ruiz et al., 2003; Saito et al., 2001; Wu et al., 2010), Cu-diamond (Weber &

Tavangar, 2007; Weidenmann et al., 2009; Yoshida & Morigami, 2004), and Cu-CNF^(Ti,Zr) (carbon nano-fiber) (Lee et al., 2007) have also attracted interest in electronics production.

Electrical properties are extremely sensitive to the amount and type of impurity elements (Caron, 2001a). The impurities present in a solid solution may precipitate during the heat treatment thus decreasing the electrical conductivity as compared to pure copper. A rough estimation of decrement in electrical conductivity with an alloying addition is about 0.1 wt.% for most elements (Caron, 2001a). Still, the addition of as little as 0.023% Fe in a solid solution of copper lowers its conductivity to 86%IACS, an amount of 0.3% Zn lowers the conductivity to 85%IACS, 1.25% Al to 70%IACS and 0.1% P to 50%IACS (Davis, 2001; Kaczmar et al., 2000). Fig. 1.3 summarizes the effect of impurity elements on the electrical conductivity of Cu. Likewise, the greater the void content (porosity) the lower the electrical conductivity.

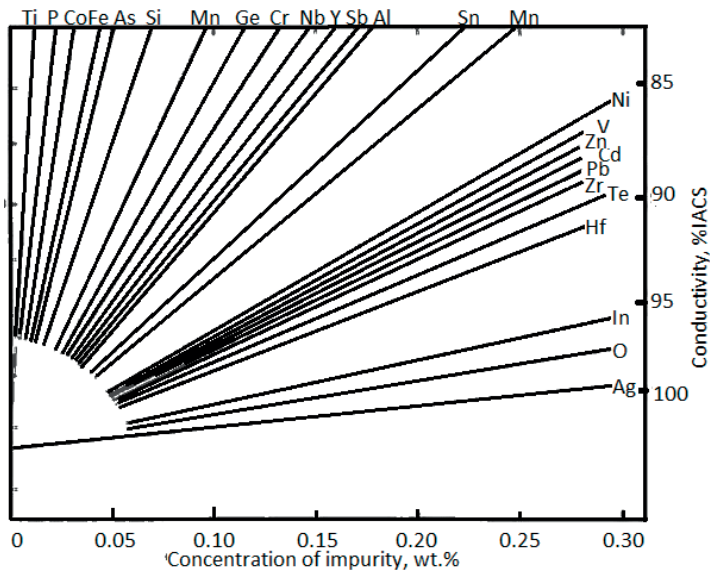


Fig. 1.3. Approximate effect of impurity elements on the electrical conductivity of copper (© Copper Development Association, 2013).

Cu-composites for heat transfer

Nowadays, the increased performance and packing density of electronic devices generates more heat than before. As a consequence, thermal management has become a significant issue in preventing a premature performance failure. The most common electronics cooling system is a heat sink with the aid of free convection or accompanied by a fan to improve heat transfer. A heat sink is a heat reservoir that can absorb a notable amount of heat without significantly changing

temperature. The sinks can also transport elevated heat fluxes to cooling medium such as water. In heat sink applications, Cu and Cu-composite materials are favorable due to their good thermal conductivity and low electrical resistance. Recently suggested heat sink materials for cooling within electronic packaging, operated at moderate temperatures, cover Cu-SiC^{Mo} (Schubert et al., 2007), Cu-diamond^(Cr,Si,W) (Abyzov et al., 2012; Nunes et al., 2011; Rosinski et al., 2012; Schubert et al., 2008a,b; Shen et al., 2010; Xia et al., 2009; Yoshida & Morigami, 2004), Cu-MWCNT (multi-walled carbon nanotubes) (Chu et al., 2010b) and Cu-TiB₂ (Chen et al., 2009). More traditional alternatives include Cu-Mo, Cu-Invar or Cu-W (Zweben, 1998 & 2005).

Active cooling parts made of heat resistant materials with good thermal conductivity are necessary for certain high temperature (700-1100 K) applications (Groza, 1992; Groza & Gibeling, 1993). Such applications include a variety of advanced power generation and aerospace devices, such as, rotating-source neutron targets, rocket nozzles, combustor walls and chamber liners, leading edges in advanced aircraft and rocket propulsion systems (Groza, 1992; Groza & Gibeling, 1993). A Cu matrix with low impurity content and low elastic modulus is advantageous to assure good thermal conductivity with minimized thermal stresses in actively cooled structures. However, in Cu-composites the thermal mismatch strain caused by the difference between the thermal expansion of the Cu matrix and dispersed particles can lead to a debonding if subjected to thermal cycling (Schubert et al., 2008a,b). Moreover, materials that are used in high heat flux structures are subjected to creep deformation as well as failures by thermo-mechanical fatigue (Groza & Gibeling, 1993). Considering these demands, a Cu matrix together with MgO, CeO₂, CaO or Y₂O₃ is potential candidate for active cooling material in high-temperature applications (Groza & Gibeling, 1993). Other options suggested are Cu with TiB₂ or Al₂O₃ or alloys of CuNiBe and CuCrZr (Kalinin & Matera, 1998; Korchagin & Dudina, 2007; Leedy et al., 1996). Cu-based materials are also exploited in continuous casting molds (Nadkarni & Synk, 1984), heater elements, and heat exchanger tubes, etc.

Cu-composites for friction materials

Majority of metal-base friction materials are produced by PM due to immiscibility of constituents with each other (Davis, 2001). The subsequently sintered PM parts have their applications in the transmission of motion through friction release and for deceleration and stopping through brakes. In these, the mechanical energy, i.e. metal-to-metal friction, is converted to frictional heat, which is absorbed and dissipated by the friction material (Davis, 2001). Because of high thermal conductivity, the Cu-base materials are preferred.

Most of these friction materials contain Cu together with other metal powders, solid lubricants, oxides, and other compounds. E.g., the use of TiB₂, TiC, SiC, MoS₂, carbon, graphite/nano-graphite, h-BN or CNTs (carbon nanotube) imbedded into the copper matrix has been successfully studied (Akhtar et al., 2009; Chen et al., 2008; Dhokey & Paretkar, 2008; Fathy et al., 2012; Hashimoto et al., 2008; Kováčik et al., 2008; Moustafa et al., 2002; Rajkumar & Aravindan, 2013; Trinh et al., 2010; Tjong & Lau, 2000; Tu et al., 2003; Zhan et al., 2004). Depending on the additive element, either the self-lubricating properties or the wear resistance is enhanced. Ceramic reinforcing particles are good candidates for increasing wear resistance (Akhtar et al., 2009). Overall, Cu-based frictional materials are used as frictional brake parts such as in liners, drums, brushes for motors and generators, moving parts for switches and electrical sliding applications, current-carrying washers and other parts requiring low contact resistance (Davis, 2001; Kaczmar et al., 2000; Nadkarni & Klar, 1973; Rajkumar & Aravindan, 2013).

1.3 Preparation of Cu-composite powders

There exist several possible routes to prepare Cu-composite powders with solid phase methods. For the conventional MMCs, the reinforcing phases are prepared separately prior to composite fabrication (*ex-situ*) (Tjong & Ma, 2000). In these powders, the reinforcing phase is limited by the size of the starting powder, which might be of the order of microns to even tens of microns. Moreover, there exists a risk of contamination of reinforcements, which might lead to poor wettability (Nadkarni & Klar, 1973). The more novel methods for preparing the powders are based on *in-situ* methods, in which the reinforcements are formed within the metallic matrix during the composite fabrication. The main benefits are clean interfaces between particle and matrix, finer and more even distribution of reinforcements and thermodynamically more stable reinforcements within the matrix (Tjong & Ma, 2000).

The simplest way to prepare Cu-composite powders is through the mechanical mixing of Cu powder together with second-phase particles. The other widely used methods are mechanical alloying (MA) and selective or internal oxidation (IO) (Groza, 1992; Nadkarni & Synk, 1984). If the reinforcing phase is formed with significant heat release, it is possible to obtain a composite material by self-propagating high-temperature synthesis (SHS). The dispersion quality and costs vary substantially among these methods (Davis, 2001).

1.3.1 Mixing

The easiest method to obtain composite powders is mechanical mixing (Korchagin & Dudina, 2007). In this, the matrix powder particles should be of the order of microns or finer in size to achieve the optimum properties of the final material

(Upadhyaya, 2000). However, powders having a size of tens of microns are also employed. In order to provide a desired distribution of the dispersoids, their size should be between 1/30 and 1/250 of the diameter of the metal powder size of metal (Upadhyaya, 2000). The main problem arising, when previously synthesized particles are mixed together with a metallic matrix powder, is the difficulty in providing a uniform distribution. More challenges are encountered with surface contamination and segregation of starting powders with different sizes or densities (Kaczmar et al., 2000; Tjong & Ma, 2000).

Overall, mixing is a widely employed method to produce several types of composite powders. Commonly, Cu powder has been blended together with, e.g. alumina (Dash et al., 2012; Upadhyaya & Upadhyaya, 1995). Part of the most recent studies producing high quality advanced materials also rely on this method for powder production. For instance, Cu-diamond^(Cr) (Rosinski et al., 2012; Yoshida & Morigami, 2004), Cu-CNT^(Ni) (Kim et al., 2009), Cu-graphite^(Cu) (Chen et al., 2008; Moustafa et al., 2002; Samal et al., 2013), Cu-h-BN (Chen et al., 2008) and Cu-SiC^(Cu) (Dhokey & Paretkar, 2008; Zhan et al., 2004) composite powders have been prepared by mixing. However, quite often, the additive particles need to be pre-coated to facilitate the bonding (Kim et al., 2009; Moustafa et al., 2002). In other cases, pre-coating is carried out to avoid segregation and to guarantee a more uniform mixture of constituents when there are notable differences in their densities. For example, Ni-coated (200 - 300 nm) CNT's and Cu with similar densities allow mixing to be a suitable method (Kim et al., 2009). On the contrary, the density difference (1.8 g/cm³ for CNT vs. 8.96 g/cm³ for Cu) and the lack of an interfacial bonding between C and Cu would, without a coating, lead to difficulties in mixing, resulting in poor mechanical properties (Kim et al., 2009).

1.3.2 Mechanical alloying

Mechanical alloying (MA) is one of the most widely applied methods in producing DS materials (Kaczmar et al., 2000). MA is a solid-state high-energy ball milling process that consists of repeated deformation, welding and fracturing of the original components (Groza, 1992; Meyers et al., 2006; Suryanarayana & Al-Aqeeli, 2013; Tjong & Ma, 2000). Typically, hard ceramic or metal balls are used as grinding media, hence the term ball milling. The process can be conducted at near room temperature, with or without a protecting atmosphere (argon, nitrogen or liquid nitrogen). The milling speed is usually between 100 - 1000 rpm and time can vary from one hour up to tens of hours (Suryanarayana & Al-Aqeeli, 2013). As a result, a uniform and controlled particle distribution along with a fine mixture is obtained (Groza, 1992; Suryanarayana & Al-Aqeeli, 2013; Upadhyaya, 2000). The another advantage is the option for particle selection without regard to liquid or solid solubility limits (Groza, 1992; Suryanarayana & Al-Aqeeli, 2013). The other

benefits include such as the refinement of powder particles (Groza, 1992; Suryanarayana & Al-Aqeeli, 2013; Upadhyaya & Upadhyaya, 1995).

By using this in-situ method, e.g., diboride particles (CrB_2 , ZrB_2 and TiB_2), oxides (Al_2O_3 , MnO , SiO_2 and ZrO_2), carbides (ZrC , NbC , TiC , TaC and Fe_3C), refractory particles (Ta , Nb , Mo , V , W and Cr), graphite, nanodiamonds, and CNT's have been successfully introduced into the Cu matrix (Akbarpour et al., 2013; Dong et al., 2002; Groza, 1992; Hanada et al., 2004 & 2007; Jin et al., 2005; López et al., 2005; Morris & Morris, 1989; Trinh et al., 2010; Suryanarayana & Al-Aqeeli, 2013; Upadhyaya & Upadhyaya, 1995; Vencel et al., 2013).

1.3.3 Internal oxidation

The internal oxidation (IO) process is an in-situ method that usually results in the finest and most uniform distribution of dispersoids (Davis, 2001; Nadkarni & Klar, 1973; Nadkarni & Synk, 1984; Upadhyaya, 2000). To keep the reaction times reasonable, the diffusion distances should be small; thus PM offers a unique solution because powder particles can be internally rapidly oxidized (Nadkarni & Synk, 1984). In practice, the only commercial, internally oxidized composite is Cu- Al_2O_3 . The process involves melting a dilute solid solution alloy of copper and aluminium, and atomizing the melt by the use of a high-pressure gas such as nitrogen. The resulting powder is blended with an oxidant consisting primarily of fine copper oxide powder. The blend is then heated to dissociate copper oxide and the released oxygen diffuses, while the aluminium in the alloy preferentially oxidizes to aluminium oxide. Excess oxygen is reduced by heating the powder in hydrogen. (Groza, 1992; Nadkarni & Klar, 1973; Nadkarni & Synk, 1984)

1.3.4 Self-propagating high-temperature synthesis

Self-propagating high-temperature synthesis (SHS) also known as combustion synthesis can be utilized in preparation of composite powder (Patil et al., 1997; Merzhanov, 2004). A typical SHS process consists of pre-flame, main heat release, afterburning, structure formation and cooling down subzones (Merzhanov, 2004). This process is ideal for producing high-melting-point ceramics, such as borides, carbides, nitrides, or silicides from elementary powders. A highly exothermic reaction is the main demand for the method. The self-sustaining reaction and in-situ method provides a high degree of conversion, and partial self-purification from impurities resulting in clean surfaces and good bonding (Merzhanov, 2004; Tjong & Ma, 2000). SHS is also simple and an energetically economic method to prepare thermodynamically stable phases (Kashinath et al., 1997). By conventional SHS it is difficult to obtain ceramic phase particles less than 1 micron of size. However, by mechanical activation (ball-milling) beforehand a reduced particle size is produced so that lower ignition/combustion temperatures can be achieved (Patil et

al., 1997; Korchagin & Dudina, 2007; Kwon et al., 2006). The mechanical treatment of diluting is also suitable in preparing materials with a higher content of metallic constituents (Kwon et al., 2006).

1.4 Preparation of bulk UFG and nanosized Cu-composites

Sintering is a thermal treatment for bonding particles into a predominantly solid structure via mass transport. The driving force of sintering is the excess surface free energy available in the materials. Both densification and grain coarsening reduces the total interfacial energy of the system. There are several ways to enhance sintering either by altering the kinetics or the driving force. The aim nevertheless, is to reduce the sintering time or temperature without compromising the degree of densification (German, 1996). Typically, the powder constituents exhibit sintering at temperatures above one half of their melting point (German, 1996). Most of the conventional methods of consolidation result in a significant growth of the grain structure, and so, the desired benefits of a fine-grained structure on material properties are not obtained (Srivatsan et al., 2002). To circumvent this, the non-conventional consolidation methods adopt high heating rates, a short sintering time, and a low sintering temperature resulting in improvements in the mechanical properties of the products due to limited grain growth during processing (Groza, 1992; Groza & Gibeling, 1993; Orrù et al., 2009; Srivatsan et al., 2002; Zhang et al., 2008 & 2009). In this work, the non-conventional method of PECS/SPS (pulsed electric current sintering/spark plasma sintering) was employed. The widely known pressure-assisted method of hot isostatic pressing (HIPing) was applied for comparison. These two methods are described in next sections.

1.4.1 Hot isostatic pressing

The conventional hot isostatic pressing (HIP) is a highly developed PM method, in which the main idea is to apply isostatic pressure to a heated component to induce plastic deformation and creep at particle-particle contacts (Meyer & Wadley, 1992; Newman, 1992). The powder container is typically heated by radiation from the enclosing furnace through an external heating element and a convection of inert gases if possible. Therefore, the sample is heated as a consequence of the conduction from the external surface of the container, thus leading to a slow heating rate (Orrù et al., 2009). Moreover, the compact is usually held for a considerably long time at a high temperature ($0.5 - 0.7 T_m$).

Helle et al. (1985) have constructed HIP diagrams for pure Cu presenting the relative density and, the densification mechanisms involved, as a function of temperature and pressure. Generally, material can transfer with different mechanisms, e.g., surface diffusion, volume diffusion, grain boundary diffusion,

Introduction

viscous flow, plastic flow, and vapour transport from neighbouring particle surfaces (Fig. 1.4). The main densification mechanisms in HIPing involve plastic yielding, power-law creep, and diffusional densification (Helle et al., 1985; Newman, 1992). Power-law creep is the dominant mechanism following an initial region of plastic yielding, the latter resulting in a considerable densification due to the low yield strength of Cu at elevated temperatures.

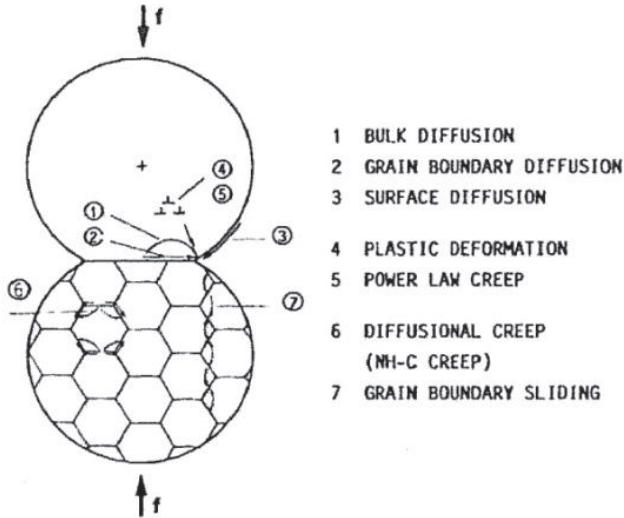


Fig. 1.4. Transport mechanisms occurring during sintering of powders (Kaysser et al., 1988, with permission from Maney Publishing).

It is proposed that the particle size has almost no effect on the densification rate (Helle et al., 1985). Densification of 15 μm -sized Cu powder was studied by Song et al. (1996). As a result, they yielded a slightly better hardness than 0.78 GPa (80 HV) and densities of 99% and 98% of T.D. with process parameters of 873 K - 50 MPa - 20 min and 773 K - 50 MPa - 60 min, correspondingly. Pavlov et al. (1983) confirmed that a full density of electrolytic Cu was attained at 1123 K under 100 MPa within a 30 min hold time by HIPing. Additionally, the simulations on the HIPing of Cu powder (10 μm) revealed that the expected grain size would be around 130 - 250 μm (Meyer & Wadley, 1992; Newman, 1992). Even though several authors have studied suitable HIPing parameters for the proper densification of Cu (Helle et al., 1985; Meyer & Wadley, 1992; Newman, 1992; Olevsky et al., 1998; Pavlov et al., 1983; Song et al., 1996), only a few have focused on grain growth during processing (Meyer & Wadley, 1992; Newman, 1992).

HIPing has been applied in order to prepare Cu-composites, such as Cu-Cu₂O, Cu-Al₂O₃, Cu-SiC and Cu-graphite. The US Patent 6,909,185 (Kondo et al., 2005) introduces a composite and its applications for a material consisting of Cu and

cuprous oxide (Cu_2O). HIP was one of the mentioned processing methods and it was applied at 1073 - 1323 K (800 - 1050° C) for about 3 hours. HIPing of Cu- Al_2O_3 composites has been carried out by Nachum et al. (2010) at 873 K (600 °C) with 100 MPa for 30 min. The strengthening was mainly attributed to the grain boundary and dispersion strengthening. For coated Cu and uncoated Cu - (0 - 50 vol.%) graphite composites HIPing at 1223 K (950 °C) for 1.5 hours with a pressure of 150 MPa was applied by Kováčik et al. (2008). Moreover, Cu - (0 - 20 vol.%) SiC composites have been prepared by HIPing at 1153 K (880 °C) with 100 MPa for 1.5 hours (Tjong & Lau, 2000). The previous studies point out that HIPing is time-consuming, and the process times required for full density Cu or Cu-based materials are in the order of hours (Kondo et al., 2005; Meyer & Wadley, 1992; Newman, 1992; Olevsky et al., 1998). An obvious consequence is that there exists a challenge to preserve the fine structure of the powder during HIPing.

1.4.2 Pulsed electric current sintering

Pulsed electric current sintering (PECS) also known as spark plasma sintering (SPS) or field assisted sintering (FAST) is a relatively new innovative technique for the consolidation of fine or nanocrystalline powders. According to Tokita (1999 & 2013), the history of the technology, related to the process in question, started in the 1930s in the USA where the first resistance heating method was patented. On the other hand, SPS was originally invented in Japan in 1962 as ‘spark sintering’ according to Inoue (1966a,b). However, only a few machines were sold at that time. The technology was commercialized in the late 1980s, and various companies started to manufacture SPS equipment based on the original technique (Omori, 2000; Orrù et al., 2009; Tokita, 1999 & 2013).

The PECS method is regarded as a solid state sintering (Ragulya, 2010; Song et al., 2006), however, in some cases it contains features of transient and/or liquid phase sintering. The technique offers significant advantages with new materials and consistently produces a highly dense compact in a shorter sintering time (order of minutes) and with finer grains than with conventional methods. Moreover, the benefits include, e.g., ease of operation and accurate control of sintering energy as well as high sintering speed, high reproducibility, safety, and reliability (Munir et al., 2011; Orrù et al., 2009; Song et al., 2006; Tokita, 1999 & 2013; Zhang et al., 2008 & 2009). As for mass transport, the mechanisms mainly involved are volume and grain boundary diffusion, viscous and plastic flow, contact melting, thermal diffusion and diffusional creep, dislocations, electromigration (in electron connectors), point defect generation, enhanced defect mobility, and dielectric breakdown (Munir et al., 2011; Ragulya, 2010; Tokita, 2013).

Several different materials and material combinations are suitable for PECS, e.g. metals, metal composites, oxides, nitrates, carbides, and polymers are widely produced. The method is getting more publicity when producing functionally graded materials (FGM), intermetallic compounds, semiconductors, ferroelectric materials, electroceramics, fiber reinforced materials, laminates as well as nanocrystalline materials and -composites. Also produced by PECS, to some extent, are transparent materials, porous materials, amorphous alloys, shape memory alloys and superconductors. This method has also been shown to be suitable for other materials, which are difficult to prepare conventionally (Eriksson, 2010; Munir et al., 2011; Omori, 2000; Orrù et al., 2009; Ragulya, 2010; Tokita, 1999 & 2013).

PECS system and compacting method

A PECS consists mainly of a hydraulic press system, specially designed upper and lower punch electrodes and punches, a sintering die/mold, a water-cooled vacuum chamber that can be evacuated or filled with shielded gas and a DC pulse generator. The computer-based process control system manages many aspects, including positioning, operating environment and water-cooling. During operation, the control system records, for example, the longitudinal displacement of punches, the temperature of the die, the pressure, the voltage between the upper and lower punches, and the current are recorded (Orrù et al., 2009; Song et al., 2006; Tokita, 1999 & 2013). The operating system also includes various interlocking safety units. A schematic picture of a PECS unit is presented in Fig. 1.5.

For consolidation, the method exploits high pulsed direct current (DC) and uniaxial pressure for converting powders to bulk form (Munir et al., 2011; Orrù et al., 2009; Tokita, 1999 & 2013). The pulsed current generates Joule heat in the die and powder, allowing use of high heating rates (Orrù et al., 2009; Tokita, 1999 & 2013), thus avoiding the grain coarsening by low temperature mechanisms (e.g. surface diffusion) (German, 1996). At the same time, the current generates a magnetic field. During the process, the graphite die is heated directly by a pulsed electric current and no insulators or external heating elements with a high heat capacity are employed (Omori, 2000; Orrù et al., 2009; Ragulya, 2010). Due to the on/off pulsed voltage, the produced electric discharge contributes to the cleaning and activation of the particle surface under relatively low pressure (Orrù et al., 2009; Song et al., 2006; Tokita, 1999 & 2013; Yanagisawa et al., 1997). Under increased temperature and pressure, the resistive heating of the compact, yields a desired densification (Orrù et al., 2009; Yanagisawa et al., 1997). The temperature measurement can be accomplished with a thermocouple (TC) or with a pyrometer. In measurements with the TC, the junction between two different materials produces a voltage related to a temperature difference. The TC can be positioned in

a hole in the die wall or in an axially drilled hole in the plunger. On the contrary, the pyrometer reads the temperature/thermal radiation optically from the external surface of the graphite die or from a borehole inside the punch. The TC starts to work at room temperature but its maximum temperature is limited, whereas, the pyrometer works only at elevated temperatures. The operation temperatures in both depend on their type (Anselmi-Tamburini et al., 2005; Eriksson, 2010).

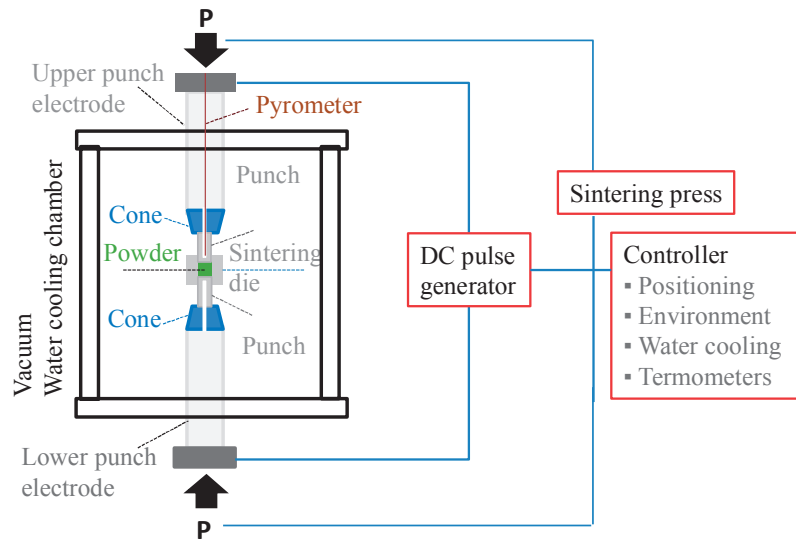


Fig. 1.5. A schematic representation of a PECS unit.

Process cycle and parameters

Before consolidation, a fixed amount of powder is placed into the mold consisting of a cylindrical die with punches at the both ends. When mounting the mold construction, graphite foils can be placed between the powder and the mold in order to shield the mold from the powder. The mold assembly is placed into the chamber, which is then closed, vacuumed, and optionally filled with an inert gas (Ragulya, 2010). The input operating parameters include the pulse: pause - sequence, pressure adjustments, voltage and current, heating rates, the holding temperature and time, and the cooling time (Munir et al., 2011; Orrù et al., 2009; Song et al, 2006)

As the process starts, a pulsed electric current and an external pressure are applied through the punches. The pressure can be increased gradually before or during the heating sequence. The die/punch assembly serves both as a pressure die and as a heating element during the compaction process (Anselmi-Tamburini et al., 2005; Song et al, 2006). The system follows the input values given from the first segment until the end (e.g. vacuuming, pressure, heating, holding, and cooling segments).

The simultaneous output of temperature and displacement (shrinkage) enables to following densification during the operation (Munir et al., 2011). In total, the cycle times are much shorter than with conventional sintering methods (Orrù et al., 2009; Ragulya, 2010).

High heating rates over 1000 K/min (400 K/min is standard) and up to 2673 K (2400 °C), with maximum voltages of 15 V and a current up to tens of kA can be used in PECS. A pulsed DC cycles that can be generated to 1 - 225 ms (on - time)/1 - 225 ms (off - time) with a FCT Systeme GmbH (Germany) or 3 - 300 ms (on)/3 - 30 ms (off) with the Sumitomo Coal & Mining Co. Ltd. (Japan) apparatus. High pressures of 600 MPa can be applied with special molds made of refractory steel (Zhang et al., 2009), or even upto 1 GPa with a special high-pressure die assembly (Anselmi-Tamburini et al., 2006). On the other hand, the temperature is usually limited by the processed material. Heating rates range typically, from below a hundred up to few hundreds K/min, and the pulse sequence applied is most often 12:2 (on/off, with each pulse duration of 3.3 ms). The mold material is typically graphite with properties such as strength and conductivity, limiting the pressure to around 100 - 140 MPa and preferring a low voltage (< 10 V) and a high current (kA) in compaction. Furthermore, the maximum process values depend on the scale and type of PECS equipment (Anselmi-Tamburini, et al, 2006; Munir et al., 2011; Song et al., 2006; Orrù et al., 2009; Ragulya, 2010).

The main drawback in PECS technology is that thermal gradients formed during the heating/cooling segments. These gradients can result in a non-uniform temperature distribution, and subsequently, inhomogeneity in the sample (Munir et al., 2011; Orrù et al., 2009; Ragulya, 2010). The temperature gradients depend on the thermal and electrical contact resistance of the material. Likewise, the heating/cooling rate, the maximum temperature during the experiment, the size of die/sample as well as the stress gradients (due to CTE and modulus) have been found to have significant effect on homogeneity (Munir et al., 2011).

1.5 PECS processed Cu-based materials and their properties

PECS has been applied for different sized Cu powders, as well as for different types of Cu-alloys and -composites. Studies relating to copper have discussed on proper process parameters, densification mechanisms, grain growth, as well as properties of the final compacts. In case of Cu-composites, the attention has also been paid to dispersoid distribution, bonding between the dispersed particles and matrix, and the overall benefits attained by the introduced additives.

PECS has been widely studied for compacting nano- and micron-sized Cu powders (Diouf, 2013; Zhang et al., 2008 & 2009; Sharma et al., 2011). E.g., Zhang et al. (2008 & 2009) obtained avg. 2.2 μm grain size and a density greater than 96% of

T.D. with micronized (1 μm) Cu powders at 1023 K (750 $^{\circ}\text{C}$). In their other study a higher density and smaller grain size was obtained with nanosized Cu powder consolidated at lower temperature with a much higher pressure. Additionally, it was revealed that a higher than optimum temperature led to notable grain growth. Diouf (2013) investigated the influence of temperature, particle size, and pressure on the densification of nanosized Cu powders. Also discussed were the effects of heating rate, holding time and mass transport phenomena. Temperature had the major effect in density, followed by particle size and pressure. It was shown that the longer holding times resulted in an increase of grain size and wide grain size distribution. During the sintering the mass transport mechanisms were particle rearrangement, plastic deformation, neck formation and growth, as well as in the final stage gradual pore elimination (Diouf, 2013).

Only one study was found about PECS of Cu powder (60 - 100 nm) for preparing Cu-Cu₂O composites (Neubauer et al., 2006). The starting powder contained Cu₂O and the concentration increased during the process. The temperature increment led to an extensive grain growth and uneven distribution of Cu₂O in compacts. At the same time, the hardness of the compacts decreased. Sharma et al. (2011) also reported that the temperature increment was observed to lead to a significant grain growth, a hardness decrement, and to a thermal expansion of the compacts.

The microstructure, density and hardness of Cu-Al₂O₃ MMCs have been studied by Dash et al. (2012). The microcomposites were consolidated by the conventional way and holding at 1173 K (900 $^{\circ}\text{C}$) for 60 min. The microcomposites showed poor mechanical properties, i.e., Cu - 15 vol.% Al₂O₃ showed hardness of 0.78 GPa (80 HV). On the contrary, the nanocomposites were prepared by PM and PECS at 973 K (700 $^{\circ}\text{C}$) - 50 MPa - 5 min resulting in enhanced mechanical properties, i.e., hardness of 1.23 GPa (125 HV) for Cu - 5 vol.% Al₂O₃. Finally, it was stated that both the distribution of Al₂O₃ and the bonding between the matrix and the reinforcement were better for nanocomposites. In another study, the nanostructured Cu-Al₂O₃ composites were prepared by ball-milling and PECS for mechanical and tribological investigations (Eddine et al., 2013). Nano-Al₂O₃ was shown to limit the grain growth of the Cu matrix, thus contributing to the strength by DS mechanism. Both the nanocomposite and coarse Cu had similar CoFs, whereas, the wear scar depth for the composite was less than half of that for Cu.

The consolidation of SHS prepared Cu-TiB₂ composite powders have been accomplished by PECS with a temperature graded mold in order to prepare FGM electrode material (Jin et al., 2005). Regardless of the notable difference in melting points between copper and TiB₂, dense microstructures and a good bonding between the layers were achieved. Also Kwon et al. (2006) used SHS as a precursor in preparing Cu-TiB₂ composite powders for PECS. The PECS resulted

in densities up to 95.5% of T.D. With a greater amount of TiB₂, the hardness increased at the expense of electrical conductivity.

Quite recently, diamond dispersed Cu-composites have attracted a growing interest. For instance, Hanada et al. (2007) studied mechanically milled nanocomposites containing 0 - 30 at.% (i.e. about 0 - 8 wt.%) nanodiamonds (ND). The PECS at 873 K (600 °C) with a pressure of 33 MPa for 3 min resulted in a high sample density with a low hardness of 0.57 - 0.69 GPa (58 - 70 HV) and diamond agglomerates, whereas, a homogeneous microstructure and higher hardness of 0.78 GPa (80 HV) was achieved by hot pressing and subsequent hot extrusion (HP + HE). Generally, the biggest challenge reported was poor wettability between Cu and diamond leading to a weak interfacial bonding (Bai et al., 2013; Chu et al., 2010a; Schubert et al., 2008a,b; Weber & Tavangar, 2007; Weidenmann et al., 2009; Xia et al., 2009), and thus a high CTE and low hardness. Several studies have shown that the interfacial reactions can be facilitated with carbide-forming alloying elements, e.g. Cr, B, Si, Ti, W and Mo (Bai et al., 2013; Chu et al., 2010a; Schubert et al., 2007 & 2008a,b; Weber & Tavangar, 2007; Xia et al., 2009; Zhang et al., 2011). Compared to uncoated composites, the densification, thermal conductivity and interfacial bonding of coated composites were significantly improved (Bai et al., 2013; Chu et al., 2010a; Xia et al., 2009; Zhang et al., 2011). On the other hand, e.g. Nunes et al. (2011) demonstrated by microhardness measurements that the effective bonding between Cu and ND's can be achieved by mechanical alloying without Cr doping. Lately, Cu with graphite (Samal et al., 2013) and Cu with CNTs have been prepared by PECS (Cho et al., 2010; Chu et al., 2010b; Guiderdoni et al., 2011). In these studies, the main interest has been the effect of dispersion on the mechanical properties (Samal et al., 2013), the enhancement of thermal conductivity Cu by introducing CNTs (Cho et al., 2010) or MWCNTs (multi-walled carbon nanotube) (Chu et al., 2010b), and the lubricative properties by introducing DWCNTs (double-walled carbon nanotube) (Guiderdoni et al., 2011). It has been shown that the distribution and interfacial properties closely relate to the final properties of composites.

1.6 Aim of the work

The basic attributes of Cu, its alloys and composites will continue to be the driving force for applicative use in industries. This means that good electrical conductivity, thermal management, fluid handling capabilities as well as corrosion and wear resistance of these materials should be maintained, if not improved. Due to increasing demands on device performances, the applicative requirements are becoming more stringent and improvements in new material design or manufacturing methods are sought after. The exposure to high temperatures during service demands a higher resistance against softening. On the other hand,

connector and electronics industries need better dimensional and interfacial stability of the materials, e.g. thermal expansion matching that of the base system or the components they are attached to. Moreover, higher reliability and ever-increasing miniaturization demand for materials with higher strength and thermal stability with thinner gauges (Caron, 2001b). These issues have given the course for this work, with the focus especially on the following aspects:

- To exploit the innovative pulsed electric current sintering method (PECS) for manufacturing fine-grained Cu-based materials.
- To study the dispersion-strengthened (DS) Cu-composites with differing types, contents, sizes, and distributions of dispersoids in the matrix.
- To evaluate the microstructural features, including the grain size and grain growth as well as the size, type, amount, and distribution of the dispersoids in Cu matrix.
- To reveal the correlation between the microstructural features and respective mechanical, thermal, tribological, and electrical properties.
- For comparison, the more conventional powder metallurgical (PM) method of hot isostatic pressing (HIP) is exploited.

The selection of additives, all with a higher hardness than plain Cu, consisted of: (i) semiconductive Cu_2O possessing low CTE (Kondo et al., 2005; Martínez-Ruiz et al., 2003; Mishina et al., 2001; Neubauer et al., 2006; Saito et al., 2001; Shao et al., 2009), (ii) thermally conductive diamonds possessing low CTE with good stability at moderate temperatures (He et al., 2008; Yoshida & Morigami, 2004), (iii) electrically non-conductive and thermally stable Al_2O_3 (Tian et al., 2006), and (iv) electrically conductive and thermally stable TiB_2 (Kim et al., 2006; Kwon et al., 2006). The composite powders were prepared using different methods, including mechanical alloying (MA), internal oxidation (IO), experimentally via a chemical route, self-propagating high-temperature synthesis (SHS), and the natural oxidation of Cu. Subsequently, these composite powders were subjected for consolidation by the non-conventional and fast sintering method of PECS (pulsed electric current sintering). For comparison, the more conventional and widely known pressure-assisted method of HIPing (hot isostatic pressing) was chosen for compacting Cu- Cu_2O composite powders.

It is supposed that dispersion strengthened (DS) Cu-composites can enhance the mechanical, thermal and tribological properties, without too extensive deterioration in electrical conductivity as compared to plain Cu. In this work, the above-mentioned issues were carefully studied and the results are believed to be helpful in

Introduction

the further development of such composites. The studied composites are expected to be potential candidates for applications where strength, good conductivity, and low thermal expansion are desired. Overall, provided that the ultrafine-grained structure is maintained during compaction, a notable improvement of the mechanical and functional properties can be expected (Hannula et al., 2004; Sanders et al., 1997).

2. Experimental

2.1 Preparation and characteristics of Cu matrix composite powders

Several different types of Cu and Cu-composite powders were exploited in preparing Cu-based bulk materials. The Cu matrix composite powders are summarized below together with a short description of the characteristics of the powders. In most cases, the structure and morphology of the initial powders were studied by θ -2 θ X-ray diffraction, XRD (Philips PW3830) and scanning electron microscopy, SEM (Hitachi FE-SEM S-4700 equipped with Inca EDS). Details are given in Publications I-VI. Altogether, eight different powders or powder mixtures, with different amounts of additive elements, were prepared for compaction:

(1) Submicron-Cu (sm-Cu): two pure submicron-sized Cu powders were obtained from Ferro (Cu10K1, $d_{50} < 1.5 \mu\text{m}$ and Cu10K2, $d_{50} < 1.0 \mu\text{m}$). The Cu10K2 powder was used to prepare pure sm-Cu reference samples by PECS. The powder showed an average Cu particle size of 580 nm, calculated from ten SEM-images. Cu10K1 powder was applied to some powder mixtures (specified below). In XRD, only Cu peaks were detected from both powders. [Publications IV-V]

(2) Cu-Cu₂O composite powders: these powders were oxidized from pure commercial Cu powder (99 %) received from MKnano (a division of M.K. Impex Canada). The nominal particle size of the raw powder was -625 mesh with an average between 0.50 to 1.5 μm . Based on image analysis with a set of SEM micrographs of the raw powder, the average particle size was estimated to be 410 nm [Fig. 1 in Publication I]. Since the powder was not stored or handled in a shielding atmosphere, oxidation was expected (Neubauer et al., 2006) and the actual starting powder was a Cu-Cu₂O composite powder. The oxidation was confirmed with the XRD measurements by verifying the peaks of Cu₂O [Fig. 3 in Publication I]. The amount of Cu₂O in the powder was influenced by the exposure time to air, so that the resulting powders had about 2 wt.% (2.9 vol.%), 16 wt.% (21.8 vol.%) and 28 wt.% (36.2 vol.%) of cuprite. [Publications I and III]

(3) Cu-Al₂O₃ (IO): the commercial internally oxidized composite powders chosen for PECS were Cu - 1.2 vol.% (0.5 wt.%) Al₂O₃ (UNS-C15725) and Cu - 2.5 vol.% (1.1 wt.%) Al₂O₃ (UNS-C15760) (Kundig & Cowie, 2006) [Figs. 1a-b in Publication II]. These powders were used without any pre-treatments. Based on

Experimental

SEM analysis, the Cu particle size distribution was wide, ranging mainly from 5 to 100 μm . The SEM and SEM-EDS observations revealed that the commercial powders had a fine distribution of Al_2O_3 particles (about 30 to 300 nm in size) located both on the surface and inside the Cu particles. The XRD could detect only the Cu peaks. [Publication II]

(4) Cu- Al_2O_3 (Exp.): the composite powders with contents of 2.5 vol.% (1.1 wt.%) and 6 vol.% (2.75 wt.%) Al_2O_3 were experimentally prepared via a chemical route [Figs. 1c-d in Publication II]. In the preparation, Cu_2O was introduced in an aqueous solution of aluminium nitrate and then the cuprite was preferentially reduced at 673 K by hydrogen. To prevent oxidation, the powders were placed in a glove box and immediately compacted with PECS. The size of Cu particles ranged mainly between 5 and 15 μm , as defined by SEM. The XRD demonstrated only Cu peaks, however, the presence of Al_2O_3 particles on the surface of Cu particles were ensured with SEM-EDS analysis. [Publication II]

(5) Cu- TiB_2 composite powders: the starting powders for SHS were a milled mixture of elemental Ti (Micron metals, < 325 mesh), B (Alchemia, < 325 mesh) and c-Cu. The subsequent SHS resulted in a porous 'cake', which was then crushed, milled and sieved. This Cu - 79 vol.% TiB_2 (65.5 wt.%) composite powder comprised large particles consisting of several grains of Cu and TiB_2 . The structure was identified with cross sectional analysis of particles by SEM. In order to prepare Cu- TiB_2 composite powders with different contents of TiB_2 , the particles larger than 32 micron were sieved from the SHS powder. After this, the rest of the powder particles were mixed with copper using high-energy vibratory ball milling at VTT. The procedure resulted in powders with 12, 20, and 36 vol.% of TiB_2 (i.e. about 6.5, 11.2, and 22.0 wt.%). The XRD study revealed only peaks of Cu and TiB_2 with no residual elements. [Publications V and VI]

(6) Cu-diamond (Cu-D) powders: these powders were prepared by milling in an argon atmosphere using a SPEX 8000 high-energy vibratory ball mill. The starting powders were pure sm-Cu powders (Ferro Cu10K1, $d_{50} < 1.5 \mu\text{m}$ and Cu10K2, $d_{50} < 1.0 \mu\text{m}$) and diamond powders (Intel-Diamond, LLC; ND, 50 nm and SMD 250 nm). The resulting composite powders (Cu-ND and Cu-SMD) consisting of 3 and 6 vol.% of diamonds, indicated good milling results based on SEM and SEM-EDS observations. The well distributed diamonds were attached onto the surface of the Cu particles with the Cu particle size reflecting that of the starting powder. For example, for Cu-6SMD (Cu with 6 vol.% submicron-sized diamond) the average powder size was larger due to the larger particle size of the Cu starting powder (Cu10K1), whereas, for other composite powders the smaller-sized Cu starting powder (Cu10K2) was used. In the course of milling, the size of Cu starting powders (Cu10K1 and Cu10K2) was reduced. The SEM observations on the milled

powders revealed that the resulting Cu particle sizes were about 320 - 340 nm and 600 nm, respectively, when Cu10K2 or Cu10K1 starting powders were used. The XRD revealed only Cu peaks. [Publication IV]

(7) Cu-nanoD (Cu with single-digit-diamond): the starting powders were pure sm-Cu powder (Cu10K2, $d_{50} < 1.0 \mu\text{m}$) and 6 vol.% diamond powders (Carbodeon Ltd Oy, 4 - 6 nm). The diamond powder was heated up to 773 K (500 °C) to remove moisture before milling the powder mixture in an argon atmosphere by a SPEX 8000 high-energy vibratory ball mill. The XRD showed only Cu peaks.

(8) nCu-nanoD (nanocopper with single-digit-diamonds): the powder was prepared by milling in an argon atmosphere by a SPEX 8000 high-energy vibratory ball mill. The starting powders were alkyl coated stabilized nano-Cu powder (Hongwu Nanometer, 40 nm) and 6 vol.% diamond powders (Carbodeon Ltd Oy, 4-6 nm). These starting powders were milled without any pre-treatment. The powder was studied by XRD indicating only copper peaks.

In high-energy vibratory ball milling the ball to powder ratio employed was 1:1.

2.2 Consolidation of the powders

2.2.1 Pulsed electric current sintering

The pulsed electric current sintering (PECS) was performed with a FCT HP D 25 PECS equipment at FCT Systeme GmbH, Germany, at the Catholic University of Leuven, Belgium (Cu-Cu₂O composite powders) and at Aalto University (all the other powders). Fig. 2.1 presents a FCT HP D 25 -type PECS equipment and a typical mold assembly.

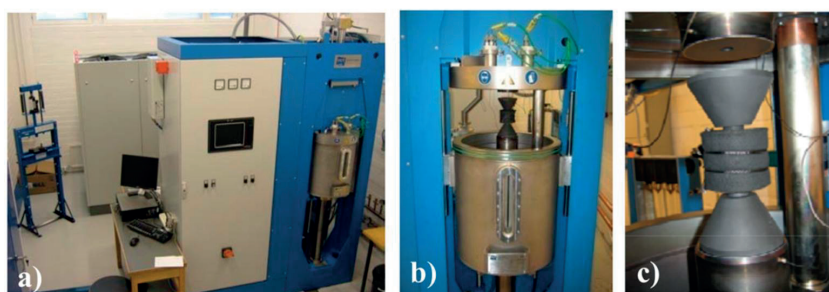


Fig. 2.1. (a) A FCT HP D 25 -type PECS equipment, (b) a vacuum chamber, and (c) a mold assembly placed in the chamber between the electrodes.

For consolidation, about 12 g of powder was placed into a graphite mold with a 20.8 mm inner diameter. When mounting the mold construction, graphite foils (0.4 mm in thickness) were placed between the powder and the mold in order to shield

Experimental

the mold from the powder. After loading the powder into the mold, the mold was placed into the PECS processing chamber, which was then closed and vacuumed.

During the process, the temperature was measured with a pyrometer through a bore-hole in the punch. The operational temperature range for the pyrometer starts at 673 K. According to the specifications given by the manufacturer, the pyrometer used in the PECS setup has a response time of 2 ms and accuracy of 0.3 % for the temperature measurements. Based on the finite element modelling work of the PECS process at Aalto, it was found that the temperature difference between the spot from where the pyrometer gets its reading and the actual sample is approximately 5 K at a temperature of 1073 K (800 °C) for 20 mm samples. The temperature difference is affected by the graphite properties, die dimensions, and the temperature dependent electrical and thermal conductivities of the sintered material. In the present study, the temperature difference between the sample and the reading of the pyrometer was quite small due to the rather small sample and die size as well as the moderate process temperatures. The used DC pulse sequence, i.e. the current pulse-pause ratio, was 12:2 when producing the Cu-Cu₂O composites and 10:5 for all the others. A pulse sequence of 12:2 means a set of 12 pulses with a current (each of 3.3 ms) followed by 2 periods with no current (each of 3.3 ms). Thus, the pulsed current is on for 39.6 ms and off for 6.6 ms. For the 10:5 sequence the pulses are on for 10 ms and then off for 5 ms. The applied heating rates were varied to obtain optimum compaction. Rates from 25 to 78 K/min were applied. Pressures were either 50, 65, 75 or 100 MPa (applied before or during the heating segment) and holding times from 0 up to 6 minutes. Sintering temperatures were varied from 773 to 1323 K depending on the type of the powder and the dispersed phase. The sintering atmosphere was either vacuum (7 - 15 Pa) or argon, depending on the facilities and the type of the employed powder. In most cases, the experiments were carried out in an argon atmosphere to prevent oxidation. The last segment of processing was a cooling stage of 4 min, after which the chamber was flooded with an inert gas and then opened. The sintering resulted in specimens of about Ø 20 mm (or 25 mm) in size (depending on the mold) with a height of 3 - 7 mm. The studied process parameters are presented in Table 2.1.

To conduct the process optimization for all the studied powders it took from three to eight experiments with each. In the process optimization, the first objective was to achieve a proper densification of the samples, i.e., to achieve density close to that of the theoretical value (%T.D.). For this purpose, several process parameters were varied and different approaches were applied, e.g. pressure increment before or during the heating time as well as heating rate changes in the last segment.

Table 2.1. Process parameters used in the experiments for Cu-composite powders showing the sintering temperature, holding time, pressure, and heating rate.

Powder	Temperature (K)	Pressure (MPa)	Holding time (min)	Heating rate (K/min)
Cu-Cu ₂ O	873 - 1073	50 - 100	1 - 6	75(or 78)
Cu-Al ₂ O ₃ (IO)	1073 - 1223	50/100	6	75
Cu-Al ₂ O ₃ (Exp.)	823 - 1173	50/100	0 - 6	75
Cu-TiB ₂	773 - 1323	50/75	0 - 6	75
Cu-SMD	773 - 923	50/75/100	0 - 3	75/37.5
Cu-ND	823 - 923	50/75/100	0 - 2	75/37.5
Cu-nanoD	923 - 1073	50/100	0 - 5	75/37.5
nCu-nanoD	823 - 1148	50	2 - 5	50 (/25)

2.2.2 Hot Isostatic Pressing

To compare the resulting properties of the PECS processed Cu-Cu₂O composite samples with a more traditional sintering method, hot isostatic pressing (HIP) method was also employed. [Publications I and III]

For HIPing, the starting powder was packed in a seamless stainless steel tube, then vibratory densified, vacuum evacuated, and weld sealed for processing. The consolidation was performed with a laboratory size HIP unit (ABB Autoclave systems Inc MiniHIP at VTT). At the start of HIPing, the tubes were heated at a rate of 13 K/min. An isostatic pressure of 100 MPa with an argon gas atmosphere was applied and kept constant during the process. Three experiments were performed, the first one at 948 K for 30 min (HIP 1), the second at 1073 K for 30 min (HIP 2) and the third one at 1073 K for 120 min (HIP 3).

2.3 Sample preparation for materials characterization

After compaction, the graphite foils applied before PECS processing were removed by sand blasting and the samples were ground with sand grit papers down to 1200 mesh. The HIP sample was cut out from the steel container with a diamond saw and then ground down to 1200 mesh.

To provide a smooth surface for mechanical characterization, the samples were further polished using 6, 3, and 1 μm diamond paste. To evaluate the properties of the different material combinations, the bulk samples were further prepared as explained in the next section.

2.4 Characterization of the bulk samples

2.4.1 Density

The densities of the sintered compacts were measured by applying the Archimedes' principle using water as a medium. Measurements were carried out by a Sartorius CPA224S balance, with an accuracy of 0.1 mg, for the polished samples. The density was measured by taking m_d for dry weight and m_w for wet weight and ρ_{H_2O} as the density of water as follows:

$$\rho = (m_d \times \rho_{H_2O}) / (m_d - m_w) \quad (2.1)$$

The theoretical density of the compacts was calculated by considering the presence of the dispersed particles and applying the rule of mixtures. The densities used for different constituents were 8.94 - 8.96 g/cm³ for Cu (García et al., 2008; Nadkarni & Synk, 1984), 6.00 - 6.14 g/cm³ for Cu₂O, (Anthony et al., 1995; García et al., 2008) 4.5 g/cm³ for TiB₂, (Munro, 2000) 3.89 - 3.95 g/cm³ for Al₂O₃ (Rajkovic et al., 2008, © 2013 Accuratus) and 3.52 g/cm³ for diamonds (Yoshida & Morigami, 2004). The density values for the bulk samples were then reported as a % of T.D.

2.4.2 Microstructure

A set of techniques including optical microscopy (Reichert Me F 300/734 and Leica DMRX), scanning electron microscopy, SEM (Hitachi FE-SEM S-4700 equipped with Inca EDS) and transmission electron microscopy, TEM (FEG-TEM Tecnai F20), were used to investigate the phase composition and microstructure of the sintered composites.

In order to reveal the grain boundaries and to determine the Cu grain size, the mechanically polished samples were further electropolished/-etched for about 30 s in a nitric acid-ethanol solution at 243 - 253 K (-30 to -20 °C). In preparing samples for the dispersoid size and distribution investigations, mechanical polishing with a colloidal silica slurry of 0.02 µm was found to be a more suitable method. Mechanical polishing was especially useful when preparing samples with Al₂O₃ or diamond dispersoids because some of the smallest dispersoids were etched away during electropolishing, thus selectively affecting the dispersoids' appearance and boundary areas in the compact surface.

The chemically/electrically polished samples were then studied by SEM and the micrographs were carefully analyzed using the line analysis method or ImageJ image-analysis. In addition, SEM-EDS was carried out to evaluate the chemical composition. For more detailed microstructural observations and phase evaluations, transmission electron microscopy (FEG-TEM Tecnai F20 G2 200kV FEG S-Twin with EDX and GIF) was applied to the selected samples. TEM foils

were cut from sintered materials and mechanically ground to a thickness of about 100 μm prior to electro-thinning with a nitric acid-methanol (1:3) solution using 10 - 12 V at 243 K (- 30 °C). A thin sample, which enables sufficient electron beam penetration, was then cut for TEM studies. TEM bright field (BF) imaging [Publications III and IV], STEM imaging [Publications II-IV], energy dispersive X-ray (EDX) spectroscopy measurements [Publications II-IV], and selected area diffraction patterns (SADP) [Publications II and III] were obtained mostly at 200 kV. More details of the analysis can be found in Publications II-IV.

The phase composition of the compacted samples was also evaluated by θ -2 θ XRD (Philips PW3830) measurements (Cu-K $_{\alpha}$ radiation, 2θ of about 20 - 90°, scan speed of 0.02 °/s). The XRD was exploited for a few composites of each type. However, the detection limit for any phases present lies at around 3 wt.%, so it was expected that the patterns for Cu-Al₂O₃ and Cu-diamond composites would reveal only the copper peaks. Whenever other elements were found, rough estimates of the contents were defined using X'pert HighScore Plus Software.

2.4.3 Mechanical and nanomechanical properties

After sample preparation, the Vickers hardness (HV1) was measured with a Zwick&Co.KG Z323 hardness tester at a load of 9.81 N. The average hardness from five to ten measurements of each sample was converted to GPa.

For nanoindentation, the samples were further polished automatically with silica slurry of 0.02 μm to provide smooth surfaces for indenting. Nanoindentation was performed for the chosen samples using a TriboIndenter® (Hysitron Inc, USA) nanomechanical testing instrument. The aim was to investigate the mechanical response of the composites at a sub-micron scale. Moreover, by exploiting the fine tip the behaviour of different phases could be studied.

Each indentation cycle was carried out in a load control mode using a Berkovich tip. The loading/unloading rate was set to 25 $\mu\text{N/s}$ with the maximum load of either 250 μN [Publications I-IV] or 1000 μN [Publication I]. The loading time to the maximum load was set to 10 s, while the maximum load was held for 5 or 10 s, before unloading within 10 s. Multiple indents at several locations on the sample surface with a size between (3 x 3) and (10 x 10) μm^2 were performed in order to gain high statistical significance in the data analysis [Publications I-IV].

2.4.4 Oxygen content

The oxygen content was measured for selected samples using an oxygen analyser TC-436 DR at Outotec Research Center in Pori. In this method, a weighed sample is melted in a graphite crucible in a stream of helium. The oxygen in the sample

Experimental

combines with carbon to form CO, which is then converted by a catalyst to CO₂. An infrared cell determines the CO₂ content, from which the weight % of oxygen in the sample is calculated. For Cu-Cu₂O composite samples, the high measured oxygen contents were transformed to the contents of Cu₂O [Publications I and III].

2.4.5 Electrical properties

The electrical conductivity values were measured for different types of composites by the Sigmatest 2.069 instrument at Luvata Inc. This is an eddy current instrument, which measures the electrical conductivity of non-ferromagnetic metals based on the complex impedance of the measuring probe. It is fast to use and provides a reliable determination of electrical conductivity with high accuracy. The instrument converts the complex impedance value to an electrical conductivity value given as %IACS (+/- 0.1% of the measured value). IACS is the International Annealed Copper Standard, which prescribes the electric conductivity of annealed unalloyed copper to 100% IACS (about 57.8 MS m⁻¹).

For the measurement, the samples were polished with diamond paste down to 1 micron to provide a smooth surface. The flat samples with a minimum diameter of 8 mm were prepared for testing. In each case, three to five measurements were accomplished to give an average value. An overview on the electrical behaviour of different types of composites is given in Publication V.

2.4.6 Thermal properties

Thermal properties were investigated in order to estimate the high-temperature applicability of different types of composites in comparison to pure copper. Particularly, properties of thermal stability and thermal expansion are reported in Publications II, IV and V.

Thermal stability

The thermal stability of different types of Cu matrix composites was evaluated by annealing treatments. For Cu-Cu₂O, Cu-diamond, Cu-TiB₂ and sm-Cu samples the experiments were carried out in glass ampules, which also incorporated titanium flakes to react with any remaining free oxygen after vacuuming the ampules. For Cu-Al₂O₃ composites and coarse Cu the annealing was performed in an argon atmosphere [Publication II].

All the studied samples were annealed at 623 and 873 K (350 and 600 °C) while the Cu-composites with Al₂O₃ (1.2 and 2.5 vol.%) or TiB₂ (12, 36, and 79 vol.%) were also treated at a higher temperature of 1023 K (750 °C) for one hour. The microhardness values (HV1) were measured, both before and after the heat

treatment to reveal the resistance against thermal softening. An average of five measurements was then transformed to GPa. [Publication V]

Thermal expansion

Dense materials were chosen for thermal expansion studies in order to minimize the effect of porosity in expansion. Four samples of Cu-diamond, three of Cu-TiB₂, and two of both Cu-Al₂O₃ and Cu-Cu₂O were studied. These composites consisted of different content/size of dispersoids while the two reference samples of plain copper had an average grain size close to 10 microns (c-Cu) and 650 nm (sm-Cu). [Publications II, IV-VI]. For the measurements, the samples were prepared to sizes of about (3 x 3 x 10) mm³. To ensure the accuracy of the measurement and to prevent bending during the experiments, the flat surfaces of the samples ends were aligned parallel to each other.

A Netzsch DIL 402C device was applied for annealing the samples in an argon atmosphere, with the heating rate of 10 K/min. The temperature range for different types of composites was selected based on the knowledge gathered from the thermal stability experiments. Thus, for c-Cu, Cu-Al₂O₃ and Cu-TiB₂ the CTE was determined from 473 K (200°C) up to 973 K (700 °C), for Cu - 6 vol.% diamond (6SMD and 6ND) up to 673 K (400 °C), and sm-Cu, Cu-Cu₂O and Cu - 3 vol.% diamond (3SMD and 3ND) up to 623 K (350 °C). The CTEs were determined based to the 1st heating ramp, as shown in Fig. 5b in Publication II [Publications II, IV and V].

After the CTE measurements, the values were compared to the theoretical expectations proposed by Turner in Eq. (1.8) and by Kerner Eq. (1.9), (see section 1.1.2). The parameters used in the calculations were $\alpha_{Cu} = 18.5 \times 10^{-6} \text{ K}^{-1}$ (Nix & MacNair, 1941), $\alpha_{sm-Cu} = 19.6 \times 10^{-6} \text{ K}^{-1}$ (473 - 523 K (200 - 250 °C)) from the present study, $K_{Cu} = 1.4 \times 10^{11} \text{ Pa}$ (Yoshida & Morigami, 2004), $G_{Cu} = 4.9 \times 10^{10} \text{ Pa}$ (Yoshida & Morigami, 2004), $\alpha_{Cu_2O} = 2.7 \times 10^{-6} \text{ K}^{-1}$ (Kondo et al., 2005), $K_{Cu_2O} = 1.08 \times 10^{11} \text{ Pa}$ (Martínez-Ruiz et al., 2003), $\alpha_{TiB_2} = 8.0 \times 10^{-6} \text{ K}^{-1}$ (Munro, 2000), $K_{TiB_2} = 2.4 \times 10^{11} \text{ Pa}$ (Munro, 2000), $\alpha_{Al_2O_3} = 8.4 \times 10^{-6} \text{ K}^{-1}$ (© 2013 Accuratus, MatWeb™), $K_{Al_2O_3} = 2.3 \times 10^{11} \text{ Pa}$ (© 2013 Accuratus), $\alpha_D = 2.3 \times 10^{-6} \text{ K}^{-1}$ (Yoshida & Morigami, 2004), $K_D = 5.8 \times 10^{11} \text{ Pa}$ (Yoshida & Morigami, 2004).

2.4.7 Tribological properties

The tribological properties were investigated with a UMT-2 versatile nano-micro tribometer, using the dry reciprocating sliding method with a ball-on-flat technique (Holmberg & Matthews, 2009). The tests were operated at a 1 N normal force at room temperature (25 °C) in air with a relative humidity of about 45%. The load

Experimental

was chosen based on the Hertz contact stress evaluation, so that in a static situation it would not cause plastic deformation in coarse copper.

The materials studied were pulsed electric current sintered (PECS) samples of pure c-Cu, sm-Cu and different types of Cu-composites. The size of the studied disc shaped samples was either 20 or 25 mm in diameter and 3 to 6 mm in height. The friction and wear tests were carried out at a displacement amplitude of 5 mm with a sliding frequency of 5 Hz for up to 3,000 cycles at the Tallinn University of Technology. Two different counterparts were applied; a metallic counter ball made of Cr-steel and a ceramic counter ball made of alumina, both 3 mm in diameter. The hardness of the metallic ball was 700 HV (6.86 GPa) and that of the ceramic ball 1700 HV (16.7 GPa). During the experiments the coefficient of friction (CoF) was recorded as a function of time.

After the sliding tests, the width and surface of the wear tracks as well as the surface of the counter balls were studied with an optical microscope and a scanning electron microscope (Hitachi FE-SEM S-4700 equipped with Inca EDS). The cross sections of the wear tracks was measured by a Dektak 6m stylus profilometer at three to five different locations along the tracks, to calculate the average worn areas. Based on the average cross-section areas and the longitude stroke length (5000 μm), the volume loss was calculated. Subsequently, the specific wear rates (W) [mm^3/mN] were expressed according to ISO 20808 (ISO 20808:2004(E)) as the volume loss (V) per distance (L) and applied load (F_p):

$$W = V/(L \times F_p) \quad (2.2)$$

A few samples were prepared in order to study the subsurface of the worn tracks with SEM. To estimate the work-hardening, the microhardness values (HV 0.2) were measured from the worn tracks after the reciprocated sliding against Cr-steel [Publication VI].

3. Summary of the Results

3.1 The microstructural characteristics of Cu and Cu-composites

3.1.1 Pure copper

Two copper samples were prepared by PECS as reference materials. These were submicron-sized copper (sm-Cu) and coarse copper (c-Cu). The grain size of sm-Cu was 650 nm after being densified by PECS using 50 MPa pressure and a one-minute exposure at 823 K. The c-Cu showed about 10 micron grain size after PECS at 1023 K for 6 minutes with 50 MPa. In both cases, the XRD showed peaks only for copper. The measured oxygen content was 0.077 wt.% for sm-Cu and 0.063 wt.% for c-Cu.

3.1.2 Cu-Cu₂O composites

The Cu-Cu₂O composite powders with different amounts of cuprite were consolidated by PECS and HIP methods to study the densification, microstructure and mechanical properties of the samples. Special attention was given to evaluate the grain growth during the processing and the role of cuprite in the grain size control.

Both the XRD [Fig. 3 in Publication I] and SEM (Fig. 3.1) verified the presence of Cu₂O within the samples. The intensity of Cu₂O XRD peaks was most pronounced for Samples HIP 1 and 3, as well as for PECS 3, which was in agreement with the results of the oxygen analysis, i.e. in these samples the oxygen content was the highest [Table 2 in Publication III]. Since oxygen has an extremely low solubility in copper at ambient temperature, it was assumed that most of the oxygen was in the form of Cu₂O (Horrigan, 1977; Rhines & Mathewson, 1934). Moreover, the TEM study [Publication III] verified that copper oxide appears as crystalline Cu₂O particles.

The amount of cuprite was 6.8 vol.% at its lowest (Sample HIP 2) and 38.7 vol.% at its highest (Sample HIP 3). Thus it had a clear influence on the appearance of the microstructure, as depicted in Fig. 3.1. When the amount of cuprite was small, i.e. about 7 vol.% (Sample HIP 2, Fig. 3.1e), the cuprite grain size was much smaller than that of Cu, and the small oxide particles were typically located at the boundaries between the copper grains. With a cuprite content of around 20 vol.%

Summary of the Results

(samples PECS 1, 2, 4 in Figs. 3.1a-c), the Cu_2O particles were quite evenly distributed between the slightly larger copper grains with only some clusters present. However, when the amount of cuprite was at its highest, i.e., more than 30 vol.% (HIP 1, 3 and PECS 3 in Figs. 3.1d,f), the somewhat smaller Cu_2O grains formed a uniform network consisting of several banded or clustered Cu_2O grains (Cu_2O particles grouped in pairs, trios or quartets) in the Cu matrix.

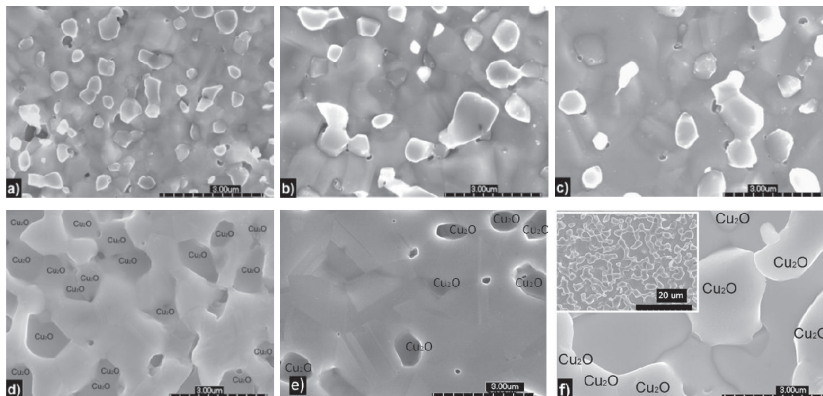


Fig. 3.1. Microstructures of the samples after etching: (a) PECS 1 (873 K/6 min), (b) PECS 2 (973 K/3 min), (c) PECS 4 (1073 K/1 min), (d) HIP 1 (948 K/30 min), (e) HIP 2 (1073K/30min), and (f) HIP 3 (1073 K/120 min) with a small insert in the top-left corner indicating the distribution of Cu_2O particles appearing with light borders. In (a) to (c) Cu_2O particles appear lighter than the Cu matrix [Publication III].

After PECS at 873 K (the lowest temperature used), the average grain size of the compacted Cu- Cu_2O sample was 460 nm (when considering both Cu and Cu_2O) (Fig. 3.1a), which indicated only a slight increase from the initial particle size (410 nm) [Publication I]. PECS at a higher temperature of 1073 K doubled the initial size of the powder leading to the grain size of 830 nm during a one-minute exposure (Fig. 3.1c). In contrast, in the case of HIPing at 1073 K for 120 min, the grain size grew 4.5 times from that of initial powder (1860 nm) during processing (Fig. 3.1f).

SEM observations of the compacted samples indicated low porosity and when the cuprite content was taken into account, the densities were found to vary from 97.6 to 99.7% of T.D. after PECS [Publication I]. Thus, the presence of Cu_2O had no significant effect on powder consolidation. However, its role in inhibiting grain growth and enhancing the mechanical properties (section 3.2) was clearly detected. The grain sizes of both phases, Cu and Cu_2O , in Cu- Cu_2O compacts are illustrated in Fig. 3.2 as a function of process temperature. Depending on the process temperature, the grain sizes for Cu_2O were somewhat smaller than those of Cu

(Fig. 3.2). When comparing the grain size of Cu and Cu₂O in bulk compacts, with those reported by Zhang et al. (2008), i.e., to pure micrometer-sized copper powder after PECS at 973, 1023 and 1073 K, the sizes remained much smaller, with the effect being more pronounced at higher temperatures.

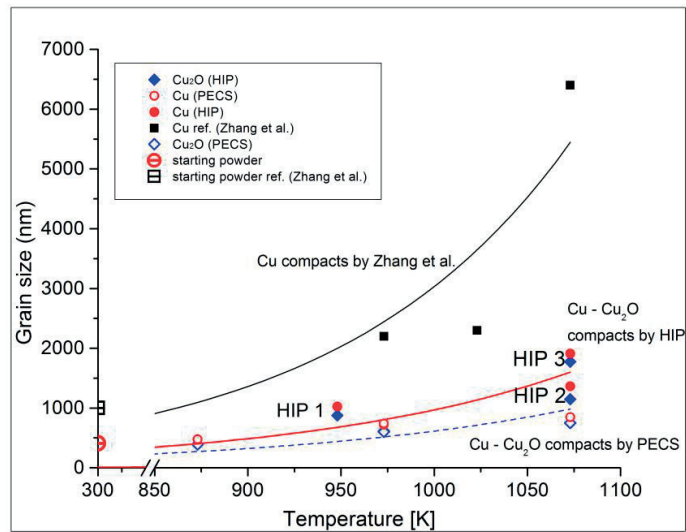


Fig. 3.2. The grain size of Cu and Cu₂O present in compacted Cu-Cu₂O samples as a function of process temperature in comparison with the values reported by Zhang et al. (2008) for (1 μm) Cu powder by PECS [Publication III].

3.1.3 Cu-Al₂O₃ composites

Two types of Cu-Al₂O₃ composite powders, both with two grades of Al₂O₃, were applied to PECS in order to evaluate the microstructural characteristics and their effect on the mechanical properties. These commercial internal oxidized (IO) powders comprised 1.2 and 2.5 vol.% Al₂O₃ and experimentally prepared (Exp.) powders consisting of 2.5 and 6 vol.% Al₂O₃. The dissimilarities detected in the consolidated samples constitute the main focus of this study. The bulk samples are denoted as 1.2Al₂O₃ (IO), 2.5Al₂O₃ (IO), 2.5Al₂O₃ (Exp.) and 6.0Al₂O₃ (Exp.), the numbers denoting the vol.% of Al₂O₃.

After process optimization, the PECS resulted in compacts having densities between 98.6% and 99.6% of T.D. The microstructural variations of the compacts are illustrated in Fig. 3.3. The main dissimilarities are in the grain size of the Cu matrix and the size of the dispersed Al₂O₃ particles. The average grain size for samples made from IO powders was 25 μm (with a wide grain size distribution between 2 and 100 μm). For the samples made from the experimentally prepared powders the average grain size was 10 μm (with a narrower grain size distribution

Summary of the Results

between 5 and 15 μm). These reflected the sizes of the initial powders, and no coarsening was observed.

The finer size and more even distribution of Al_2O_3 was seen in compacts made from the commercial IO powders (Fig. 3.3a) as compared to the ones made from the Exp. powder (Fig. 3.3b), in which the alumina was either coarser or more segregated at the grain boundaries.

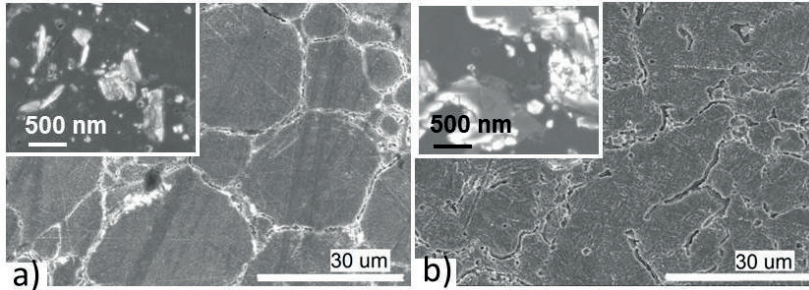


Fig. 3.3. The microstructures of the composite samples: (a) $2.5\text{Al}_2\text{O}_3$ (IO) and (b) $2.5\text{Al}_2\text{O}_3$ (Exp.). Inserts in the top-left corners show Al_2O_3 particle distributions [Publication II].

Due to the small amount of Al_2O_3 , it could not be detected with XRD from the powders or the samples. However, the TEM images in Fig. 3.4 verified the presence of Al_2O_3 in the bulk samples and also revealed, in more detail, the observations made about its distribution by SEM. Figs. 3.4a-b are STEM micrographs of the sample $2.5\text{Al}_2\text{O}_3$ (IO), showing fine nano- and submicron-sized alumina particles in the Cu matrix. The selected area diffraction (SAD) pattern indicated gamma-alumina ($\gamma\text{-Al}_2\text{O}_3$) (Gamma-alumina JCPDS 50-741). Figs. 3.4c-d show the STEM micrographs of the sample $2.5\text{Al}_2\text{O}_3$ (Exp.). The SAD indicated agglomerates of $\gamma\text{-Al}_2\text{O}_3$ [Publication II].

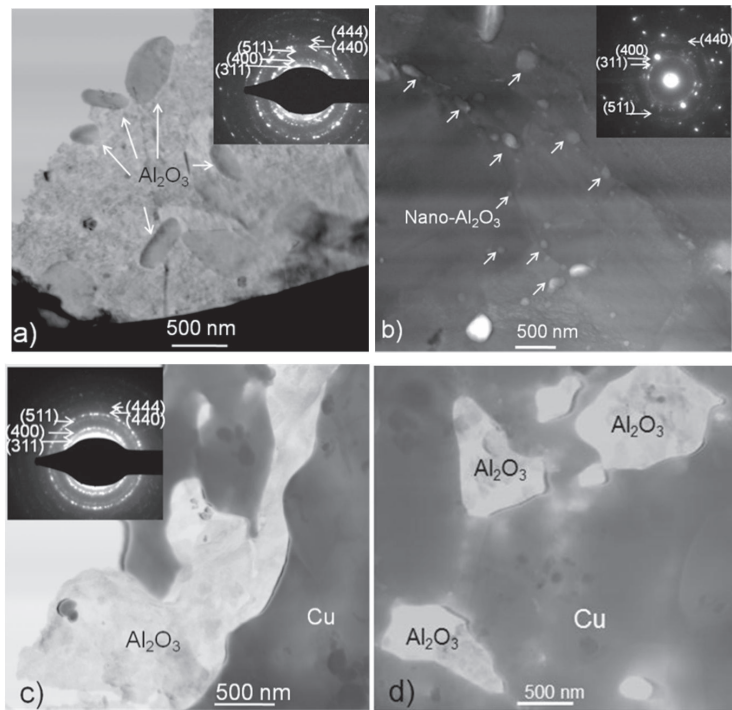


Fig. 3.4. (a) - (b) STEM micrographs of the sample $2.5\text{Al}_2\text{O}_3$ (IO) with SAD and (c) - (d) STEM micrographs of the sample $2.5\text{Al}_2\text{O}_3$ (Exp.), the former with SAD.

3.1.4 Cu-TiB₂ composites

The Cu-TiB₂ composite powders with different amounts of TiB₂ were compacted by PECS. The bulk samples are denoted as 12TiB₂, 20TiB₂, 36TiB₂, and 79TiB₂, the numbers indicating vol.% of TiB₂.

Dense samples with a T.D. higher than 98.6% were achieved for the majority of the samples. However, the sample with the highest amount of TiB₂ was an exception having a density of only 94.3% of T.D., probably because of the insufficient temperature for proper densification. All the bulk samples showed a wide size range of TiB₂ grains (30 - 2000 nm) distributed in the Cu matrix (Fig. 3.5). After etching the samples, it was evident that most of the dispersoids were located at the grain boundaries of the Cu matrix.

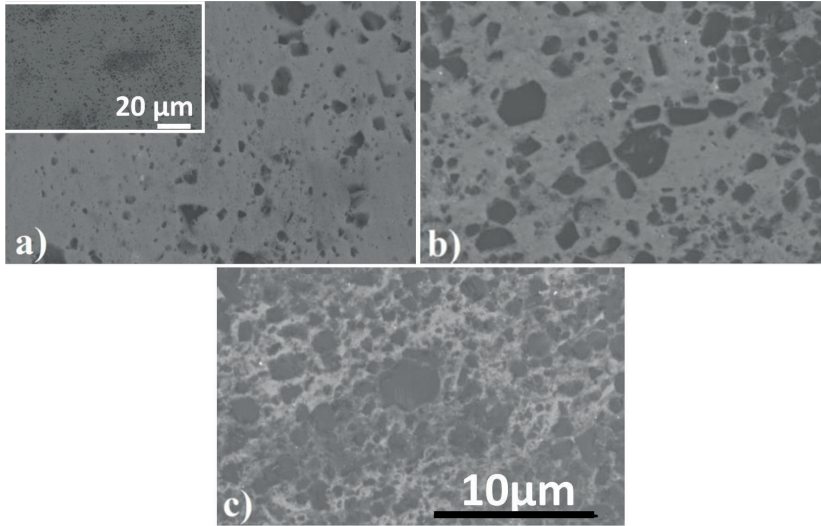


Fig. 3.5. Optical microscopy images of Cu-TiB₂ -composites: (a) 12TiB₂, (b) 36TiB₂, and (c) 79TiB₂. TiB₂ appears darker in the micrographs.

Microstructural observations demonstrated a slightly inhomogeneous distribution of TiB₂ for the 12TiB₂ sample (insert in Fig. 3.5a), probably due to the Cu dilution of the SHS-produced composite powder. A more homogeneous distribution was achieved for the samples made with the original SHS powder (79TiB₂) and the powder with 36TiB₂. The XRD results verified the amounts of TiB₂ with no oxide phases or residual Ti or B present (Fig. 3.6). However, the oxygen analysis revealed a slightly increased oxygen content of 0.64% for the 36TiB₂ sample.

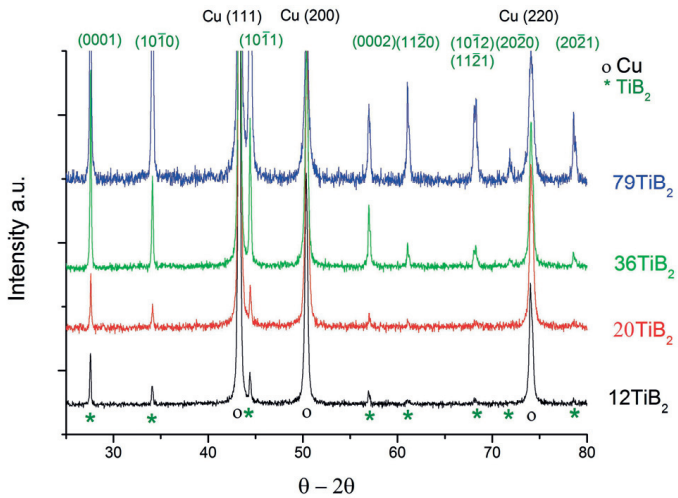


Fig. 3.6. XRD results of the Cu-TiB₂ composite samples.

3.1.5 Cu-diamond composites

The submicron and nanosized copper powders together with different sizes and amounts of diamonds were ball-milled prior to PECS compactions. The main idea behind choosing such a wide selection of different-sized starting powders was to distinguish, which of the following factors has a major influence on their properties: (i) amount of dispersoids, (ii) size of the dispersoids, or (iii) the matrix grain size [Publication IV]. In addition, the distribution of diamonds was investigated.

After process optimization, the compaction yielded over 97% of T.D.s for samples with submicron-sized Cu matrix, whereas a much lower density was achieved for the sample, which had nanocopper as a matrix (nCu-nanoD). The compacted samples were designated as SMD, ND and nanoD, denoting Cu-composites with submicron-sized (250 nm), nanosized (50 nm) and single-digit-sized (5 nm) diamonds, respectively. The numbers denote vol.% diamonds, i.e. 3SMD, 6SMD, 3ND, 6ND, 6nanoD.

The microstructures of the compacts with a submicron-sized Cu matrix together with 6 vol.% diamonds after PECS can be seen in Fig. 3.7. The samples with a submicron-sized (250 nm) or nanosized diamonds (50 nm) are shown to be homogeneously distributed, with visibly distinct diamond particles (Figs. 3.7a-b), whereas single-digit diamonds are highly agglomerated, Fig. 3.7c.

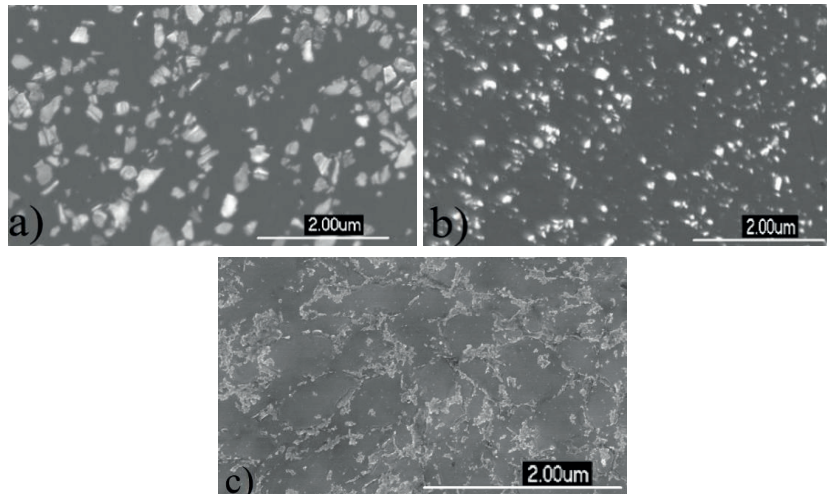


Fig. 3.7 SEM micrographs of the Cu-composite samples: (a) 6SMD (Cu - 6 vol.% submicron-sized diamonds), (b) 6ND (Cu - 6 vol.% 50 nm diamonds), and (c) 6nanoD (Cu - 6 vol.% 5 nm diamonds). Diamonds appear light in all micrographs.

Summary of the Results

The EFTEM and STEM micrographs together with the carbon map in Fig. 3.8 reveal the size and distribution of nanodiamonds in the 6ND sample. During sample preparation by electrothinning, most of the large diamonds were etched away, leaving only holes or shallow dimples of their original places. This can be observed in the STEM image (Fig. 3.8c), which also verifies that part of the nanodiamonds are located inside the copper grains (indicated by arrows) and not only decorating the grain boundaries. The EFTEM image (at 100 kV) in Fig. 3.8a shows the microstructure of the sample, and the corresponding carbon map in Fig. 3.8b illustrates the remaining diamond agglomerates that can be seen inside the holes and deep dimples.

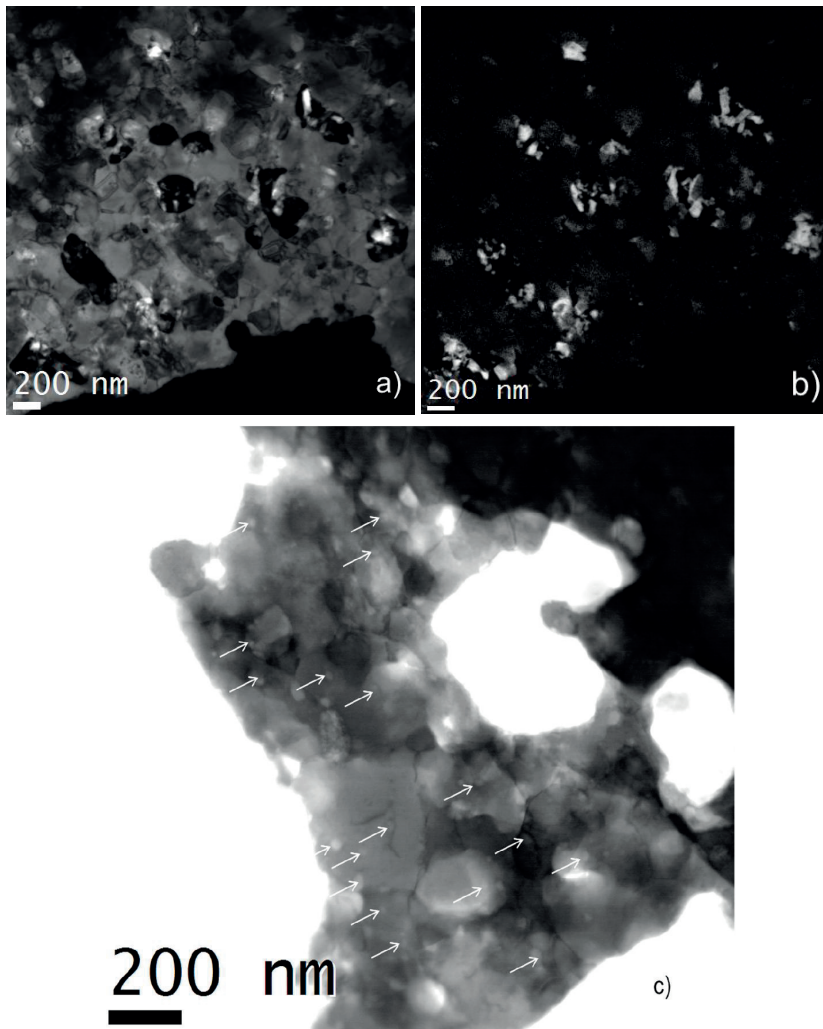


Fig. 3.8. (a) EFTEM micrograph of the Cu sample with 6 vol.% nanodiamonds (6ND), (b) the corresponding carbon map, and (c) STEM micrograph showing lighter spots, which indicate the sizes and placement of nanodiamonds in sample 6ND [Publication IV].

Only Cu diffraction peaks were found by XRD; the diamond peaks were too small and partially overlapped by the Cu peaks to be detected, as has been reported earlier (He et al., 2008; Yamamoto et al., 2007). The oxygen contents of samples 6SMD and 6ND were 0.091% and 0.19%, respectively, thus indicating very low oxidation of the powders.

3.2 The mechanical properties of Cu-composites

3.2.1 Microhardness

The properties of selected PECS compacts are compiled in Table 3.1, showing the matrix grain sizes, size and amount of dispersoids as well as the microhardness and density of the samples. The effectiveness of the second-phase particulates in increasing the microhardness is evident as compared to pure copper. Only the samples with a notably large matrix grain size (i.e. Cu-Al₂O₃ (Exp.) composites) led to a lower microhardness.

Table 3.1. Properties of the PECS samples.

Composite	Matrix grain size (nm)	Dispersoids		Micro-hardness (GPa)	Density % of T.D.
		Amount (vol.%)	Avg. size (nm)		
c-Cu	10000	-	-	0.58	99.2
sm-Cu	650	-	-	1.02	97.0
Cu-Cu ₂ O	480	20	390	1.24	98.0
	850	20	750	1.02	98.8
	740	37	600	1.35	99.1
Cu-Al ₂ O ₃ (IO)	25000	1.2	110	1.22	98.6
	25000	2.5	150	1.58	99.1
Cu-Al ₂ O ₃ (Exp.)	10000	2.5	500	0.78	98.7
	10000	6	500	0.93	99.6
Cu-TiB ₂	260	12	350	1.78	98.6
	200	36	440	2.50	98.8
	160	79	290	3.94	94.3
Cu-SMD	560	3	250	1.31	97.4
	630	6	250	1.26	97.5
Cu-ND	350	3	50	1.46	97.1
	340	6	50	1.77	97.9
Cu-nanoD	345	6	5	2.01	97.2
nCu-nanoD	40	6	5	1.08	90.1

When the microhardness values of the Cu-Cu₂O composites are compared to those reported for pure nanocopper (Chokshi et al., 1989; Das et al., 2006; Khan et al.,

Summary of the Results

2008; Youngdahl et al., 1997), a large difference can be observed (see Fig. 3.9). However, at a fixed grain size, the Cu-Cu₂O composite samples seemed to have a higher hardness than pure copper. The samples with more than 30 vol.% Cu₂O (filled marks and pointed with arrows in Serie E; HIP 1, HIP 3 and PECS 3) also showed increased hardness compared to those containing less Cu₂O (6 - 20 vol.%) at a similar grain size.

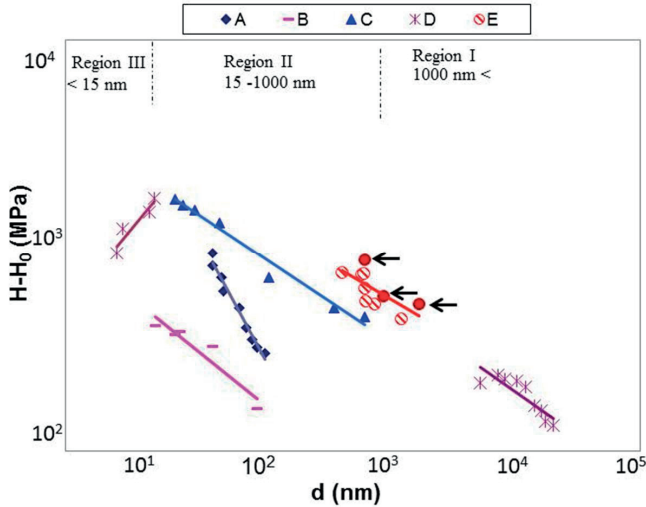


Fig. 3.9. The hardness increment ($H - H_0$) as a function of grain size (d) obtained through the study of Cu-Cu₂O in comparison with the earlier reported values for Cu. Sources for the points marked with A - Das et al. (2006), B - Youngdahl et al. (1997), C - Khan et al. (2008), D - Chokshi et al. (1989), and E - present study. The samples of the present study with more than 30 vol.% Cu₂O are emphasized with filled marks and arrows. The trendlines are fitted for each data series [Publication III].

The matrix grain size (d) in the presence of particles has been shown to follow the critical grain size R_c inversely proportional to the volume fraction of particles (f_v) and directly proportional to the particle radius (R), as in Eq. 1.2 and first presented by Zener (Smith, 1948). However, a uniform distribution and a lower volume fraction of second-phase particles are typically assumed, without noticing particle clusters, which decrease the effective surface, leading to a larger critical grain size (R_c) (Flores et al., 2004). In order to take into account the clustering of the second-phase particles, the following expression has been proposed (Flores et al., 2004):

$$R_c = R (6f_v - 0.6f_v^2 - 19.2f_v^3)^{-1} \quad (3.1)$$

where R_c is the critical radius, R is the particle radius and f_v is the volume fraction of the second-phase. This relation was found to describe several two-phase systems. The critical radius for Cu in this study has been calculated as proposed by Flores (Flores et al., 2004), following the Eq. (3.2):

$$R_c = r_e (6f_v)^{-1} \quad (3.2)$$

where r_e is the effective average radius, i.e. the radius of every particle when taking a cluster to be a single particle. The orders (particles grouped by pairs, trios, quartets, and so on), amounts and frequency of clusters were analyzed for samples with different contents of Cu_2O based on image analysis with a set of ten SEM micrographs. As a consequence of particle agglomeration, the average radius R (radius of Cu_2O) is lower than the effective radius r_e (radius of typical clusters), and the ratio R/r_e decreases with increasing volume fractions. Based on Fig. 3.10a, the higher amount of Cu_2O led to a greater amount of clusters, and hence, to a decrease of effectiveness when compared to isolated particles. The results in Fig. 3.10b together with those of Flores et al. (2004) indicate that the effectiveness of Cu_2O on grain growth control increases up to about 20 vol. % of Cu_2O and remains at the same level beyond that.

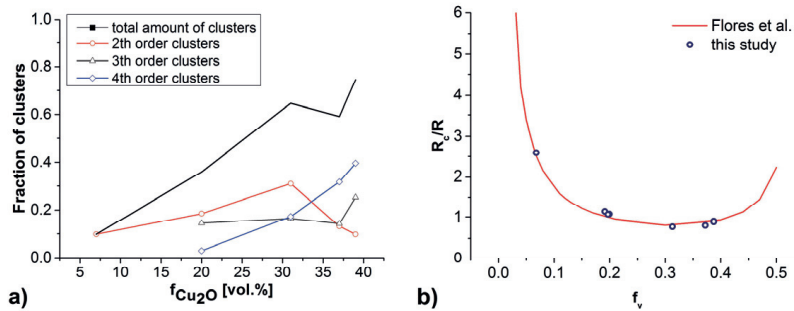


Fig. 3.10. (a) Fraction of clusters present in samples as a function of Cu_2O content and (b) dependence of the R_c/R ratio on the volume fraction of the second-phase as a comparison to the model presented by Flores et al. (2004) [Publication III].

Overall, the hardness closely relates to the grain size of the matrix material and the distribution of the second-phase particles in the matrix. Thus, the effectiveness of the dispersed particles in increasing the hardness depends on their ability to prevent grain growth and to retain the hardness of the matrix material. This is supported by the results presented in Publications II and IV. In Publication II, the samples consisting of clustered Al_2O_3 demonstrated a much lower microhardness than the samples with the same amount of Al_2O_3 but more evenly distributed, the corresponding microhardness values being 0.78 and 1.58 GPa (Table 3.1). Moreover, the results in Publication IV showed a high microhardness of 1.77 GPa

Summary of the Results

for the sample with 6 vol.% of 50 nm diamonds (ND), whereas the sample with less of the same-sized diamonds (3 vol.%) yielded the corresponding value of 1.46 GPa. As the grain size is about the same in both samples, the microhardness difference can be attributed to the different amounts of diamonds. The microhardness values in Table 3.1 also confirm that a high amount of TiB₂ (79 vol.%) leads to the highest microhardness of Cu-TiB₂ composites due to the homogenous distribution of hard TiB₂ grains (Fig. 3.5c). On the whole, the results indicated that the hardness increment was at its highest with a larger amount of homogeneously distributed small-sized dispersoids [Publications II-V].

The yield strength

The yield strengths of the composites were estimated from the hardness measurements by applying the Tabor relation ($H \approx 3\sigma_y$ (Tabor, 1951)). These values were then compared with the theoretical ones (Fig. 3.11) calculated by assuming a simple summation of the single well-established relations given in literature. The contributions of the various strengthening mechanisms considered include: (1) grain size strengthening based on the Hall-Petch (H-P) relation as in Eq. (3.3) (Hall, 1951; Hwang, 2011; Petch, 1953; Tian et al., 2006), (2) dispersion strengthening (DS) based on the Orowan equation (OR) as in Eq. (3.4) (Hwang, 2011; Kocks, 1977; Tian et al., 2006), and (3) the increase in yield stress due to the dislocation pile-up mechanism as in Eq. (3.5) (Guo et al., 2009).

$$\sigma_{HP} \text{ (MPa)} = \sigma_o + k_H d^{-1/2}, \quad (3.3)$$

$$\Delta\sigma_{OR} \text{ (MPa)} = 0.84 (2T / b\lambda), \quad \text{where } \lambda = R (2\pi / 3f_v)^{1/2}, \text{ and} \quad (3.4)$$

$$\Delta\sigma_Y \text{ (MPa)} = [M\mu b\sigma_{TiB_2} / (\pi (1-\nu) (\lambda - 2R(\pi/4)))]^{1/2}, \quad (3.5)$$

where k_H (0.18 MPa m^{1/2}) and σ_o (157 MPa) are material -dependent constants, d is the average grain size, T the line tension (10⁻⁹ N), b the Burgers vector (2.56 x 10⁻¹⁰ m) of the dislocation, f_v the volume fraction, λ the distance between the dispersoids, R their radius, M the Taylor factor of polycrystalline Cu (3.1), μ the shear modulus of the matrix (45.5 GPa), σ_{TiB_2} the fracture strength of TiB₂ phase (0.3 GPa) and ν the Poisson ratio (0.34) of Cu (Guo et al., 2009; Hwang, 2011; Lee et al., 2000; Tian et al., 2006). The Cu grain size as well as the distribution and size of the dispersoids were determined by Image analysis (Image J) to define R , λ and d . Fig. 3.11 presents the contribution of the above-mentioned strengthening mechanism to the final strength, calculated on the basis of the relations (3.3) - (3.5).

The grains of the matrix and dispersoids of over 300 nm in size influence the strength mainly via grain boundary strengthening (Hall-Petch). When the dispersoids are 300 nm or less in size, single dislocations bypass the hard and fine

particles, leaving a dislocation loop behind thus contributing by the Orowan strengthening mechanism (OR). In OR the size and distance between the dispersoids play an important role. When coarse and hard obstacles cannot be bypassed by dislocations, the stress induced dislocation pile-ups form in the neighboring soft grain. This applies for large, hard and stiff TiB_2 dispersoids, which inhibit both dislocation penetration and glide (Guo et al., 2009). On the other hand, the contribution of pile-ups to the strengthening of Cu-Cu₂O is negligible due to the low tensile strength of submicron-sized Cu₂O and as a consequence, the strength of these composites can be explained by the Hall-Petch contribution only. The results in Fig. 3.11 confirm that the measured values correlate well with the theoretical ones with a few exceptions. Even for 79TiB₂ with more TiB₂ than Cu, a rough estimate of the strength by DS is justified. Since there exists a copper connection through the material (Fig. 3.5c), copper acts as a ‘glue’ between the clearly distinguishable TiB₂ phase grains. It is realistic to assume that the properties of the composite with second-phase dispersoids in the matrix are close to those of pure Cu.

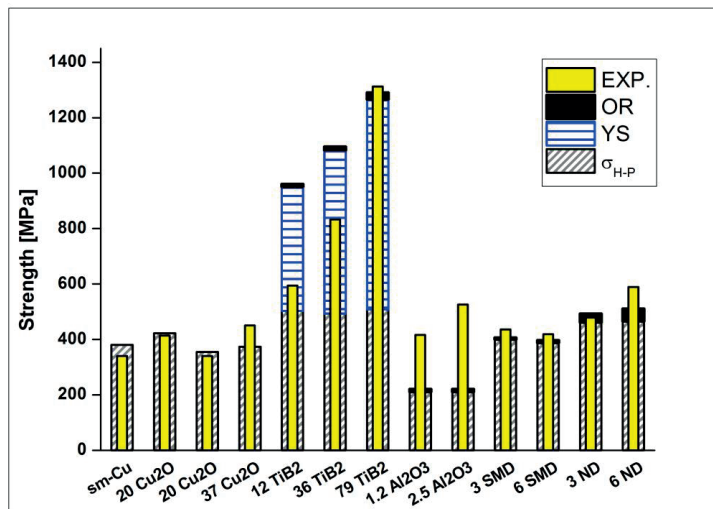


Fig. 3.11. Comparison of the experimental (exp.) and theoretical strengths (stacked bars). The numbers indicate the vol.% of dispersoids [Publication V].

3.2.2 Nanomechanical properties of Cu-composites

Nanoindentation was applied to Cu-Cu₂O, Cu-Al₂O₃ and Cu-SMD samples. The main foci were slightly different depending on the type of the composite:

- (1) Cu-Cu₂O composite: to study the properties of different phases separately,

Summary of the Results

- (2) Cu-Al₂O₃ composites: to verify the notable difference detected in the microhardness measurements for the two different types of composites (IO and Exp.),
- (3) Cu-SMD composites: to separately study the properties of different phases and to verify the strong interface between the matrix and the dispersed particles.

The nanoindented regions of the samples were studied using scanning probe microscopy (SPM) in order to connect the results of the indentation with the respective sample structure.

The SPM image in Fig. 3.12a shows the indent marks on the surface of Sample HIP 3. The measured nanohardness values for both phases, Cu and Cu₂O, ranged between 2.4 and 3.0 GPa on average (with a 250 μ N load) [Publications I and III], whereas the elastic modulus (Young's modulus) ranged between 45 and 73 GPa for Cu₂O and between 133 and 143 GPa for the Cu matrix [Publication III]. Thus, the elastic modulus of the oxide particles was significantly lower than that of the surrounding material. The load displacement curves in Fig. 3.12b also indicate the different mechanical response of the two phases, in which the elastic recovery upon unloading was greater for the lighter Cu₂O particles. A more detailed examination can be found in Publications I and III.

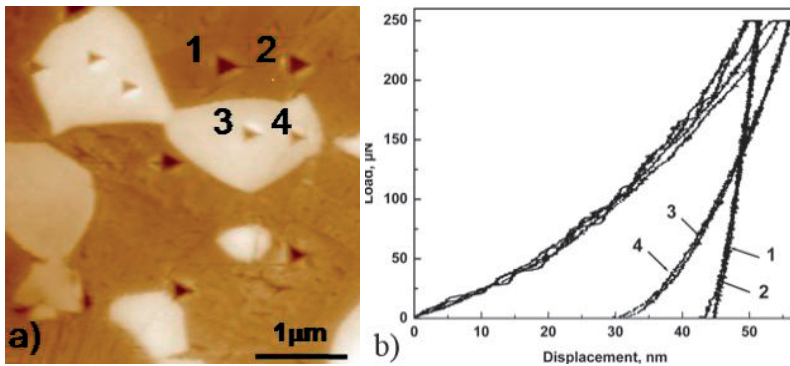


Fig. 3.12. (a) The SPM image after indentation on HIP 3 and (b) the nanoindentation load-displacement curves corresponding to the points in (a) [Publication III].

In the case of Cu-Al₂O₃ composites, three to five locations on the sample surfaces were studied by means of nanoindentation [Publication II, Fig. 3]. The nanohardness results support the microhardness values, verifying that the samples compacted from the commercial IO powders were evidently harder (3.1 and 3.8 GPa) than those made from the Exp. powder (2.3 and 2.6 GPa), the higher values

referring to the samples with the higher amount of Al_2O_3 . The average elastic moduli were also higher for samples made from IO powders (144 and 154 GPa) than for those made from Exp. powder (127 and 138 GPa). More details can be found in Publication II.

Fig. 3.13a is an example of the scanning probe microscopy (SPM) image for a sample of Cu with 6 vol.% submicron-sized diamonds (6SMD). It shows the marks from a (3 x 4) indent pattern and also the dispersed diamonds on the sample surface. Fig. 3.13b shows the load vs. displacement curves for the three indicated indents in Fig. 3.13a. The indentation curve 1 and the corresponding properties, i.e. high hardness (52 GPa) and elastic modulus (568 GPa), are close to those reported for diamond in nanoindentation studies (Couvry et al., 2011; Richter et al., 2000; Yanchuk et al., 2004). The shape of indentation curve 3 is almost that of a Cu matrix (Fig. 3.12), with a somewhat higher hardness (4 GPa) and elastic modulus (172 GPa) obviously due to the influence of nearby diamonds. Indentation curve 2 is made from the boundary of the matrix and diamonds and is influenced by both phases. It shows the value of 9 GPa for the hardness and 204 GPa for the elastic modulus, both being notably higher than those for Cu (2.4 - 3.0 GPa and 119 - 143 GPa) [Publications I and III]. In the SEM study of the indents, no cracking of interfaces could be observed [Publication IV].

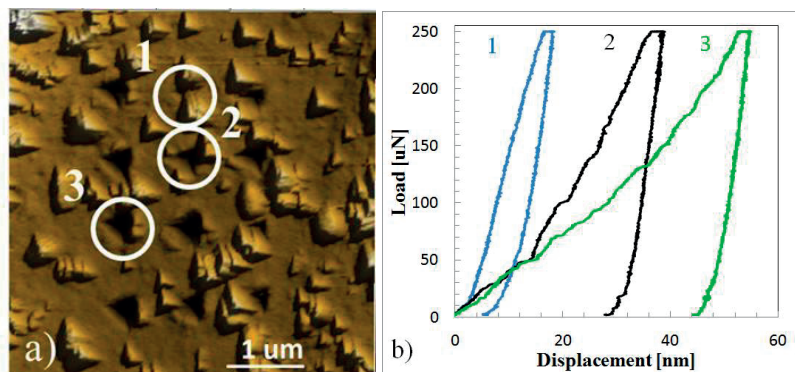


Fig. 3.13. (a) An SPM image of sample 6SMD (Cu with 6 vol.% submicron-sized diamonds) showing elevated lighter formations (diamonds) above the polished surface and marks from the (3 x 4) indent pattern and (b) the load vs. displacement curves for the indicated indents shown in (a) [Publication IV].

3.3 Thermal stability and thermal expansion of Cu-composites

In general, the softening temperature corresponds to the temperature, which leads to the hardness loss of 20% during heating (Liang & Fan, 1999). The microhardness values (HV1) were measured both before and after heat treatment to reveal the resistance against thermal softening. In Fig. 3.14, 'PECS' denotes the

microhardness values (GPa) of the samples before the treatment, whereas the temperatures (623, 873 and 1023 K) denote the microhardness values after the treatments at the indicated temperatures. This demonstrates that for sm-Cu the softening temperature is about 673 K (as in Tian et al., 2006). For Cu-ND, Cu-SMD and Cu-Cu₂O the softening temperatures are below or around 873 K, depending on the size and content of the dispersoids. In contrast, the softening temperatures are much higher for Cu-Al₂O₃ and Cu-TiB₂, i.e., above 1023 K. [Publications II, IV and V]

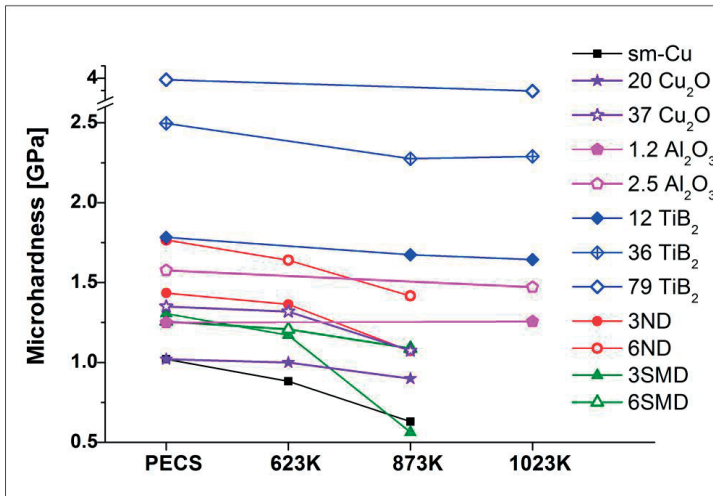


Fig. 3.14. Influence of one-hour (1h) heat treatment on the hardness of the compacts [Publication V].

Similar to thermal softening, the high values of the coefficient of thermal expansion (CTE) are characteristic of pure copper (Groza, 1992; Nadkarni & Synk, 1984; Tian et al., 2006). In order to decrease the high CTE of plain Cu, particles with lower CTE can be introduced to the matrix (Groza, 1992; Nadkarni & Synk, 1984; Tian et al., 2006). Fig. 3.15 demonstrates how the additions of Cu₂O, Al₂O₃, TiB₂ and diamond can theoretically decrease the CTEs as a function of the volumetric amount (Turner, 1946). The experimental values in Fig. 3.15 reveal the change in CTEs as the temperature is increased, starting from 473 K (200 °C). The numbers denote the samples; (1) sm-Cu, (2) Cu, (3) Cu-Cu₂O, (4) Cu-TiB₂, (5) Cu-Al₂O₃, (6) Cu-SMD and (7) Cu-ND. Fig. 3.15 confirms that sm-Cu presents a larger variation of CTE in comparison to coarse Cu as the temperature is increased. The same applies to Cu-diamond samples with a lower amount of diamonds (3 vol.%), as compared to the samples with a higher amount (6 vol.%). The most notable differences in the thermal expansion coefficients can be observed for the Cu-Cu₂O samples; at higher temperatures the CTE values are increased. On the other hand, Cu-Al₂O₃ (IO) and Cu-TiB₂ show stable CTEs at higher temperatures.

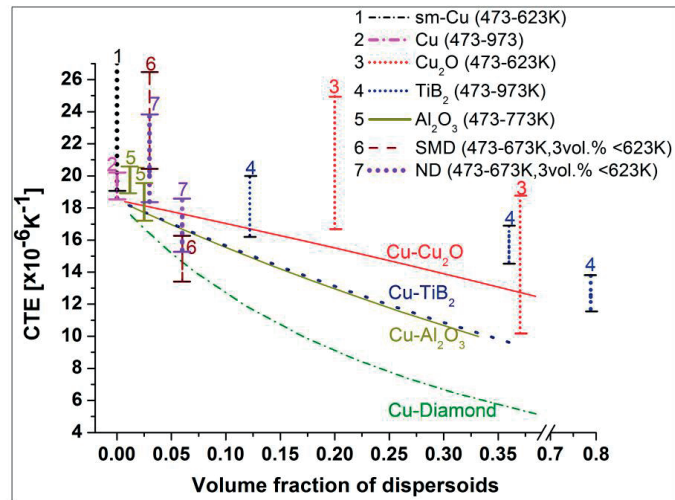


Fig. 3.15. The measured CTE values between the marked temperature ranges and the theoretical predictions based on Eq. (1.8) [Publication V].

3.4 Electrical properties

Since copper possesses high electric conductivity, the dispersed particles most often decrease the conductivity. Among others, the type of dispersed particles, their size, their distribution and amount, as well as any impurities and porosities have a major effect on the electrical properties of composites, as pointed out earlier. In the present study [Publication V], the measured electrical conductivity values (%IACS) of both types of Cu-Al₂O₃ (IO) and Cu-Al₂O₃ (Exp.) samples varied between 78.8 and 92.6%IACS. Similar conductivities were measured for Cu-diamond composites, ranging from 77.8 to 87.3%IACS. Both the above-mentioned composites contained small amounts (few vol.%) of electrically non-conductive dispersoids. On the other hand, Cu₂O and TiB₂ are more electrically conductive dispersoids, and even with a relatively large amount (≥ 10 vol.%) of these dispersoids, the composites have sufficient electrical conductivity. For instance, the results revealed that the 37Cu₂O and 36TiB₂ samples show about 45%IACS, the values showing a decreasing trend for increasing amounts of dispersoids.

3.5 Friction and wear properties of Cu-composites

The friction coefficients were recorded during reciprocating sliding tests consisting of 3,000 cycles. When the test materials were sliding against a Cr-steel ball, notable fluctuations were observed and a considerable time was needed to reach the steady state CoF value [Fig. 1a in Publication VI]. It seemed that the CoF values converged at the end of the tests closer to the CoF values of the copper samples, thus, the copper matrix dominated and the type or amount of the

Summary of the Results

dispersoids had a lesser influence. On the contrary, while sliding against alumina balls smoother sliding and low CoFs were observed and the steady state was reached faster [Fig. 1b in Publication VI]. The difference in the CoF values remained large and relatively stable throughout the test, and thus the type of dispersoids had a notable effect. In both cases, the highest CoF values at the end of the tests were for 79TiB₂ samples and lowest for 37Cu₂O samples. Fig. 3.16 presents the average steady state friction coefficients taken from the stable region (i.e. between 400 s and 600 s of the test) as a function of dispersoid content (vol.%). Typically 0.2 - 0.4 higher CoFs were found against Cr-steel than against alumina. When sliding against the Cr-steel counterpart, the increased fraction of Cu₂O decreased the CoFs, whereas for other composites the trend was opposite. The trends were similar when sliding against alumina, except for Cu with 5 nm diamonds (nanoD), which had a CoF similar to sm-Cu, and sample 1.2Al₂O₃ (IO) with a low CoF.

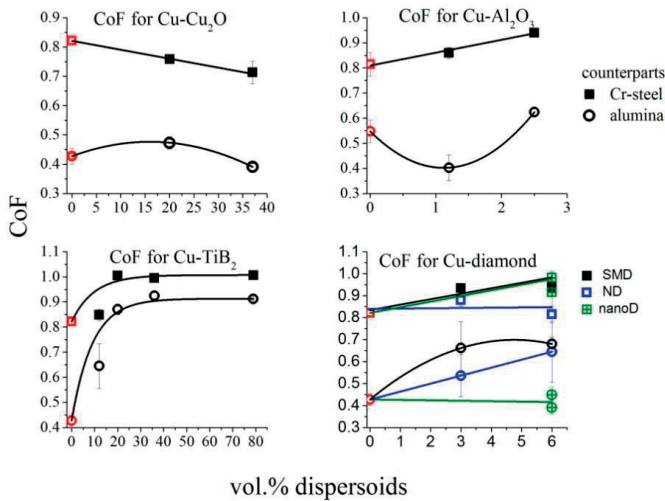


Fig. 3.16. The steady state coefficient of friction (CoF) as a function of vol.% dispersoids against Cr-steel and alumina counter balls. Note that the scales are different. The red marks are reference values for Cu (c-Cu for Cu-Al₂O₃ composites, and sm-Cu for others) [Publication VI].

The size of the wear tracks was much wider when sliding against Cr-steel than against alumina. Similarly, much higher CoFs were detected against Cr-steel than against alumina. Fig. 3.17 presents the optical images of the wear tracks for the samples c-Cu, 37Cu₂O and 6ND after sliding against alumina (upper images), against Cr-steel (middle images), and the Cr-steel ball surfaces after sliding (lower images). Oxidational wear plays the most significant role when the test samples were sliding against ceramic alumina balls (e.g. upper images in Fig. 3.17), thus

inducing smooth and slight wear tracks [Figs. 3 and 5 in Publication VI]. On the other hand, both oxidational and abrasive wear led to somewhat wider tracks for c-Cu (middle image in Fig. 3.17a), sm-Cu, Cu-Cu₂O (middle image in Fig. 3.17b) and Cu with ≥ 20 vol.% TiB₂ [Figs. 3, 4, 6 and Table 2 in Publication VI]. However, the most notable wear was caused by adhesion, which was the main reason for wide wear tracks found for Cu-Al₂O₃ and Cu-diamond (middle image in Fig. 3.17c) after sliding against Cr-steel [Figs. 3 and 6 and Table 2 in Publication VI]. The optical image taken from the Cr-steel ball surface after the test with 6ND verifies the adhesive wear with pile-ups of copper on the ball surface (lower image in Fig. 3.17c). In comparison, the ball surfaces with furrows and some wear debris at the end of furrows after the tests with c-Cu and 37Cu₂O indicate abrasive wear (lower images in Figs. 3.17a-b).

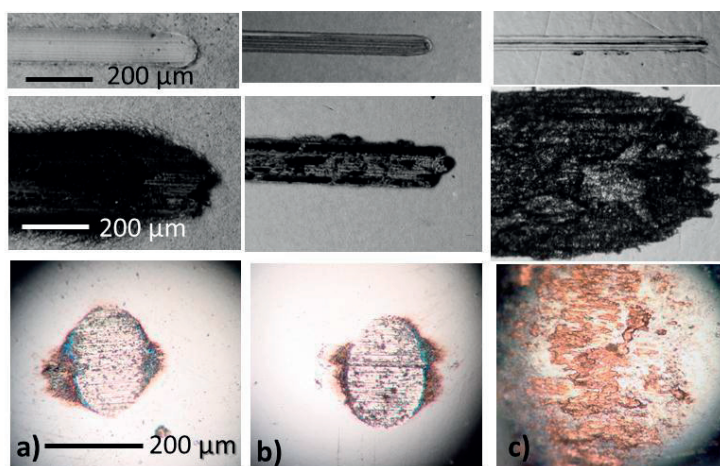


Fig. 3.17. Optical images for (a) c-Cu, (b) 37Cu₂O, and (c) 6ND showing wear tracks after sliding against alumina (upper images) and Cr-steel (middle images), as well as ball surfaces after sliding against Cr-steel (lower images).

The wear profiles in Fig. 3.18 support the optical observations revealing extensive wear against Cr-steel compared to the smooth profiles and only slight wear against alumina. The depth of wear tracks in the samples after sliding against Cr-steel were much greater in 2.5Al₂O₃, 12TiB₂ and 6ND samples than in c-Cu, whereas in sm-Cu, 37Cu₂O and 79TiB₂ samples, the depths were clearly smaller. Also, the wear rates and plots in Fig. 3.19 (logarithmic scale) indicate higher wear rates of samples after sliding against the Cr-steel ball when compared to those sliding against the alumina ball. The increase in Cu₂O content decreased the wear rate against Cr-steel, whereas the addition of Al₂O₃ or diamonds obviously increased wear as compared to pure sm-Cu. The sample 12TiB₂ showed a high wear rate against the Cr-steel counter material, although decreasing wear rate was observed

Summary of the Results

when the content of TiB_2 increased. Overall, the materials studied had high wear rates between 1.3×10^{-5} and $5.7 \times 10^{-3} \text{ mm}^3/\text{Nm}$ against Cr-steel [Table 2 in Publication VI].

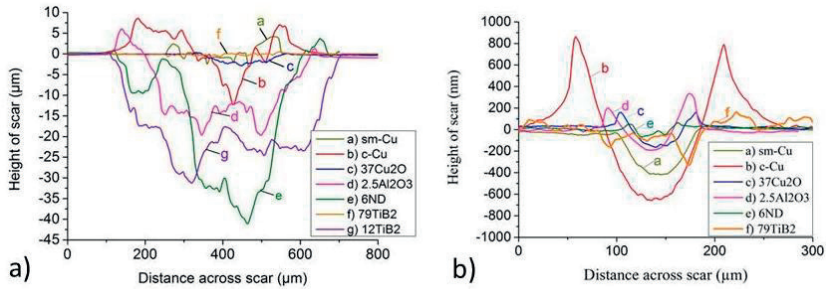


Fig. 3.18. Typical wear profiles of the tracks made by (a) the Cr-steel and (b) the alumina counter ball [Publication VI].

The increasing amount of dispersoids showed a tendency to decrease the wear rates against alumina as compared to the corresponding bare Cu samples. Overall, oxidative wear led to rather low wear rates between 1.4×10^{-7} and $6.1 \times 10^{-6} \text{ mm}^3/\text{Nm}$ against alumina [Table 2 in Publication VI]. The lowest wear rate was measured for Cu-diamond composites. A more detailed description of the observed wear mechanisms can be found in Publication IV.

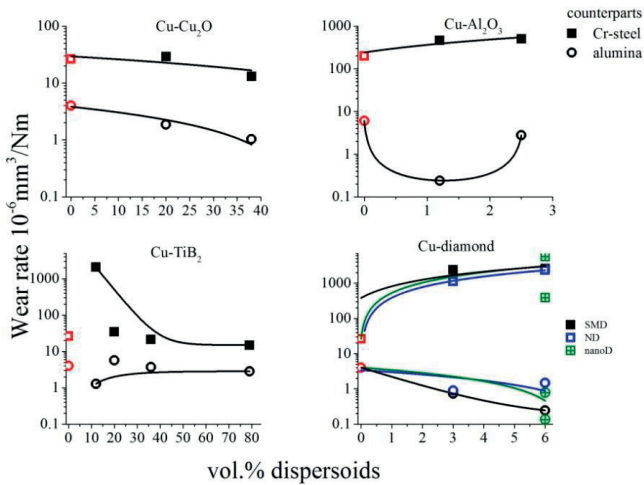


Fig. 3.19. Logarithmic presentation of the wear rates as a function of vol.% dispersoids against Cr-steel and alumina. The reference Cu values are marked as red (values of c-Cu for $\text{Cu-Al}_2\text{O}_3$ composites due to the coarse matrix and sm-Cu for others) [Publication VI].

4. Discussion

4.1 Densification of Cu-composite powders

The consolidation by PECS resulted in highly dense materials close to the theoretical densities (T.D.). According to Table 3.1, c-Cu, Cu-Cu₂O, Cu-Al₂O₃ and Cu-TiB₂ (≤ 36 vol.% TiB₂) samples reached densities of over 98% of T.D., and Cu-diamond and sm-Cu samples over 97% of T.D. Only the sample with the highest amount of TiB₂, i.e., 79TiB₂, and the sample of n-Cu with nanodiamonds (5 nm) resulted in a low density, i.e., 94.3% and 90.1% of T.D. at best, correspondingly.

Cu and Cu-based powders can be consolidated with various sintering methods. Dense materials have been achieved e.g., with PECS and HIPing. While a high holding temperature together with high pressure assists densification (Orrù et al., 2009; Tokita, 2013; Yanagisawa et al., 1997), the maximum pressure in PECS is limited by the strength of the graphite mold (Munir et al., 2011; Orrù et al., 2009; Ragulya, 2010) and the maximum temperature by the melting point of copper. Additionally, the temperature increase from the optimal can cause grain growth and thus decrease the strength (Zhang et al., 2008 & 2009). Fig. 4 and Table 2 in Publication I demonstrate that the higher the PECS temperature, the more noticeable the grain growth along with a lower microhardness of Cu-Cu₂O composites, while there is not necessarily a systematic increase in the density with an increase of the hold temperature. Nevertheless, since the compact densities were from 97.6 to 99.7% of T.D., it can be concluded that the presence of Cu₂O has no significant effect on the powder consolidation [Publications I and III].

With HIPing, the densities of the Cu-Cu₂O composite samples ranged from 93.0 to 99.1% of T.D. depending on the holding time and temperature. To reach the highest density (99.1%), the holding time needed was 120 min at 1073 K, while 30 min at the same temperature led to only 95.1% of T.D. The long holding time needed for proper densification with HIPing is well documented (Helle et al., 1985; Meyer & Wadley, 1992; Newman, 1992; Kondo et al., 2005; Kováčik et al., 2008; Olevsky et al., 1998; Tjong & Lau, 2000). The main differences between HIP and PECS include the heating technique and the heating rate and thus, subsequently, the diffusion and densification mechanisms. The imposition of an electrical

current/field during PECS provides a number of advantages. The field activation enhances, for example, the sintering kinetics and material transfer towards the neck area. It can also accommodate the thermal and electrical breakdown phenomena, enhance electrotransport, facilitate interparticle bonding, and the coupling of field, temperature and pressure effects. These phenomena promote higher densities at lower temperatures and/or shorter processing times than the conventional sintering methods (Groza & Zavaliangos, 2000), e.g., HIPing.

The low density of 94.3% of T.D. for the 79TiB₂ sample after PECS could have been caused by a too low temperature for proper densification of TiB₂ (Jin et al., 2005). On the other hand, a higher temperature could have melted the Cu matrix. Nevertheless, this density value correlates well with those reported, e.g., by Kwon et al. (2006) ranging from 90.3% to 95.5% of T.D. for Cu with 2.5 - 10 wt.% (~ 5 - 18 vol.%) TiB₂. Generally, with a lower TiB₂ content there is enough Cu to fill the pores during sintering, thus leading to higher densities (Jin et al., 2005) than with higher amounts of TiB₂ (Jin et al., 2005; Kwon et al., 2006; Yih & Chung, 1997).

For Cu-diamond composites, the highest holding temperatures applied led to a slight expansion in samples resulting in lower densities. On the other hand, with the optimum parameters the densities were over 97% of T.D. for Cu-ND and Cu-SMD samples. The low density of the nCu-6nanoD (40 nm-sized n-Cu with 6 vol.% of 5 nm-sized diamonds) sample could have arisen from the nature of the powder. The powder was likely to contain diamond agglomerates, which may result in interagglomerate pores or entrapped gases after evaporation due to adsorbed moisture on the diamonds. The sample having a n-Cu matrix also contained stabilizing agents on the particle surfaces and this may not have been fully removed during PECS, resulting in entrapped gases. The sample of Cu-6nanoD (sm-Cu matrix with 6 vol.% of 5 nm-sized diamonds) yielded a much higher density of 97.2% of T.D. In this case, the Cu powder was not treated with a stabilization agent, and additionally, the diamond powder was heated up to 773 K (500 °C) to remove any moisture before milling the powder mixture.

4.2 Influence of the dispersoids on the hardness and grain growth

4.2.1 Microhardness

The Cu₂O, Al₂O₃, TiB₂ and diamond dispersoids were found to noticeably improve, at room temperature, the mechanical properties of copper as compared to plain sm-Cu (Table 3.1). The effectiveness of the reinforcement type, size and amount was studied in Publication V.

The microhardness values of Cu-Cu₂O (1.02 - 1.35 GPa) composites by PECS were much higher than that of fully-annealed copper (0.39 - 0.50 GPa) (García et

al., 2008; Han et al., 2006) or even cold-worked pure copper (0.98 GPa) (MatWebTM). It was also evident that the PECS samples were somewhat harder than the HIPed samples (0.94 - 1.07 GPa), the difference being mostly attributed to the finer grain size in PECS compacts due to the shorter process time. It is proposed that one of the main reasons for high hardness is the fine grain size maintained during the PECS process. Another factor suggested is the amount of Cu₂O particles distributed in the Cu matrix. The hardness grew with an increasing amount of Cu₂O. For example, with the same grain size and density, a composite with about double the amount of cuprite (i.e. 37.2 vs. 19.7 vol.% Cu₂O) was 20% harder [Table 2 in Publication III]. In Fig. 3.9., the microhardness values of the Cu-Cu₂O composites are compared to those reported for pure n-Cu. This confirms that the Cu₂O secondary-phase in Cu matrix can markedly increase the hardness of Cu at a fixed grain size level.

For Cu-Al₂O₃ composites, there exists a notable difference in the microhardness values measured from compacts made of commercial IO powders, as compared to those made of Exp. powders synthesized by a chemical method. With the same amount of 2.5 vol.% alumina in a bulk sample, the former yielded a microhardness (1.58 GPa) two times higher than the latter (0.78 GPa), even though the Cu grain size was smaller in the Exp. compact. The overall difference in hardness can be attributed to the size and distribution of alumina in the compacts. The fine and more evenly distributed Al₂O₃ in IO compacts clearly resulted in a higher hardness than those in Exp. compacts, in which the alumina was more segregated at the grain boundaries [Publication II]. These agglomerated regions of alumina were verified with SEM and TEM studies, whereas isolated Al₂O₃ was observed in the IO samples (Figs. 3.3 and 3.4). The results are in line with those obtained by PECS and conventional compaction methods (Fathy et al., 2012; Ferkel, 1999; Nachum et al., 2010; Rajkovic et al., 2008; Vencl et al., 2013). However, it is noteworthy to point out that the hardness values in literature present quite large variations depending on the powder processing and compaction methods, as well as on the amount and size of reinforcement; i.e., values from 0.79 to 2.60 GPa have been reported (Dash et al., 2012; Hwang, 2011; Ferkel, 1999; Nachum et al., 2010; Tian et al., 2006; Vencl et al., 2013). Similar to Al₂O₃ strengthened Cu-composites, the nanodiamonds (ND) were more effective reinforcements than the submicron-sized diamonds (SMD). Both composites clearly reveal higher values than the bare sm-Cu (1.02 GPa) [Publication IV]. The increasing amount of ND also resulted in improvements in the microhardness, i.e., 1.77 GPa for 6ND as compared to 1.46 GPa for 3ND. The slightly smaller Cu grain size explains the higher hardness of compact 3SMD (H = 1.31 GPa) than that of 6SMD (H = 1.26 GPa), even if the amount of dispersoids was half as much in the former as compared to the latter (see

Table 3.1). The present Cu-diamond composites, without the addition of carbide forming elements, show that high hardness values can be obtained by PECS.

Overall, the smaller size and higher amount of dispersoids were beneficial in increasing the hardness (Table 3.1). The small and evenly distributed hard particles act as reinforcing phases being obstacles to the movement of dislocations (Ferkel, 1999; Rajkovic et al., 2008; Tian et al., 2006). The non-coarsening and fine Al_2O_3 and diamond particles showed the highest capability in hardness increment. For example, the microhardness for the reference sm-Cu sample, 3ND, 6ND, $2.5\text{Al}_2\text{O}_3$ (IO) were 1.02, 1.43, 1.77 and 1.58 GPa, respectively. The highest microhardness values (from 1.78 GPa up to 3.94 GPa) were, however, obtained for Cu- TiB_2 due to the high amount (from 12 up to 79 vol.% TiB_2) of hard and non-coarsening TiB_2 . Regarding the large amount of Cu_2O (6.8 - 38.7 vol.%), its capability in increasing the hardness of sm-Cu falls clearly behind the above-mentioned composites due to the greater size, lower hardness, and the coarsening tendency of Cu_2O .

4.2.2 Grain growth

Grain size is closely related to the hardness of materials, as the Hall-Petch relation (Eq. (1.1)) announces. It has also been widely reported that the dispersed non-coarsening particles have a great potential in controlling grain growth during consolidation and in further treatments. However, not as much attention has been addressed to the grain growth of the matrix in the presence of particles with a tendency to coarsening. To study this phenomenon, the grain size and grain growth of Cu and Cu_2O were analyzed separately in PECS and HIP compacts.

The initial particle size of Cu, with an oxide layer surrounding it, was on average 410 nm [Fig. 1 in Publication I]. The lowest temperature applied by PECS resulted in an average grain size of 460 nm (Fig. 3.1a), which shows only a slight increase from the initial powder size. The higher sintering temperature in PECS led to larger grain size in the samples, which, however, still remained much smaller than in the HIPed samples. The overall results also confirm that the distributed Cu_2O in a Cu matrix has a function in preventing grain growth. This is evident from Fig. 3.2, where the grain growth of the composite is compared to that of pure Cu. The Cu- Cu_2O compacts clearly show less grain growth than pure Cu, especially at high temperatures. This observation is in agreement with earlier studies (García et al., 2008; Wood, 1957; Zhang et al., 2008). However, based on the results and observations depicted in Figs. 1 - 3 in Publication III, the smallest amount of Cu_2O might not have prevented the growth of Cu grains as effectively as when the Cu_2O volume fraction was about 20 vol.% or more. The results also verify that the Cu_2O phase prevented the grain growth in the HIPed composites. Even at a high

temperature (1073 K) the grain growth factor was 4.54, which is much smaller than that between 13 and 25 predicted for pure copper at 800 K by HIP simulations (Meyer & Wadley, 1992; Newman, 1992).

4.2.3 Strengthening

The overall strength of each type of composite can be attributed to the fine grain size and dispersoids of 300 nm or less due to the Hall-Petch and Orowan strengthening (Results, section 3.2.1). The hard and over 300 nm-sized dispersoids also play a noticeable role in the yield stress increment of Cu-TiB₂ composites, as pointed out earlier by Lee et al. (2000) and Guo et al. (2009). By comparison of the experimental strengths calculated using Tabor's rule $HV \approx 3\sigma$ (Tabor, 1951) with the theoretical calculations (Eq. (3.3) - (3.5)) shown in Fig. 3.11, the following observations can be presented: (i) the experimental strengths are close to the theoretical expectations for sm-Cu, Cu-Cu₂O, Cu-diamond and Cu - 79 vol.% TiB₂, (ii) a clear difference between the experimental and theoretical strengths can be noticed for Cu-Al₂O₃ and Cu - 12 vol.% TiB₂ samples. For the Cu - 12 vol.% TiB₂ composite, the somewhat inhomogeneous dispersion of TiB₂ due to the combined method of SHS and MA can explain the difference between the experimental and theoretical values presented in Fig. 3.11. The unevenly distributed dispersoids in the matrix can lead to early deformation of the matrix at a lower stress (Akbarpour et al., 2013). For Cu-Al₂O₃ the contribution of strengthening, resulting from the residual plastic strain due to the thermal mismatch (CTEs) between Al₂O₃ particles and the Cu matrix during post-processing cooling has been proposed, e.g., by Eddine et al. (2013). In their calculations, the difference in CTE values between the constituents, the difference between the processing and measuring temperature, and the content and size of reinforcements were taken into account. However, calculations based on the present data indicate that the thermal mismatch difference can not explain the strengthening in such a straightforward way. On the other hand, Tian et al. (2006) have suggested that internally oxidized Cu-Al₂O₃ composites may also have other strengthening mechanisms involved, e.g., interface strengthening, the strong pinning effect of extremely small (10 - 30 nm) nano-Al₂O₃ and sub-grain boundaries. In the current work, the observed high strength is suggested to result from: (i) the higher amount of small nano-Al₂O₃ in compacted samples, and (ii) the notable amount of twins present in the Cu matrix. Cu-Al₂O₃ (Exp.) resulted in a much lower strength than Cu-Al₂O₃ (IO) because of coarser and agglomerated Al₂O₃. Akbarpour et al. (2013) have stated that reinforcements with a smaller size lead to smaller distances between dispersoids than the coarser/segregated dispersoids at the grain boundaries. As a consequence, smaller reinforcements are more effective in enhancing the strength and restricting the grain growth.

The observed strength of the experimental materials as a function of the copper grain size is depicted in Fig. 4.1. The base line (grain size dependence of the strength of pure copper) has been selected based on Khan et al. (2008), which was also found to accurately describe the strength of pure copper in the current work (see, Fig. 3.9). The arrows indicate how the Cu grain size and strength are affected by the presence of dispersed particles in the final Cu-composites as compared to the initial Cu-powder grain sizes with strengths assumed by the base line (Khan et al., 2008). Based on the data shown in Fig. 4.1, it is evident that with a higher amount of dispersoids: (i) a smaller Cu grain size can be retained due to a more effective restriction of grain growth, (ii) the overall strength is contributed by the amount and size of reinforcements, and (iii) all the reinforcements clearly improve the strength as compared to pure reference Cu by Khan et al. (2008). The arrows in Fig. 4.1. indicate the strengthening effect of reinforcements as compared to plain Cu.

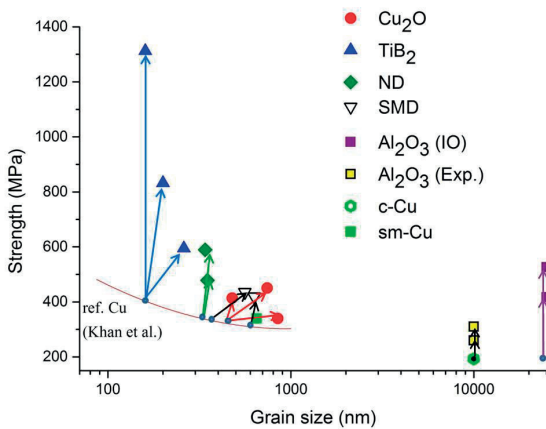


Fig. 4.1. Contribution of the reinforcements to the strength of Cu. Reference values for Cu have been taken from Khan et al. (2008).

4.2.4 Nanomechanical properties

The low load nanoindentation measurements made it possible to obtain information from a more confined region to reveal, for e.g., the nanohardness and elastic properties of the desired phases.

In the nanoindentation studies the Cu₂O phase, with a white and irregular-shaped appearance in the SPM image (Fig. 3.12a), turned out to have about the same hardness as the surrounding material (both between 2.4 and 3.0 GPa) [Fig. 5c in Publication I and Table 3 in Publication III]. The nanohardness of the Cu matrix is at the same level as the values reported for Cu with a 500 nm grain size and a highly-twinned structure (2.0 - 2.6 GPa) (Lu et al., 2005) or for pure Cu with a 100

nm grain size (2.42 GPa) (Srivatsan et al., 2001). Thus, it is clearly higher than those of Cu with a 500 nm grain size with a low-twinned structure (1.7 - 2.0 GPa) or a non-twinned structure (1.4 - 1.6 GPa) (Lu et al., 2005), and also higher than that of an ECAP processed Cu with a 190 nm grain size (1.67 GPa) (Chen et al. 2006). For comparison, the microhardness of Cu_2O is between 1.8 GPa and 2.2 GPa (Anthony et al., 1995). It is also evident that the apparent nanohardness of the matrix is somewhat higher when the indentation load is decreased from 1 mN to 0.25 mN [Table 3 in Publication I]. The hardness increase along with a decreasing indentation depth is typical of the indentation size effect (Hannula et al., 2004; Nachum et al., 2010). Overall, the high nanohardness value is consistent with high microhardness values.

Even with similar nanohardness values, the load-displacement curves in Fig. 3.12b demonstrate a clear difference in the elastic behavior of Cu and Cu_2O . For the Cu matrix, the elastic recovery upon unloading is small resulting in large indent marks and near-vertical unloading curves. The elastic recovery of the Cu_2O phase is comparably higher revealing more inclined unloading curves, thus resulting in smaller indent marks. The higher-than-actual elastic modulus measured from the Cu_2O phase can be explained by the influence of the surrounding Cu with a higher modulus. More precisely placed indents on large Cu_2O particles in the HIP 3 Sample yielded values closer to its bulk value [Table 3 in Publication III].

In the case of Cu- Al_2O_3 composites the ratio of the nanohardness values (3.8 GPa and 2.3 GPa for $2.5\text{Al}_2\text{O}_3$ (IO) and $2.5\text{Al}_2\text{O}_3$ (Exp.), respectively) was clearly smaller than that of the microhardness values (1.58 GPa and 0.78 GPa for $2.5\text{Al}_2\text{O}_3$ (IO) and $2.5\text{Al}_2\text{O}_3$ (Exp.), respectively). This indicates that the local difference within the two materials is less than the overall difference in hardness of the starting materials. This difference may arise, in addition to the intrinsic property variation from point to point over the sample surface, for several other reasons, including the different scales applied, the indentation size effects, and the existence of hardened surface layers. Because nanohardness represents a material property of small volumes, it is sensitive to local microstructural features, such as local particle densities and even surface roughness. These are expected when explaining the large data scattering found in nanoindentation [Publication II]. Similar scattering was observed by Nachum et al. (2010). Additionally, they noticed pronounced size effects with different indentation depths, e.g., in Cu - 1 vol.% Al_2O_3 , the hardness almost doubled when the contact depth was reduced from 1 μm (1.3 - 1.4 GPa measured with Vickers) to 0.1 μm (2.3 - 3.5 GPa measured with nanoindentation). The composite with 5 vol.% Al_2O_3 yielded a microhardness of 2.2 - 2.35 GPa, whereas the nanohardness resulted in a wide variety of values between 2.8 and 4.3 GPa. The difference between the microhardness and nanohardness (from one of the

test setups of the present study) for selected samples in Fig. 4.2 reveals a notable scattering in nanohardness. This difference might be caused by the variations arising from hard particles, grain boundary areas, pores, surface roughness, etc.

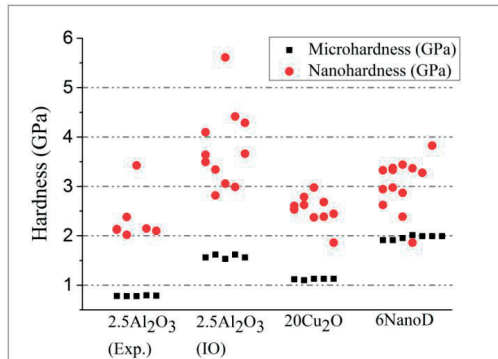


Fig. 4.2. Comparison of micro- and nanohardness values for selected samples.

The modulus values obtained in the present study are close to the results reported earlier for both Cu and Cu-Al₂O₃, which lie between 115 and 150 GPa (Eddine et al., 2013; Nachum et al., 2010; Nadkarni & Synk, 1984). Since DS copper contains small amounts of aluminium oxide as discrete particles in an essentially pure Cu matrix, its physical properties, e.g., the modulus of elasticity is expected to resemble that of pure copper (Nadkarni & Synk, 1984).

The indentation curves for the 6SMD sample in Fig. 3.13 clearly show the different behaviour of Cu, diamond, and the boundary area of the matrix and a diamond particle. It is noteworthy that all the curves have a similar initial loading path in Fig. 3.13b. Thus, the copper matrix has an influence on each of the curves resulting in somewhat lower analyzed values, e.g., such as with diamonds, as compared to its actual values. With high nanohardness (52 GPa at indent depth of 15 nm) and an elastic modulus of 568 GPa, with only minor plastic deformation observed in the indentation curve 1 (Fig. 3.13b), this approaches the values reported earlier for diamond; i.e., the nanohardness between 30 and 62 GPa and modulus between 400 and 707 GPa (Couvry et al., 2011; Yanchuk et al., 2004). The load-displacement curves of diamond by Couvry et al. (2011) and Richter et al. (2000) illustrated that in loading, the indent depths were less than 10 nm and about 15 nm, respectively, when the load was 250 μ N. Their results are close to the ones obtained from the measurement presented in Fig. 3.13. The nanohardness and elastic modulus values are higher for Cu in Cu-diamond compacts than for plain Cu due to the influence of nearby diamonds. During indentations no cracking and almost no pull-outs were noticed, indicating a good bonding between the phases.

4.3 Thermal properties of Cu MMCs

4.3.1 Thermal stability

Ultrafine-grained Cu is usually unstable when exposed to moderate temperatures as a result of recovery of the dislocation structure and grain growth (Akbarpour et al., 2013; Vencl et al., 2013). There is a lack of thermal stability at temperatures higher than the temperature range of the primary recrystallization 448 - 523 K (175 - 250 °C) (Lebedev et al., 1996). To enhance the resistance against softening, the introduction of stable particles was found to be an appropriate way (Tian et al., 2006; Vencl et al., 2013).

The results in Fig. 3.14 illustrate how the size and amount of different types of dispersoids influence the softening resistance of Cu-composites. It should be noted, that the softening temperature for sm-Cu and 3SMD was about 673 K (400 °C), whereas for 3ND, 6ND, 6SMD and Cu-Cu₂O composites it was estimated to be roughly around 823 - 873 K (550 - 600 °C) [Publications IV and V]. In contrast, Cu-Al₂O₃ (IO) and Cu-TiB₂ composites showed almost no softening below 1023 K (850 °C). Overall, these results agree quite well with those reported. The softening temperature of 673 K (400 °C) for sm-Cu in the present study falls between the softening range of 448 K and 673 K (175 °C and 400 °C) reported by Lebedev et al. (1996), Liang & Fan (1999), and Tian et al. (2006). Additionally, the present study revealed that the samples with nanodiamonds (3ND and 6 ND) or the sample with a higher amount of submicron-sized diamonds (6SMD) retained their hardness much better than the sample with less submicron-sized diamonds (3SMD). Earlier He et al. (2008) have shown that the amount of nanodiamonds affects the softening temperature. This varies from about 673 to 873 K (400 to 600 °C), the range corresponding to Cu - 1 wt.% (2.5 vol.%) ND, Cu - 3 wt.% (7.3 vol.%) and Cu - 8 wt.% (18.2 vol.%) ND. The longer interparticle distance between the dispersed diamonds may lead to an insufficient prevention of grain growth, subsequently resulting in softening. For example, 3SMD had a much smaller Cu-powder size after milling (340 nm) than that of 6SMD (595 nm), whereas the corresponding grain sizes of 560 and 630 nm after PECS indicated a notable grain growth for sample 3SMD. On the contrary, the other samples (6SMD, 3ND and 6ND) with more and/or finer diamonds resulted in only about a 25 - 45 nm increase in grain size in PECS as compared to that of the starting powder. This indicated a more significant grain growth control and thermal stability [Publication IV].

Kim et al. (2006) and Ferkel (1999) reported that Cu - 4.5 vol.% TiB₂ and Cu - 3 vol.% nano-Al₂O₃ composites can resist softening up to 1173 K (900 °C). These results are well in line with the present study and those reported by Tian et al. (2006), Vencl et al. (2013), and Liang & Fan (1999). In Publication II, it was

shown that the softening behaviour of Cu-Al₂O₃ composites depended on the size of Al₂O₃ dispersoids. Finely dispersed Al₂O₃, clearly retains hardness better than larger/agglomerated dispersoids (Fig. 5a in Publication II). This is due to the dependence of the pinning effect on grain boundaries on dispersoid spacing. Hence, copper grains next to and between these particles can grow more rapidly at higher temperatures than those pinned by fine particles (Afshar & Simchi, 2008). Generally, the softening resistance of Cu-Al₂O₃ and Cu-TiB₂ composites can be attributed to thermally stable and non-coarsening particles, which can efficiently prevent the recrystallization, resulting in strength retention even after high-temperature exposure (Groza, 1992; Kim et al., 2006; Tian et al., 2006; Vencl et al., 2013).

The results in Publication V showed that even a high content (≥ 20 vol.%) of sintered Cu₂O in the Cu matrix could not fully restrict the softening of the composite at temperatures above 873 K (600 °C). This can be partly because of the coarsening behaviour of Cu₂O as the temperature increases [Publication III]. On the other hand, it is possible that the notable difference in the elastic properties of copper and cuprite may have led to high internal stresses and stress relaxation when exposed to high temperatures, thus resulting in a diminishing of the softening resistance. Nevertheless, no earlier studies have been conducted on the thermal stability of Cu-Cu₂O composites in high temperature annealing.

4.3.2 Coefficient of thermal expansion

The coefficient of thermal expansion (CTE) values reflect the level of misfit strains introduced in the matrix, e.g., due to reinforcements with distinct properties or due to microstructural changes (Levy-Tubiana et al., 2003; Qian et al., 2002; Weiss, 2000). The grains of different phases have different physical properties, shapes or volumes leading to residual stresses at boundaries after thermal treatment (Kassner & Hayes, 2003; Levy-Tubiana et al., 2003; Weiss, 2000). These stresses can be transmitted without the expansion of Cu or the debonding of boundaries, provided that a strong interface exists between the Cu matrix and the reinforcements (Weidenmann et al., 2009). As a consequence, a high CTE of Cu can be lowered with reinforcements possessing lower CTE. Yoshida & Morigami (2004) have pointed out that the volume fraction is the main factor, which counts for the composites' CTEs. In the present study, the higher amount of the same additive systematically led to lower measured CTEs. When these experimental CTEs were compared to the theoretical predictions in Fig. 3.15, it can be concluded that the values coincided quite well for c-Cu, Cu-Al₂O₃, Cu-TiB₂, and Cu - 6 vol.% diamond samples. Moreover, these were in good accordance with the values given in literature for Cu and its composites prepared by other means; i.e., $17.6 - 33.0 \times 10^{-6} \text{ K}^{-1}$ for Cu (Fathy & El-Kady, 2013; Kondo et al., 2005; Nadkarni & Synk,

1984; Saito et al., 2001), $16.6 - 20.4 \times 10^{-6} \text{ K}^{-1}$ for Cu-Al₂O₃ (Fathy & El-Kady, 2013; Nadkarni & Synk, 1984; Nadkarni et al., 1988), and $10.2 \times 10^{-6} \text{ K}^{-1}$ for Cu - 48vol.% TiB₂ (Yih & Chung, 1997). For sm-Cu, Cu-Cu₂O, and Cu - 3 vol.% diamond samples, steady CTEs were expected without a large difference between the high and low temperature values in the studied range of 423 K to 623 K (150 °C and 350 °C). However, there is no detailed description of high-temperature CTEs for Cu-Cu₂O and Cu-diamond composites in the literature for comparison. Kondo et al. (2005) and Saito et al. (2001) measured CTEs between $10.8 - 13.5 \times 10^{-6} \text{ K}^{-1}$ for Cu - (30 - 40) vol.% Cu₂O and Yoshida & Morigami (2004) obtained a CTE of $12 \times 10^{-6} \text{ K}^{-1}$ for Cu - 50 vol.% diamonds; however, measurements were made only up to 573 K (300 °C). [Publications II, IV and V]

In the present investigation, the Cu-diamond composites without carbide formers showed average CTEs of $14 \times 10^{-6} \text{ K}^{-1}$ for 6SMD and $17 \times 10^{-6} \text{ K}^{-1}$ for 6ND in the temperature range of 473 - 573 K (200 - 300 °C), thus corresponding well to the theoretical predictions (Fig. 3.15). However, much lower CTEs of about $6 - 7 \times 10^{-6} \text{ K}^{-1}$ and $10 \times 10^{-6} \text{ K}^{-1}$ (between 413 K and 433 K) corresponding to Cu-B and Cu-Cr with 60 vol.% of 200 µm diamonds were obtained by Weber & Tavangar (2007). Also, Schubert et al. (2008b) reduced the CTEs to about $11 \times 10^{-6} \text{ K}^{-1}$ (303 - 473 K (30 - 200 °C)) by an improved interfacial bonding between the Cu matrix and the diamond (42 vol.%, 100 - 125 µm) by applying gas atomized, pre-alloyed Cu (Cr) instead of pure Cu. Recently, great attention has been focused on the issue of interfacial bonding between Cu and diamond. It is claimed that the low values indicate good bonding, whereas the CTE and moduli differences between Cu and second-phase particles may initiate thermal stresses, weakening the bonding at higher temperatures (Levy-Tubiana et al., 2003; Weiss, 2000). One inherited issue is the effect of grain size. It has been shown that the CTE values of a nanocrystalline structure can be noticeably greater than those of coarse grain structures (Birringner & Gleiter, 1988; Klam et al., 1987). This suggestion is also supported by the presented results, e.g. for c-Cu ($19.0 \times 10^{-6} \text{ K}^{-1}$ (473 - 973 K (200 - 700 °C))) and for sm-Cu $19.6 \times 10^{-6} \text{ K}^{-1}$ (473 - 523 K (200 - 250 °C)). The same reason may also partly explain the difference in CTE values of 6SMD and 6ND samples. According to Birringner & Gleiter (1988), nanocrystalline copper with an average grain size of 8 nm has a thermal expansion coefficient of $31 \times 10^{-6} \text{ K}^{-1}$, which is almost twice as large as that of coarse-grained copper. Based on Klam et al. (1987), the thermal expansion of the grain boundary in copper was from 40 to $80 \times 10^{-6} \text{ K}^{-1}$, which is about 2.5 to 5 times the expansion of a Cu-crystal. It has been suggested that the reason for greater CTEs in nano-regimes is the larger fraction of boundaries, which add less well-bonded areas to the volume compared to the coarser grained bulk form (Birringner & Gleiter, 1988). Other reasons suggested include a higher defect density, atomic vibrations at grain boundaries,

and the effect of microstrains originating from the microstructure changes of the grain boundaries (Klam et al., 1987; Qian et al., 2002). The above-mentioned issues are also expected to play a role in the present composites and help explain the observed differences in thermal stability and higher CTEs for sm-Cu, Cu-Cu₂O and Cu - 3vol.% diamonds at higher temperatures as compared to Cu - 6 vol.% diamond, Cu-Al₂O₃ and Cu-TiB₂ composites. In addition, the measured CTEs can partly reflect the release of internal stresses from PECS compaction [Publications IV and V].

4.4 Electrical properties of Cu-composites

Generally, if there is no continuous copper network (i.e., Cu grains attached to each) the electrical conductivity in a particle-reinforced Cu matrix composite is decreased. The high volumetric amount of the insulating element decreases the conductivity, similar to pores and debonded interfaces in the material (Akhtar et al., 2009; Rajkumar & Aravindan, 2013). The presence of small and isolated particles do not prevent the continuity of electron pathways in the copper phase, which might result in a smaller effect on conductivity (Rajkumar & Aravindan, 2013). On the other hand, it is suggested that the nanoparticles in the Cu matrix increase the scattering surfaces for conduction electrons and therefore reduce the electrical conductivity of the composite (Tu et al., 2003).

The electrical conductivities of Cu-ND and Cu-Al₂O₃ composites measured in the present work are in accordance with the previous studies by He et al. (2008), Nadkarni & Synk (1984), Tian et al. (2006) and Upadhyaya & Upadhyaya (1995). For example, Nadkarni et al. (1988) obtained 78%IACS for internally oxidized Cu - 2.5 vol.% Al₂O₃, whereas in blended or mechanically alloyed Cu - (0 - 3 wt.%) Al₂O₃ composites, the conductivities ranged between 73 and 84%IACS (Upadhyaya & Upadhyaya, 1995). He et al. (2008) showed that the homogeneous dispersion of the ND as non-conductive reinforcement does not greatly damage the electrical conductivity of the composite. Even the high weight fraction of 8 wt.% ND yielded more than 70%IACS. On the contrary, the reported conductivity values for Cu-TiB₂ showed much more variation. Overall, the conductivity values reported for Cu-TiB₂ composites varied between 11.8 and 83%IACS with TiB₂ contents varying between 1 and 18 vol.% (Kim et al., 2006; Kwon et al., 2006; López et al., 2005; Tu et al., 2003). Generally, the conductivity showed a decreasing trend as the amount of TiB₂ increased, e.g., from 75 to 45%IACS as the content of < 250nm-sized TiB₂ increased from 2.5 to 10 wt.% (i.e., about 5 vol.% to 18 vol.%) (Kwon et al., 2006). It also seems that the processing method and size of TiB₂ might have some effect on the wide variations in the reported values. Oxygen in Cu is also known to decrease the electrical conductivity, (Boucher, 2005; © Copper Development Association, 2013), see e.g. Fig. 1.3.

4.5 Tribological characteristics of Cu-composites

The tribological properties of materials under different operating conditions involve the composite's composition, the metallurgical structure including interfaces, and the properties of the constituents (e.g., hardness/strength, grain size, wear resistance, ability for work-hardening or the formation of a transfer layer, thermal conductivity, and load bearing ability) (Eddine et al., 2013; Han et al., 2006; Holmberg & Matthews, 2009; Peterson & Winer, 1980; Tu et al., 2003; Zhan et al., 2004). Additionally, during contact in the running-in, steady state, and breakdown period the material and especially its surface properties change (Holmberg & Matthews, 2009; Peterson & Winer, 1980; Zhan et al., 2004).

4.5.1 Coefficient of friction

The CoF demonstrated much more fluctuations, a longer running-in period [Fig. 1 in Publication VI] and higher average values when sliding against Cr-steel than against an alumina counter ball (Fig. 3.16). There are a few main reasons proposed to explain this. Firstly, the combination of sliding materials, which have higher reactivity against each other, e.g., metal-metal contact, tends to have a higher CoF and wear rate (Peterson & Winer, 1980). Secondly, decohesion, material transfer and adhesion between the counterparts can cause destructive or unstable behaviour (Bouchoucha et al., 2004; Zhan et al., 2004). Thirdly, frictional heating during sliding in an air environment can cause oxidation of the copper surface (resulting mainly in the formation of Cu_2O (Peterson & Winer, 1980)) and the repetitive forming and destruction of a film can occur, influencing the behaviour of friction (Bouchoucha et al., 2004; Eddine et al., 2013). Moreover, it is possible that the fluctuation in sliding may be due to the pull-off of the hardened layer (Han et al., 2006). Based on Fig. 1a in Publication VI, the CoFs in the latter part of the test with the Cr-steel ball were mainly influenced by the Cu matrix and did not depend so much on the type or amount of the dispersed particles. This led to friction values approaching those reported for a copper-steel sliding pair [Table 2 in Publication VI]. On the contrary, in the tests with the alumina ball, the CoFs varied more, depending on the type and amount of dispersoids, but were more stable throughout the test [Fig. 1b in Publication VI].

The reference Cu samples (c-Cu and sm-Cu) both had CoFs of about 0.8 against Cr-steel. Against alumina the CoF was 0.55 for c-Cu and 0.42 for sm-Cu. It has been reported that fine-grained Cu leads to a lower CoF due to the higher boundary area, which allows for easier oxidation and thus a lubricative contact (Han et al., 2006). Of the reinforcements, only Cu_2O decreased the CoF in sliding. This happened against both the Cr-steel and alumina counter balls when compared to the reference Cu. The sample of Cu with the finest diamonds (5 nm) also resulted

in a slight decrease of CoF against alumina (Fig. 3.16). Even if the lubricating effect of diamonds is established, it is nevertheless closely related to the surface properties, the carbon bonding on the surface, the size of diamonds, and the atmosphere and its humidity and pH (Gubarevich et al., 2005). The suggested threshold size for diamonds is approximately 100 nm, the smaller being better solid lubricants in vacuum conditions. Overall, the CoFs in this study are slightly higher against Cr-steel than those reported elsewhere, while the CoFs against alumina are somewhat smaller than those reported previously [Table 2 in Publication VI].

4.5.2 Wear track profiles

The counter material had a clear influence on the wear behaviour of Cu and its composites. While the Cr-steel counter material resulted in extensive wear with deep and wide wear tracks, the alumina counter material led to low wear with smooth wear tracks [Publication VI]. When comparing the tracks made by Cr-steel to those made by alumina balls, the tracks in 37Cu₂O, sm-Cu, 2.5Al₂O₃ and 6ND samples were 2, 2.5, 7 and 10 times wider for the Cr-steel balls. These also agreed well with the wear depths, see Figs. 3.18a and b. Since c-Cu has a low hardness, the reciprocating sliding can cause more material pile-up onto the sides of the tracks (Fig. 3.18) and repetitive work-hardening in the worn surface (Eddine et al., 2013; Han et al., 2006; Holmberg & Matthews, 2009; Zhan et al., 2004). This also explains the extensive increase of over 70 % in hardness for c-Cu after sliding against Cr-steel. For other samples, the work-hardening was less pronounced due to the initial harder structure. Additionally, the worn substructure revealed that the deformation layer of c-Cu extended deeper than that of sm-Cu or 37Cu₂O, whereas, the substructure of 6SMD showed deformation and large areas of spalling-off material covering part of the worn surface [Fig. 9 in Publication VI]. This indicates that some of the surface material in 6SMD sample has been deformed and fractured due to the cyclical stresses and then moved to another place during sliding, which might also be related to the fluctuation of CoF during the sliding tests as well. Even if the Cu-diamond composites performed poorly against Cr-steel, they still performed much better against alumina, showing smaller tracks with the decreasing size of diamond dispersoids. It has been widely recognized that the carbon in diamond can diffuse into steel at higher temperatures and so diamond is not suitable e.g., for the tooling of ferrous alloys (Holmberg & Matthews, 2009; Lane et al., 2010; Peterson & Winer, 1980). For example, Lane et al. (2010) reported that comparable wear on a diamond tool from steel, with a similar hardness, was encountered at cutting distances 1000 times less than for aluminium. Moreover, they pointed out that water absorption from the air can make the surface more sensitive to adhering so that the surface state of diamonds can affect the adhesion sensitivity in sliding.

4.5.3 Wear rate and mechanisms

The main reason for the extensive wear of samples when sliding against Cr-steel is the wear mechanism involved in sliding operation. The transfer of material from one surface to another is the primary symptom of adhesion (Peterson & Winer, 1980). Careful analysis of the Cr-steel counter ball surfaces after sliding revealed severe adhesive wear of Cu-diamond and Cu-Al₂O₃ (e.g. Fig. 3.17c) and correspondingly very high wear rates (Fig. 3.19). The same composites also showed very high CoFs at the beginning of the experiments [Fig. 1a in Publication VI]. While the tracks in c-Cu, 2.5Al₂O₃ and 6ND samples had a rough surface with some oxygen, the samples of sm-Cu, 37Cu₂O and 79TiB₂ presented smoother surfaces with a higher content of oxygen. It is suggested that non-uniform oxidational wear (the forming and destruction of oxide films) can play a role in sliding.

Generally, the samples which revealed abrasive and/or oxidational wear in sliding contact with Cr-steel revealed a much lower wear rate and also, initially, lower CoFs than the materials exposed to adhesive wear. Abrasive wear, with typical parallel and uniform furrows (Peterson & Winer, 1980), was identified in Cr-steel balls after tests against c-Cu, sm-Cu, Cu-Cu₂O and Cu-TiB₂ (≥ 20 vol.%). Further proof was obtained as abrasive particles and wear debris was found at the end of furrows, primarily at the entrance/exit points of the balls. Detached wear debris particles have an abrasive effect when caught in the contact area (Zhan et al., 2004). For Cu with TiB₂ (≥ 20 vol.%) or Cu₂O, the wear rate decreases as the amount of dispersoids increases. On the other hand, the samples with an addition of Al₂O₃ or diamonds increased the wear rate (Fig. 3.19) and were unsuitable in contact with Cr-steel. The wear rates and the identified wear mechanisms are defined in Table 2 in Publication VI. On the whole, the studied materials showed high wear rates between 1.3×10^{-5} and 5.7×10^{-3} mm³/Nm against Cr-steel. The same test samples indicated oxidational wear after sliding against alumina, as identified in SEM and SEM-EDS analysis [Figs. 3 and 5 in Publication VI]. The smooth profiles of the worn surfaces (Fig. 3.18b) and the low wear rates were caused by the non-reactive contact parts, with a lubricative surface oxidation induced by environmental and frictional conditions. For Cu with Cu₂O, TiB₂ (≥ 20 vol.%) or diamond, the wear rate shows a decreasing trend as the amount of dispersoids increases (Fig. 3.19). The sample with a lower amount of Al₂O₃ in Cu led to lower wear rates against alumina than that with the higher amount. This might be due to slight changes in the wear mechanism, as has been pointed out by Zhou et al. (2009), who showed that more than 2 wt.% Al₂O₃ led to an increase in wear rate due to the change in wear mechanism. With 1 wt.% Al₂O₃ the mechanism was adhesive wear, associated with oxidational wear, whereas for 2 wt.% Al₂O₃ slight

abrasive wear was noticed. Even higher amount (5 wt.%) of Al_2O_3 led to abrasive wear and delaminating fatigue. Additionally, their friction tests illustrated higher CoFs with Al_2O_3 additions than without. Overall, the oxidational wear in the present study led to low wear rates between 1.4×10^{-7} and $6.1 \times 10^{-6} \text{ mm}^3/\text{Nm}$ against alumina [Table 2 in Publication VI]. The lowest wear was measured for Cu-diamond composites.

The lower wear rate of fine-sized Cu (sm-Cu) as compared with the coarse Cu (c-Cu) is an obvious result of the higher hardness of sm-Cu (Table 3.1). A similar hardness dependence of copper wear rates has been reported earlier, e.g., by Han et al. (2006). When comparing the wear performance of different composites in this study, it is clear that adhesively worn samples, against Cr-steel, had the highest wear rates. Much lower wear rates were observed when the same samples were tested against a ceramic alumina ball due to the change of wear mechanism from adhesive to oxidational wear. Usually, the deterioration in wear resistance has been attributed to an increase in reinforcement breakage, reinforcement pull-out, and/or poor reinforcement-matrix interfacial bonding (Rajkumar & Aravindan, 2013; Zhan et al., 2004). When the interfacial bonding is good, the wear resistance increases, e.g., due to the enhanced load-bearing ability, as the amount of dispersoids increases (Tu et al., 2003; Zhan et al., 2004). The nanoindentation studies conducted in this work have shown that a well-bonded interface between the diamonds and the Cu matrix is achieved by PECS [Publication IV]. Thus, it is suggested that the high wear rates of Cu-diamond composites against Cr-steel are not because of the non-bonded interfaces but are more likely due to the interaction of diamonds with iron. This is supported by the fact that the diamond-containing samples performed well against the ceramic alumina balls, indicating mainly oxidational wear well below the level of plain copper.

5. Conclusions

The objective of this work was to extend the knowledge of the PECS method in compacting Cu-based materials and to correlate the observed microstructural features to the resulting properties. On the basis of the results presented in this thesis and the attached publications, the following conclusions can be drawn:

- The composite powders were prepared with a variety of techniques, including high-energy ball milling, i.e. mechanical alloying (MA), self-propagating high-temperature synthesis (SHS) accompanied with MA, via a chemical route, and natural oxidation of Cu. Additionally, commercial internally oxidized (IO) Cu-Al₂O₃ powders were employed. The consolidation of these powders by PECS resulted in highly dense Cu and Cu-composites. Typically, densities over 97% of T.D. were reached. It is noteworthy also to point out that as the density of Cu-Cu₂O composite was 99.7% of T.D. at best, the presence of Cu₂O (up to 37 vol.%) seemed not to have any negative effect on the PECS consolidation.
- The comparison between PECS and HIP processed Cu-Cu₂O composite samples revealed clear differences in the microstructure of the samples. With PECS, a highly dense and fine-grained structure was easily obtained, while with HIPing, grain growth was noticeable due to the long process time needed for proper densification. The finer grain size retained by PECS also resulted in superior mechanical properties as compared to those by HIPing.
- It has been widely reported that non-coarsening dispersoids have a great potential in controlling the grain growth of the matrix during consolidation and further treatments. This applies for Cu-Al₂O₃ or Cu-TiB₂ composites in the present study as well as for the Cu-diamond composites. In comparison to the non-coarsening dispersoids, not much attention has been given to the grain growth of the matrix in the presence of coarsening particles. Therefore, the grain size and growth of Cu and Cu₂O were separately studied. A linear relationship was observed between Cu and Cu₂O grain growth, independent of the process conditions and sintering method, suggesting that the rate controlling mechanism, i.e. grain boundary diffusion, remains the same in the studied regimes. It was shown that during high-temperature exposure, the grain growth in Cu-Cu₂O composites was

Conclusions

suppressed by the presence of Cu_2O , the effectiveness increasing up to about 20 vol.%. The higher amount of Cu_2O increased the fraction of clusters in the samples and yielded no additional effectiveness in grain growth control.

- The reinforcements applied in the present study, i.e., Cu_2O , Al_2O_3 , TiB_2 and diamonds, were found to noticeably improve the microhardness of the composite as compared to plain sm-Cu. For instance, the hardness values for sm-sized Cu- Cu_2O composites were comparable to those reported for pure n-Cu, with a near-Hall-Petch -type of relationship for hardness dependence on grain size. In addition, the hardness was found to increase with increasing amount of Cu_2O . However, the nanosized dispersoids (e.g., ND and nano- Al_2O_3 in Cu- Al_2O_3 (IO)) were found to be more effective in increasing the hardness than sm-sized Cu_2O or the sm-sized or agglomerated dispersoids (i.e., submicron-sized diamonds or Al_2O_3 in Cu- Al_2O_3 (Exp.)). This is due to the smaller interparticle distance between the reinforcements, which generally is a consequence of either a higher amount or a smaller size of isolated reinforcements. The overall strength of the compacts was attributed to Hall-Petch and Orowan strengthening, whereas the coarse and hard TiB_2 also contributed by the dislocation pile-up mechanism in Cu- TiB_2 compacts. Overall, Cu- TiB_2 composites resulted in the highest strengths due to the high amount of hard TiB_2 and the restricted grain growth of Cu.
- The differences in constituent properties can be separately studied by applying low load nanoindentation measurements. For Cu- Cu_2O , the results revealed a similar nanohardness for both the Cu and the Cu_2O , although with a clear difference in elastic properties. For Cu with submicron-sized diamonds, the different hardness and amount of elastic deformation, as well as the good interface between the two phases, were verified. Nanoindentation was applied to Cu- Al_2O_3 in order to confirm the difference in the microhardness values between the two different types of composites (IO and Exp.).
- As expected, higher amount of the same additive systematically led to lower measured CTEs. A good correlation between the measured and theoretically predicted values was observed for c-Cu, Cu- Al_2O_3 , Cu- TiB_2 , and Cu with 6 vol.% diamond samples. In contrast, for sm-Cu, Cu- Cu_2O , and Cu with 3 vol.% diamond samples the CTEs showed a notable variation when comparing the high and low temperature CTE values in the studied range of 423 K to 623 K (150 °C and 350 °C). Generally, the CTE values reflect the level of misfit strains introduced into the matrix, e.g., due to reinforcements with distinct properties or due to microstructural changes. Also, a fine microstructure can lead to greater CTEs than coarse structures because of the contributions of grain boundaries in the nano-regimes (Birringer & Gleiter, 1988; Klam et al., 1987; Qian et al., 2002).

- Based on thermal evaluations, sm-Cu, Cu-Cu₂O and Cu with 3 vol.% submicron-sized diamonds are suitable for use at moderate temperatures up to 623 - 673 K (350 - 400 °C), after which the softening and changes in CTEs associated with recovery and grain growth restrain their use. Copper with 3 vol.% of nanodiamonds is suitable up to about 823 K (550 °C), whereas samples with 6 vol.% of either sub- or nanosized diamonds have an estimated softening temperature of around 873 K (600 °C). On the other hand, Cu-Al₂O₃ (IO) and Cu-TiB₂ composites can retain their mechanical properties even at high temperatures and are suitable above 1023 K (850 °C). The Cu-Al₂O₃ (Exp.) samples resulted in a much lower temperature stability due to the agglomerated alumina, which cannot resist softening as effectively as when well distributed.
- As expected, the higher volumetric amount of dispersoids decreased the electrical conductivity in each type of Cu-composite. The effect was greatly influenced by the non-conducting/conducting behaviour of the additives. In most cases, however, the conductivity clearly yielded over 50%IACS, which is required for Cu-based alloys in high-temperature applications (Grant et al., 1984).
- The ball-on-flat test results showed a strong dependence of wear rate and wear mechanism on the CoF of used counterpart material. The Cr-steel counterpart material indicated reactivity against the majority of the metallic Cu and Cu-composite test samples. This mainly led to adhesive wear, high CoFs and high wear rates. The Cu-Cu₂O composites showed the lowest CoF, with abrasive and oxidational wear mechanisms. These mechanisms led to a notably lower wear rate in c-Cu, sm-Cu and Cu-TiB₂ samples as compared to Cu-Al₂O₃ and Cu-diamond samples, which suffered from extensive adhesive wear. It is believed that the carbon in diamonds reacted with the steel counterpart material, leading to an accelerated wear in the Cu-diamond composites. The same samples performed well against alumina, indicating mainly oxidational wear well below the level of plain Cu. The lowest wear rates against alumina were found for Cu-diamond composites. Altogether, the alumina counterpart material showed no reactivity against the test materials, the oxidational wear and pile-up formation being the main wear mechanisms, thus leading to low CoFs and wear rates. All the composites performed better than the plain Cu against alumina.

This study shows that PECS can be used to produce fine-grained, high quality Cu-composites with superior properties as compared to those of sm-Cu. These materials are considered to be promising candidates for applications where enhanced thermal properties together with high mechanical properties are desired. While the mechanical properties of the Cu-composites were carefully studied in the present thesis, more detailed work focusing on the electrical and thermal conductivities and concomitant changes within the microstructure at higher

Conclusions

temperatures is suggested. In order to achieve a more uniform distribution of dispersoids, it is recommended that in further studies the mixing of nanoCu and nanoDiamond should be accomplished by using liquid solvents. More detailed work on Cu-Al₂O₃ and its strengthening mechanisms is proposed as well.

Bibliography

Abyzov, A.M., Kidalov, S.V. & Shakhov, F.M. (2012) High thermal conductivity composite of diamond particles with tungsten coating in a copper matrix for heat sink applications. *Applied Thermal Engineering*, 48, 72-80.

Addleman, R.L. & Webster, G.A. (1973) A simple model of uniaxial creep recovery and stress relaxation based on residual-stress redistribution. *Journal of Strain Analysis*, 8 (2), 99-107.

Afshar, A & Simchi, A. (2008) Abnormal grain growth in alumina dispersion-strengthened copper produced by an internal oxidation process. *Scripta Materialia*, 58 (11), 966-969.

Akbarpour, M.R., Salahi, E., Hesari, F.A., Simchi, A. & Kim, H.S. (2013) Fabrication, characterization and mechanical properties of hybrid composites of copper using nanoparticulates of SiC and carbon nanotubes. *Materials Science and Engineering A*, 572, 83-90.

Akhtar, F., Askari, S.J., Shah, K.A., Du, X. & Guo, S. (2009) Microstructure, mechanical properties, electrical conductivity and wear behavior of high volume TiC reinforced Cu-matrix composites. *Materials Characterization*, 60 (4), 327-336.

Anselmi-Tamburini, U., Garay, J.E. & Munir, Z.A. (2006) Fast low-temperature consolidation of bulk nanometric ceramic materials. *Scripta Materialia*, 54, 823-828.

Anselmi-Tamburini, U., Gennari, S., Garay, J.E. & Munir, Z.A. (2005) Fundamental investigations on the spark plasma sintering/synthesis process II. Modeling of current and temperature distributions. *Materials Science and Engineering A*, 394, 139-148.

Anthony, J., Bideaux, R., Bladh, K., & Nichols, M. (1995) *Handbook of Mineralogy*. Mineralogical Society of America, Chantilly, USA.
<http://www.handbookofmineralogy.org/pdfs/cuprite.pdf>

Ardell, A.J. (1972) On the coarsening of grain boundary precipitates. *Acta Metallurgica*, 20 (4), 601-609.

Arzt, E. (1998) Size effects in materials due to microstructural and dimensional constraints: a comparative review. *Acta Materialia*, 46 (16), 5611-5626.

Ashby, M.F. (1974) A first report on sintering diagrams. *Acta Metallurgica*, 22, 275-289.

- Bai, H., Ma, N., Lang, J. & Zhu, C. (2013) Effect of a new pretreatment on the microstructure and thermal conductivity of Cu/diamond composites. *Journal of Alloys and Compounds*, 580, 382-385.
- Birringier R. & Gleiter, H. (1988) Nanocrystalline materials. In: *Advances in Materials Science, Encyclopedia of Materials Science and Engineering*, 1, Cahn, R.W. (editor), Pergamon Press, Oxford, 339-349.
- Boucher, R. (2005) The electrical property dependence of disordered copper oxide on oxygen content. *Journal of Physics and Chemistry of Solids*, 66, 1234-1239.
- Bouchoucha, A., Chekroud, S. & Paulmier, D. (2004) Influence of the electrical sliding speed on friction and wear processes in an electrical contact copper-stainless steel. *Applied Surface Science*, 223, 330-342.
- Brock, J. (2001) Copper Alloys: Corrosion. In: *Encyclopedia of Materials: Science and Technology*, 2nd edition, edited by Buschow, K.H.J., Cahn, R.W., Flemings, M.C., Ilschner, B., Kramer, E.J., Mahajan, S. and Veysière, P., Elsevier, ISBN: 978-0-08-043152-9, Oxford, 1662-1664.
- Brodhag, S.H. & Herwegh, M. (2010) The effect of different second-phase particle regimes on grain growth in two-phase aggregates: insights from in situ rock analogue experiments. *Contributions to Mineralogy and Petrology*, 160, 219-238.
- Cai, B., Kong, Q.P., Lu, L. & Lu, K. (1999) Interface controlled diffusional creep of nanocrystalline pure copper. *Scripta Materialia*, 41 (7), 755-759.
- Caron, R.N. (2001a) Copper: alloying. In: *Encyclopedia of Materials: Science and Technology*, 2nd edition, edited by Buschow, K.H.J., Cahn, R.W., Flemings, M.C., Ilschner, B., Kramer, E.J., Mahajan, S. and Veysière, P., Elsevier, ISBN: 978-0-08-043152-9, Oxford, 1652-1660.
- Caron, R.N. (2001b) Copper alloys: properties and applications. In: *Encyclopedia of Materials: Science and Technology*, 2nd edition, edited by Buschow, K.H.J., Cahn, R.W., Flemings, M.C., Ilschner, B., Kramer, E.J., Mahajan, S. and Veysière, P., Elsevier, ISBN: 978-0-08-043152-9, Oxford, 1665-1668.
- Caron, R.N. (2001c) Copper alloys: thermal and thermomechanical processing. In: *Encyclopedia of Materials: Science and Technology*, 2nd edition, edited by Buschow, K.H.J., Cahn, R.W., Flemings, M.C., Ilschner, B., Kramer, E.J., Mahajan, S. and Veysière, P., Elsevier, ISBN: 978-0-08-043152-9, Oxford, 1668-1670.
- Chandrasekaran, D. (2003) Grain size and solid solution strengthening in metals: a theoretical and experimental study. *Doctoral Dissertation*, Stockholm University, Sweden.
- Chen, B., Bi, Q., Yang, J., Xia, Y. & Hao, J. (2008) Tribological properties of solid lubricants (graphite, h-BN) for Cu-based P/M friction composites. *Tribology International*, 41 (12), 1145-1152.
- Chen, G-Q., Xiu, Z-Y., Meng, S-H., Wu, G-H. & Zhu, D-Z. (2009) Fabrication and thermo-physical properties of TiB₂/Cu composites for electronic packaging applications. *Transactions of Nonferrous Metals Society of China*, 19, S448-S452.

- Chen, J., Lu, L. & Lu, K. (2006) Hardness and strain sensitivity of nanocrystalline Cu. *Scripta Materialia*, 54, 1913-1918.
- Cho, S., Kikuchi, K., Miyazaki, T., Takagi, K., Kawasaki, A. & Tsukada, T. (2010) Multiwalled carbon nanotubes as a contributing reinforcement phase for the improvement of thermal conductivity in copper matrix composites. *Scripta Materialia*, 63, 375-378.
- Chokshi, A.H., Rosen, A., Karch, J. & Gleiter, H. (1989) On the validity of the Hall-Petch relationship in nanocrystalline materials. *Scripta Metallurgica*, 23, 1679-1684.
- Choo, H., Bourke, M.A.M., & Daymond, M.R. (2001) A finite-element analysis of the inelastic relaxation of thermal residual stress in continuous-fiber-reinforced composites. *Composites Science and Technology*, 61, 1757-1772.
- Chu, K., Liu, Z., Jia, C., Chen, H., Liang, X., Gao, W., Tian, W. & Guo, H. (2010a) Thermal conductivity of SPS consolidated Cu/diamond composites with Cr-coated diamond particles. *Journal of Alloys and Compounds*, 490, 453-458.
- Chu, K., Wu, Q., Jia, C., Liang, X., Nie, J., Tian, W., Gai, G. & Guo, H. (2010b) Fabrication and effective thermal conductivity of multi-walled carbon nanotubes reinforced Cu matrix composites for heat sink application. *Composites Science and Technology*, 70, 298-304.
- Clyne, T.W. & Withers, P.J. (1993) An introduction to metal matrix composites. Cambridge University Press, ISBN: 0-521-41808-9, Cambridge, 509.
- Coble, R.L. (1963) A model for boundary diffusion controlled creep in polycrystalline materials. *Journal of Applied Physics*, 34, 1679-1682.
- Conrad, H. (2003) Grain size dependence of the plastic deformation kinetics in Cu. *Materials Science and Engineering A*, 341, 216-228.
- Conrad, H. (2004) Grain-size dependence of the flow stress of Cu from millimeters to nanometers. *Metallurgical and Materials Transactions A*, 35, 2681-2695.
- Conrad, H. & Jung, K. (2005) Effect of grain size from mm to nm on the flow stress and plastic deformation kinetics of Au at low homologous temperatures. *Materials Science and Engineering A*, 406, 78-85.
- Couvy, H., Lahiri, D., Chen, J., Agarwal, A. & Sen, G. (2011) Nanohardness and Young's modulus of nanopolycrystalline diamond. *Scripta Materialia*, 64, 1019-1022.
- Das, D., Samanta, A. & Chattopadhyay, P.P. (2006) Mechanical properties of bulk ultrafine-grained copper. *Synthesis and Reactivity in Inorganic, Metal-Organic, and Nano-Metal Chemistry*, 36, 221-225.
- Dash, K., Ray, B.C. & Chaira, D. (2012) Synthesis and characterization of copper-alumina metal matrix composite by conventional and spark plasma sintering. *Journal of Alloys and Compounds*, 516, 78-84.

- Davis J.R. (editor) (2001) Powder metallurgy: copper and copper alloys. *ASM Specialty Handbook*, ASM International, ISBN: 0-87170-726-8, Materials Park, OH, USA, 105-120.
- Dhokey, N.B. & Paretkar, R.K. (2008) Study of wear mechanism in copper-based SiC_p (20% by volume) reinforced composite. *Wear*, 265 (1-2), 117-133.
- Diouf, S. (2013) Production of a nanostructured copper by spark plasma sintering. *Doctoral Thesis*, University of Trento, Italy.
- Dong, S.J., Zhou, Y., Shi, Y.W. & Chang, B.H. (2002) Formation of a TiB₂-reinforced copper-based composite by mechanically alloying and hot pressing. *Metallurgical and Materials Transactions A*, 33, 1275-1280
- Eddine, W.Z., Matteazzi, P. & Celis, J-P. (2013) Mechanical and tribological behavior of nanostructured copper-alumina cermets obtained by pulsed electric current sintering. *Wear*, 297, 762-773.
- El-Khozondar, R., El-Kohonzar, H., Gottstein, G. & Rollet, A. (2006) Microstructural simulation of grain growth in two-phase polycrystalline materials. *Egyptian Journal of Solids*, 29 (1), 35-47.
- Eriksson, M. (2010) Spark plasma sintering enhancing grain sliding, deformation and grain size control. *Doctoral Thesis*, Stockholm University, Sweden.
- Fan, D. & Chen, L-Q. (1997a) Diffusion-controlled grain growth in two-phase solids. *Acta Materialia*, 45 (8), 3297-3310.
- Fan, D. & Chen, L-Q. (1997b) Computer simulations of grain growth and Ostwald ripening in alumina-zirconia two-phase composites. *Journal of the American Ceramic Society*, 80 (7), 1773-1780.
- Fan, D., Chen, L-Q. & Chen, S-P.P. (1998) Numerical simulation of Zener pinning with growing second-phase particles. *Journal of the American Ceramic Society*, 81 (3), 526-532.
- Fathy, A. & El-Kady, O. (2013) Thermal expansion and thermal conductivity characteristics of Cu-Al₂O₃ nanocomposites. *Materials & Design*, 46, 355-359.
- Fathy, A., Shehata, F., Abdelhameed, M. & Elmahdy, M. (2012) Compressive and wear resistance of nanometric alumina reinforced copper matrix composites. *Materials & Design*, 36, 100-107.
- Ferkel, H. (1999) Properties of copper reinforced by laser-generated Al₂O₃-nanoparticles. *Nanostructured Materials*, 11 (5), 595-602.
- Finsy, R. (2004) On the critical radius in Ostwald ripening. *Langmuir*, 20 (7), 2975-2976.
- Flores, E., Cabrera, J.M. & Prado, J.M. (2004) Effect of clustering of precipitates on grain growth. *Metallurgical and Materials Transactions A*, 35, 1097-1103.
- García, V.G., Cabrera, J.M. & Prado, J.M. (2008) Role of Cu₂O during hot compression of 99.9 % pure copper. *Materials Science and Engineering A*, 488, 92-101.

- German, R.M. (1996) Sintering theory and practice. John Wiley & Sons, ISBN: 978-0-471-05786-4, New York, USA, 568.
- Grant, J.N., Lee, A. & Lou, M. (1984) Multiple hardening of mechanisms for high strength, high temperature, high conductivity copper base alloys. *Proceedings of the Conference on High Conductivity Copper and Aluminium Alloys*, The Metallurgical Society of AIME, California, 103-111.
- Groza, J. (1992) Heat-resistant dispersion-strengthened copper alloys. *Journal of Materials Engineering and Performance*, 1 (1), 113-121.
- Groza, J.R. & Gibeling J.C. (1993) Principles of particle selection for dispersion-strengthened copper. *Materials Science and Engineering A*, 171, 115-125.
- Groza, J. & Zavaliangos, A. (2000) Sintering activation by external electrical field. *Materials Science and Engineering A*, 287, 171-177.
- Gubarevich, A.V., Usuba, S., Kakudate, Y., Tanaka, A. & Odawara, O. (2005) Frictional properties of diamond and fullerene nanoparticles sprayed by a high-velocity argon gas on stainless steel substrate. *Diamond & Related Materials*, 14, 1549-1555.
- Guiderdoni, Ch., Estournès, C., Peigney, A., Weibel, A., Turq, V. & Laurent, Ch. (2011) The preparation of double-walled carbon nanotube/Cu composites by spark plasma sintering, and their hardness and friction properties. *Carbon*, 49 (13), 4535-4543.
- Guo, M., Shen, K. & Wang, M. (2009) Relationship between microstructure, properties and reaction conditions for Cu-TiB₂ alloys prepared by in situ reaction. *Acta Materialia*, 57, 4568-4579.
- Hall, E.O. (1951) The deformation and aging of mild steel: III discussion of results. *Proceedings of the Physical Society B*, 64, 747-753.
- Han, Z., Lu, L. & Lu, K. (2006) Dry sliding tribological behavior of nanocrystalline and conventional polycrystalline copper. *Tribology Letters*, 21, 47-52.
- Hanada, K., Matsuzaki, K. & Sano, T. (2004) Thermal properties of diamond particle-dispersed Cu composites. *Journal of Materials Processing Technology*, 153-154, 514-518.
- Hanada, K., Yamamoto, K., Taguchi, T., Ōsawa, E., Inakuma, M., Livramento, V., Correia, J.B. & Shohoji N. (2007) Further studies on copper nanocomposite with dispersed single-digit-nanodiamond particles. *Diamond & Related Materials*, 16 (12), 2054-2057.
- Hannula, S-P., Koskinen, J., Haimi, E. & Nowak, R. (2004) Mechanical properties of nanostructured materials. *Encyclopedia of Nanoscience and Nanotechnology*, 5, Nalwa, R. (editor), American Scientific Publishers, ISBN: 1-58883-001-2, USA, 131-162.
- Hansen, N. (2004) Hall-Petch relation and boundary strengthening. *Scripta Materialia*, 51, 801-806.

- Harper, J. & Dorn, J.E. (1957) Viscous creep of aluminum near its melting temperature. *Acta Metallurgica*, 5 (11), 654-665.
- Hashimoto, T., Kohri, H., Yumoto, A. & Shiota, I. (2008) Friction coefficients and wear rates of MoS₂/Cu, BN/Cu composites. *Advances in Science and Technology*, 54, 174-179.
- He, J., Zhao, N., Shi, C., Du, X., Li, J. & Nash P. (2008) Reinforcing copper matrix composites through molecular-level mixing of functionalized nanodiamond by co-deposition route. *Materials Science and Engineering A*, 490, 293-299.
- Helle, A.S., Easterling, K.E. & Ashby, M.F. (1985) Hot-isostatic pressing diagrams: new developments. *Acta Metallurgica*, 33 (12), 2163-2174.
- Herring, C. (1950) Diffusional viscosity of a polycrystalline solid. *Journal of Applied Physics*, 21, 437-445.
- Holmberg, K. & Matthews, A. (2009) Coatings tribology; properties, mechanisms, techniques and applications in surface engineering. *Tribology and Interface Engineering Series*, 56, Briscoe, B.J. (editor), 2nd edition, Elsevier, ISBN: 978-0-444-52750-9, Amsterdam, The Netherlands, 560.
- Horrigan, V.M. (1977) The solubility of oxygen in solid copper. *Metallurgical Transactions A*, 8, 785-787.
- Hwang, S.J. (2011) Compressive yield strength of the nanocrystalline Cu with Al₂O₃ dispersoid. *Journal of Alloys and Compounds*, 509 (5), 2355-2359.
- Ichikawa, K. & Achikita, M. (1991) Production and properties of carbide dispersion-strengthened coppers by compocasting. *ISIJ International*, 31 (9), 985-991.
- Inoue, K. (1966a) Electric-discharge sintering. US Patent No. 3,241,956.
- Inoue, K. (1966b) Apparatus for electrically sintering discrete bodies. U.S. Patent No. 3,250,892.
- Jacobs, M.H. (1999) Precipitation hardening. *European Aluminium Association*, 1-47.
- Jin, S., Zhang, H., Jia, S. & Li, J-F. (2005) TiB₂/Cu electrode materials fabricated via SPS. *Materials Science Forum*, 475-479, 1555-1558.
- Kaczmar, J.W., Pietrzak, K. & Włosiński, W. (2000) The production and application of metal matrix composite materials. *Journal of Materials Processing Technology*, 106, 58-67.
- Kainer, K.U (editor) (2006) Metal matrix composites: custom-made materials for automotive and aerospace engineering. Wiley-VHC Verlag & Co., KGaA, Weinheim, ISBN: 3-527-31360-5, 315.
- Kalinin, G. & Matera, R. (1998) Comparative analysis of copper alloys for the heat sink of plasma facing components in ITER. *Journal of Nuclear Materials*, 258-263, 345-350.

- Kassner, M.E. & Hayes, T.A. (2003) Creep cavitation in metals. *International Journal of Plasticity*, 19, 1715-1748.
- Kaysser, W.A., Aslan, M., Arzt, E., Mitkov, M. & Petzow, G. (1988) Microstructural development and densification during HIPping of ceramics and metals. *Powder Metallurgy*, 31 (1), 63-69.
- Kerner, E.H. (1956) The elastic and thermo-elastic properties of composite media. *Proceedings of the Physical Society B*, 69, 808-813.
- Khan, A.S., Farrokh, B. & Takacs, L. (2008) Compressive properties of Cu with different grain sizes: sub-micron to nanometer realm. *Journal of Materials Science*, 43, 3305-3313.
- Kim, C., Lim, B., Kim, B., Shim, U., Oh, S., Sung, B., Choi, J., Ki, J. & Baik, S. (2009) Strengthening of copper matrix composites by nickel-coated single-walled carbon nanotube reinforcements. *Synthetic Metals*, 159, 424-429.
- Kim, H.S., Estrin, Y. & Bush, M.B. (2000) Plastic deformation behaviour of fine-grained materials. *Acta Materialia*, 48, 493-504.
- Kim, J-S., Kum, J-W., Kang, E-H., Nguyen, D-T., Kim, J-C. & Kwon, Y-S. (2006) Microstructure and property of TiB₂-dispersed Cu-matrix composites. *The First International Forum on Strategic Technology, IEEE 2006*, 366-368.
- Klam, H.J., Hahn, H. & Gleiter, H. (1987) The thermal expansion of grain boundaries. *Acta Metallurgica*, 35 (8), 2101-2104.
- Kocks, U.F. (1977) The theory of an obstacle-controlled yield strength – report after an international workshop. *Materials Science and Engineering*, 27, 291-298.
- Kondo, Y., Kaneda, J., Aono, T., Abe, T., Inagaki, M., Saito, R., Koike, Y. & Arakawa, H. (2005) Composite material including copper and cuprous oxide and application thereof. U.S. Patent 6,909,185.
- Korchagin, M.A. & Dudina, D.V. (2007) Application of self-propagating high-temperature synthesis and mechanical activation for obtaining nanocomposites. *Combustion, Explosion, and Shock Waves*, 43 (2), 176-187.
- Kováčik, J., Emmer, Š., Bielek, J. & Keleši, L. (2008) Effect of composition on friction coefficient of Cu-graphite composites. *Wear*, 265, 417-421.
- Kundig, K.J.A. & Cowie, J.G. (2006) Copper and Copper Alloys. In: *Mechanical Engineers' Handbook: Materials and Mechanical Design*, 1, 3rd edition, Kutz, M. (editor), John Wiley & Sons, Inc., ISBN: Hoboken, NJ, USA, ISBN: 978-0-471-77744-1, 117-220.
- Kwon, Y.J., Kobashi, M., Choh, T. & Kanetake, N. (2004) Fabrication and simultaneous bonding of metal matrix composite by combustion synthesis reaction. *Scripta Materialia*, 50, 577-581.
- Kwon, D-H., Nguyen, T.D., Huynh, K.X., Choi, P-P., Chang, M-G., Yum, Y-J., Kim, J-S. & Kwon, Y-S. (2006) Mechanical, electrical and wear properties of Cu-TiB₂ nanocomposites fabricated by MA-SHS and SPS. *Journal of Ceramic Processing Research*, 7 (3), 275-279.

- Lane, B.M., Shi, M., Dow, T.A. & Scattergood, R. (2010) Diamond tool wear when machining Al6061 and 1215 steel. *Wear*, 268, 1434-1441.
- Langdon, T.G. (2006) Grain boundary sliding revisited: developments in sliding over four decades. *Materials Science*, 41, 597-609.
- Lebedev, A.B., Pulnev, S.A., Kopylov, V.I., Burenkov, Yu.A., Vetrov, V.V. & Vylegzhanin, O.V. (1996) Thermal stability of submicrocrystalline copper and Cu:ZrO₂ composite. *Scripta Materialia*, 35 (9), 1077-1081.
- Lee, J., Jung, J.Y., Lee, E-S., Park, W.J., Ahn, S. & Kim, N.J. (2000) Microstructure and properties of titanium dispersed Cu alloys fabricated by spray forming. *Materials Science and Engineering A*, 277, 274-283.
- Lee, S.B., Matsunaga, K., Ikuhara, Y. & Lee, S-K. (2007) Effect of alloying elements on the interfacial bonding strength and electric conductivity of carbon nano-fiber reinforced Cu matrix composites. *Materials Science and Engineering A*, 449-451, 778-781.
- Leedy, K.D., Stubbins, J.F., Singh, B.N. & Garner, F.A. (1996) Fatigue behavior of copper and selected copper alloys for high heat flux applications. *Journal of Nuclear Materials*, 233-237, 547-552.
- Levy-Tubiana, R., Baczmanski, A. & Lodini, A. (2003) Relaxation of thermal mismatch stress due to plastic deformation in an Al/SiCp metal matrix composite. *Materials Science and Engineering A*, 341, 74-86.
- Liang, S.H. & Fan, Z.K. (1999) Al₂O₃ particle reinforced copper matrix composite using for continuous casting mould. *Acta Metallurgica Sinica*, 12 (5), 782-786.
- Lifshitz, I.M. & Slyozov, V.V. (1961) The kinetics of precipitation from supersaturated solid solution. *Journal of Physics and Chemistry of Solids*, 19 (1-2), 35-50.
- López, M., Corredor, D., Camurri, C., Vergara, V. & Jiménez, J. (2005) Performance and characterization of dispersion strengthened Cu-TiB₂ composite for electrical use. *Materials Characterization*, 55, 252-262.
- Lu, L., Schwaiger, R., Shan, Z.W., Dao, M., Lu, K. & Suresh, S. (2005) Nano-sized twins induce high rate sensitivity of flow stress in pure copper. *Acta Materialia*, 53, 2169-2179.
- Martínez-Ruiz, A., Moreno, M.G. & Takeuchi, N. (2003) First principles calculations of the electronic properties of bulk Cu₂O, clean and doped with Ag, Ni, and Zn. *Solid State Sciences*, 5, 291-295.
- Merzhanov, A.G. (2004) The chemistry of self-propagating high-temperature synthesis. *Journal of Materials Chemistry*, 14, 1779-1786.
- Meyer, D.G. & Wadley, H.N.G. (1992) Coprime receding horizon feedback control of hot isostatic pressing. *Control Applications, First IEEE Conference*, OH, USA, 362-367.
- Meyers, M.A., Mishra, A. & Benson, D.J. (2006) Mechanical properties of nanocrystalline materials. *Progress in Materials Science*, 51, 427-556.

- Mishina E.D., Nagai, K. & Nakabayashi, S. (2001) Self-assembled Cu/Cu₂O multilayers: deposition, structure and optical properties. *Nano Letters*, 1 (8), 401-404.
- Morris, M.A. & Morris, D.G (1989) Microstructural refinement and associated strength of copper alloys obtained by mechanical alloying. *Materials Science and Engineering A*, 111, 115-127.
- Moustafa, S.F., El-Badry, S.A., Sanad, A.M. & Kieback, B. (2002) Friction and wear of copper-graphite composites made with Cu-coated and uncoated graphite powders. *Wear*, 253, 699-710.
- Munir, Z.A., Quach, D.V. & Ohyanagi, M. (2011) Electric current activation of sintering: a review of the pulsed electric current sintering process. *Journal of the American Ceramic Society*, 94 (1), 1-19.
- Munro, R.G. (2000) Material properties of titanium diboride. *Journal of Research of NIST*, 105, 709-720.
- Murty, Y.V. (2001) Electrical and electronic connectors: materials and technology. *Encyclopedia of Materials: Science and Technology*, 2nd edition, edited by Buschow, K.H.J., Cahn, R.W., Flemings, M.C., Ilshner, B., Kramer, E.J., Mahajan, S. and Veyssi re, P., Elsevier, ISBN: 978-0-08-043152-9, Oxford, 2483-2494.
- Nachum, S., Fleck, N.A., Ashby, M.F., Colella, A. & Matteazzi, P. (2010) The microstructural basis for the mechanical properties and electrical resistivity of nanocrystalline Cu-Al₂O₃. *Materials Science and Engineering A*, 527, 5065-5071.
- Nadkarni, A.V. & Klar, E. (1973) Dispersion strengthening of metals by internal oxidation. SCM Corporation, U.S. Patent 3,779,714.
- Nadkarni, A.V. Samal, P.K. & Synk, J.E. (1988) Dispersion strengthened metal composites. U.S. Patent No. 4,752,334.
- Nadkarni, A.V. & Synk, J.E. (1984) Dispersion-strengthened materials. In: *Metals Handbook: Powder Metallurgy*, 7, 9th edition., ASM, Metals Park, OH, 711.
- Neubauer, E., Angerer, P., Altenburger, A. & Korb, G. (2006) Thermophysical properties and microstructural investigations of copper-copper oxide composites. *Proceedings of the International Conference Copper'06 - Better properties for innovative products*, Wiley-VCH, 79-85.
- Newman, A.J. (1992) Neutral observer for the hot isostatic pressing nonlinear system. *IJCNN, third International Joint Conference: Neutral Networks*, Baltimore, USA, 30-35.
- Nix, F.C. & MacNair, D. (1941) The thermal expansion of pure metals: copper, gold, aluminum, nickel, and iron. *Physical Review*, 60, 597-605.
- Nunes, D., Correia, J.B., Carvalho, P.A., Shohoji, N., Fernandes, H., Silva, C., Alves, L.C., Hanada, K. &  sawa, E. (2011) Production of Cu/diamond composites for first-wall heat sinks. *Fusion Engineering and Design*, 86 (9-11), 2589-2592.

- Olevsky, E., Maximenko, A., Van Dyck, S., Froyen, L. & Delaey, L. (1998) Container influence on shrinkage under hot isostatic pressing – I. Shrinkage anisotropy of a cylindrical specimen. *International Journal of Solids and Structures*, 35 (11), 2283-3303.
- Omori, M. (2000) Sintering, consolidation, reaction and crystal growth by the spark plasma system (SPS). *Materials Science and Engineering A*, 287, 183-188.
- Orrù, R., Licheri, R., Locci, A.M., Cincotti, A. & Cao, G. (2009) Consolidation/synthesis of materials by electric current activated/assisted sintering. *Materials Science and Engineering R*, 63, 127-287.
- Patil, K.C., Aruna, S.T. & Ekambaram, S. (1997) Combustion synthesis. *Current Opinion in Solid State & Materials Science*, 2 (2), 158-165.
- Pavlov, V.A., Popov, B.V. & Kucherenko, V.G. (1983) Energy expenditure in the hot isostatic pressing of metal powders. *Powder Metallurgy and Metal Ceramics*, 22, 809-813.
- Petch, N.J. (1953) The cleavage strength of polycrystals. *Journal of Iron and Steel Research*, 174, 25-28.
- Peterson, M.B.A & Winer, W.O. (1980) *Wear Control Handbook*, ASME, 1358.
- Qian, L.H., Wang, S.C., Zhao, Y.H. & Lu, K. (2002) Microstrain effects on thermal properties of nanocrystalline Cu. *Acta Materialia*, 50, 3425-3434.
- Ragulya, A.V. (2010) Fundamentals of spark plasma sintering. *Encyclopedia of Materials: Science and Technology*, 2nd edition, edited by Buschow, K.H.J., Cahn, R.W., Flemings, M.C., Ilschner, B., Kramer, E.J., Mahajan, S. and Veysière, P., Elsevier, ISBN: 978-0-08-043152-9, Oxford, 1-5.
- Rajkovic, V., Bozic, D. & Jovanovic, M.T. (2008) Properties of copper matrix reinforced with nano- and micro-sized Al₂O₃ particles. *Journal of Alloys and Compounds*, 459, 177-184.
- Rajkumar, K. & Aravindan, S. (2013) Tripological behavior of microwave processed copper-nanographite composites. *Tribology International*, 57, 282-296.
- Rhines, F.N. & Mathewson, C.H. (1934) Solubility of oxygen in solid copper. *Transactions of the Metallurgical Society of AIME*, 111, 337-353.
- Richter, A., Ries, R., Smith, R., Henkel, M. & Wolf, B. (2000) Nanoindentation of diamond, graphite and fullerene films. *Diamond & Related Materials*, 9, 170-184.
- Rosinski, M., Ciupinski, L., Grzonka, J., Michalski, A. & Kurzydowski, K.J. (2012) Synthesis and characterization of the diamond/copper composites produced by the pulse plasma sintering (PPS) method. *Diamond & Related Materials*, 27-28, 29-35.
- Saito, R., Kondo, Y., Koike, Y., Okamoto, K., Suzumura, T. & Abe, T. (2001) Noble high thermal conductivity, low thermal expansion Cu-Cu₂O composite base plate technology for power module application. *Proceedings of 2001 International Symposium on Power Semiconductor Devices & ICs*, 51-54.

- Samal, C.P., Parihar, J.S. & Chaira, D. (2013) The effect of milling and sintering techniques on mechanical properties of Cu-graphite metal matrix composite prepared by powder metallurgy route. *Journal of Alloys and Compounds*, 569, 95-101.
- Sanders P.G., Eastman, J.A. & Weertman, J.R. (1997) Elastic and tensile behavior of nanocrystalline copper and palladium. *Acta Materialia*, 45 (10), 4019-4025.
- Schubert, Th., Brendel, A., Schmid, K., Koeck, Th., Ciupiński, Ł., Zieliński, W., Weißgärber, T. & Kieback, B. (2007) Interfacial design of Cu/SiC composites prepared by powder metallurgy for heat sink applications. *Composites: Part A*, 38, 2398-2403.
- Schubert, Th., Ciupiński, Ł., Zieliński, W., Michalski, A., Weißgärber, T. & Kieback, B. (2008a) Interfacial characterization of Cu/diamond composites prepared by powder metallurgy for heat sink applications. *Scripta Materialia*, 58, 263-266.
- Schubert, Th., Trindade, B., Weißgärber, T. & Kieback, B. (2008b) Interfacial design of Cu-based composites prepared by powder metallurgy for heat sink applications. *Materials Science and Engineering A*, 475, 39-44.
- Shao, W.Z., Feng, L.C., Zhen, L. & Xie, N. (2009) Thermal expansion behavior of Cu/Cu₂O cermets with different Cu structures. *Ceramics International*, 35, 2803-2807.
- Sharma, A.S., Biswas, K., Basu, B. & Chakravarty, D. (2011) Spark plasma sintering of nanocrystalline Cu and Cu-10wt pct Pb alloy. *Metallurgical and Materials Transactions A*, 42 (7), 2072-2084.
- Shen, W., Shao, W., Wang, Q. & Ma, M. (2010) Thermal conductivity and thermal expansion coefficient of diamond/5wt.%Si-Cu composite by vacuum hot pressing. *Fusion Engineering and Design*, 85, 2237-2240.
- Smith, C.S. (1948) (Private communication from C. Zener to C.S. Smith) Grains, phases and interphases, an interpretation of microstructure. *Transactions of the Metallurgical Society of AIME*, 175, 15-51.
- Solomatov, V.S., El-Khozondar, R. & Tikare, V. (2002) Grain size in the lower mantle: constraints from numerical modeling of grain growth in two-phase systems. *Physics of the Earth and Planetary Interiors*, 129, 265-282.
- Song, M.C., Kim, H.G. & Kim, K.T. (1996) Creep densification of copper powder compact. *International Journal of Mechanical Sciences*, 38 (11), 1197-1208.
- Song, X., Liu, X. & Zhang, J. (2006) Neck formation and self-adjusting mechanism of neck growth of conducting powders in spark plasma sintering. *Journal of the American Ceramic Society*, 89 (2), 494-500.
- Srivatsan T.S., Ravi, B.G., Naruka, A.S., Petraroli, M., Kalyanaraman, R. & Sudarshan, T.S. (2002) Influence of consolidation parameters on the microstructure and hardness of bulk copper samples made from nanopowders. *Materials & Design*, 23, 291-296.

- Srivatsan T.S., Ravi, B.G., Naruka, A.S., Riester, L., Yoo, S. & Sudarshan, T.S. (2001) A study of microstructure and hardness of bulk copper sample obtained by consolidating nanocrystalline powders using plasma pressure compaction. *Materials Science and Engineering A*, 311, 22-27.
- Suryanarayana, C. & Al-Ageeli, N. (2013) Mechanically alloyed nanocomposites. *Progress in Materials Science*, 58, 383-502.
- Tabor, D. (1951) *The Hardness of Metals*. Clarendon Press, Oxford, ISBN: 0-19-850776-3, UK, 175.
- Tian, B., Liu, P., Song, K., Li, Y., Liu, Y., Ren, F. & Su, J. (2006) Microstructure and properties at elevated temperature of a nano- Al_2O_3 particles dispersion-strengthened copper base composite. *Materials Science and Engineering A*, 435-436, 705-710.
- Tjong, S.C. & Lau, K.C. (2000) Tribological behaviour of SiC particle-reinforced copper matrix composites. *Materials Letters*, 43 (5-6), 274-280.
- Tjong, S.C. & Ma, Z.Y. (2000) Microstructural and mechanical characteristics of in situ metal matrix composites. *Materials Science and Engineering R*, 29, 49-113.
- Tokita, M. (1999) Mechanism of spark plasma sintering. *Proceeding of NEDO International Symposium on Functionally Graded Materials*, Tokyo, Japan, 23-33.
- Tokita, M. (2013) Spark plasma sintering (SPS) method, system, and applications. In: *Handbook of Advanced Ceramics*, 2nd edition, Somiya, S. (editor), Academic Press, Oxford, ISBN: 978-0-12-385469-8, 1149-1177.
- Trinh, P.V., Trung, T.B., Thang, N.B., Thang, B.H., Tinh, T.X., Quang, L.D., Phuong, D.D. & Minh, P.N. (2010) Calculation of the friction coefficient of Cu matrix composite reinforced by carbon nanotubes. *Computational Materials Science*, 49, S239-S241.
- Tu, J.P., Rong, W., Guo, S.Y. & Yang, Y.Z. (2003) Dry sliding wear behavior of in situ Cu-TiB₂ nanocomposites against medium carbon steel. *Wear*, 255, 832-835.
- Turner, P.S. (1946) Thermal-expansion stresses in reinforced plastics. *Journal of Research of NBS*, 37, 239-250.
- Upadhyaya, G.S. (2000) *Sintered metallic and ceramic materials: preparation, properties and applications*. Wiley, ISBN: 0-471-98155-9, Chichester, New York, 670.
- Upadhyaya, A. & Upadhyaya, G.S. (1995) Sintering of copper-alumina composites through blending and mechanically alloying powder metallurgical routes. *Materials & Design*, 16 (1), 41-45.
- Vencl, A., Rajkovic, V., Zivic, F., Mitrović, S., Cvijović-Alagić, I. & Jovanovic, M.T. (2013) The effect of processing techniques on microstructural and tribological properties of copper-based alloys. *Applied Surface Science*, 280, 646-654.
- Wagner, C. (1961) Theorie der alterung von niederschlägen durch umlösen (Ostwald Reifung). *Zeitschrift für Elektrochemie*, 65 (7-8), 581-591.

- Weber, L. & Tavangar, R. (2007) On the influence of active element content on the thermal conductivity and thermal expansion of Cu-X (X = Cr, B) diamond composites. *Scripta Materialia*, 57, 988-991.
- Weidenmann, K.A., Tavangar, R. & Weber, L. (2009) Mechanical behaviour of diamond reinforced metals. *Materials Science and Engineering A*, 523, 226-234.
- Weiss, D. (2000) Deformation mechanisms in pure and alloyed copper films. *Doctoral Dissertation*, Stuttgart University, Germany.
- Wood, D.L. (1957) Effect of dissolved oxygen on the grain size of annealed pure copper and Cu-Al alloys. *Journal of Metals, Transactions AIME*, 209, 406-408.
- Wu, Y., Liu, X., Zhang, J., Qin, J. & Li, C. (2010) In situ formation of nano-scale Cu-Cu₂O composites. *Materials Science and Engineering A*, 527, 1544-1547.
- Xia, Y., Song, Y-Q., Lin, C-G., Cui, S. & Fang, Z-Z. (2009) Effect of carbide formers on microstructure and thermal conductivity of diamond-Cu composites for heat sink materials. *Transactions of Nonferrous Metals Society of China*, 19, 1161-1166.
- Yamamoto, K., Taguchi, T., Hanada, K., Ōsawa, E., Inakuma, M., Livramento, V., Correia, J.B. & Shohoji, N. (2007) TEM studies of nanocarbons and nanodiamonds (ND): mechanical milling of ND and Cu. *Diamond & Related Materials*, 16 (12), 2058-2062.
- Yanagisawa, O., Matsugi, K. & Hatayama, T. (1997) Effect of direct pulse discharge on electrical resistivity of copper and iron powder compacts. *Materials Transactions, JIM*, 38 (3), 240-246.
- Yanchuk, I.B., Valakh, M.Ya., Vul, A.Ya., Golubev, V.G., Grudinkin, S.A., Feoktistov, N.A., Richter, A. & Wolf, B. (2004) Raman scattering, AFM and nanoindentation characterisation of diamond films obtained by hot filament CVD. *Diamond & Related Materials*, 13, 266-269.
- Yih, P. & Chung, D.D.L. (1997) Titanium diboride copper-matrix composites. *Journal of Materials Science*, 32, 1703-1709.
- Yoshida, K. & Morigami, H. (2004) Thermal properties of diamond/copper composite material. *Microelectronics Reliability*, 44, 303-308.
- Youngdahl, C.J., Sanders, P.G., Eastman, J.A. & Weertman, J.R. (1997) Compressive yield strengths of nanocrystalline Cu and Pd. *Scripta Materialia*, 37 (6), 809-813.
- Zhan, Y., Zhang, G. & Zhuang, Y. (2004) Wear transitions in particulate reinforced copper matrix composites. *Materials Transactions*, 45 (7), 2332-2338.
- Zhang, Y., Zhang, H.L., Wu, J.H. & Wang, X.T. (2011) Enhanced thermal conductivity in copper matrix composites reinforced with titanium-coated diamond particles. *Scripta Materialia*, 65 (12), 1097-1100.

Zhang, Z.H., Wang, F.C., Lee, S.K., Liu, Y., Cheng, J.W. & Liang, Y. (2009) Microstructure characteristic, mechanical properties and sintering mechanism of nanocrystalline copper obtained by SPS process. *Materials Science and Engineering A*, 523, 134-138.

Zhang, Z.H., Wang, F.C., Wang, L. & Li, S.K. (2008) Ultrafine-grained copper prepared by spark plasma sintering process. *Materials Science and Engineering A*, 476 (1-2), 201-205.

Zheng, Y.G., Lu, C., Mai, Y-W., Zhang, H.W. & Chen, Z. (2006) Model-based simulation of normal grain growth in a two-phase nanostructured system. *Science and Technology of Advanced Materials*, 7, 812-818.

Zhou, G., Ding, H., Zhang, Y., Hui, D. & Liu, A. (2009) Fretting behavior of nano- Al_2O_3 reinforced copper-matrix composites prepared by coprecipitation. *Metallurgija*, 15 (3), 169-179.

Zweben, C. (1998) Advances in composite materials for thermal management in electronic packaging. *The Journal of The Minerals, Metals & Materials Society*, 50 (6), 47-51.

Zweben, C. (2005) Ultrahigh-thermal-conductivity packaging materials. *Semiconductor Thermal Measurement and Management Symposium, Twenty First Annual IEEE*, 168-174.

MatWeb™, Material property Data, copper: cold-worked.
<http://www.matweb.com/search/MaterialGroupSearch.aspx>

MatWeb™, Material property Data, aluminum oxide, 99.5%.
<http://www.matweb.com/search/MaterialGroupSearch.aspx>

© 2013 Copper Development Association, UK, 2013.
<http://www.copperinfo.co.uk/>

© 2013 Accuratus. <http://accuratus.com/alumox.html>

Errata

Publication I

On page 5, conclusions row 6: (up to 20 wt.%) should be (up to 20 vol.%)

Publication IV

In reference 34 Bimger should be Birringer

On page 5, end of results: $G_{\text{Cu}} = 4.9 \times 10^{11}$ Pa should be $G_{\text{Cu}} = 4.9 \times 10^{10}$ Pa

On page 2, experimental, row 13: ratio of 1:3 should be ratio of 1:1

Publication V

On page 1, row 7: 320 or 600 nm, respectively, when Cu10K1 or Cu10K2 starting powder was used should be 320 or 600 nm, respectively, when Cu10K2 or Cu10K1 starting powder was used

On page 2, last row of the first chapter of results: powder with 22 vol.% TiB₂ should be 36 vol.% TiB₂ (i.e. 22 wt.% TiB₂).



ISBN 978-952-60-5654-8
ISBN 978-952-60-5655-5 (pdf)
ISSN-L 1799-4934
ISSN 1799-4934
ISSN 1799-4942 (pdf)

Aalto University
School of Chemical Technology
Department of Materials Science and Engineering
www.aalto.fi

**BUSINESS +
ECONOMY**

**ART +
DESIGN +
ARCHITECTURE**

**SCIENCE +
TECHNOLOGY**

CROSSOVER

**DOCTORAL
DISSERTATIONS**